STRUCTURE-PROPERTY RELATIONSHIPS IN SUSTAINABLE THERMOPLASTIC ELASTOMERS

A Dissertation

Presented to

the Faculty of the Department of Chemical & Biomolecular Engineering

University of Houston

In Partial Fulfillment

of the Requirements for the Degree

Doctor of Philosophy

in Chemical Engineering

by

Wenyue Ding

August 2019

STRUCTURE-PROPERTY RELATIONSHIPS IN SUSTAINABLE THERMOPLASTIC ELASTOMERS

Wenyue Ding

Approved:

Chair of the Committee
Megan L. Robertson, Associate Professor,
Chemical & Biomolecular Engineering

Committee Members:

Jacinta C. Conrad, Associate Professor,
Chemical & Biomolecular Engineering

Jeffrey D. Rimer, Professor
Chemical & Biomolecular Engineering

Eva M. Harth, Professor,
Chemistry

Yan Yao, Associate Professor,
Electrical & Computer Engineering

Suresh K. Khator, Associate Dean,
Cullen College of Engineering

Michael P. Harold, Professor and Chair,
Chemical & Biomolecular Engineering

Acknowledgment

Firstly, I would like to express my sincere gratitude to my advisor Prof. Megan L. Robertson for introducing me to the world of polymer science and the continuous support of my Ph.D. study. She always encourages me and provides me opportunities to attend conferences and workshops to develop professional skills such as presentation and networking. She has been supportive and has given me the freedom to pursue various projects without objection. She has also provided an insightful discussion about the research. I truly appreciate her patience, enthusiasm and immense knowledge.

Besides my advisor, I would also like to express my deepest thanks to my dissertation committee members: Prof. Jacinta C. Conrad, Prof. Jeffrey D. Rimer, Prof. Eva M. Harth and Prof. Yan Yao. I'm grateful for their time and effort on the dissertation, their great support and invaluable advice. I would especially thanks to Prof. Jacinta C. Conrad and Prof. Jeffrey D. Rimer who have also been my committee members for my qualification exam and proposal defense. Their insightful comments and crucial remarks have kept me thinking throughout my Ph.D. journey.

I'm also grateful to my collaborators, Prof. Chuanbing Tang and his student Mitra S. Ganewatta from University of South Carolina for helpful discussion on the synthesis of rosin derived methacrylic monomers, Prof. Wesley R. Burghardt form Northwestern University for his kind help on setting up the *in-situ* SAXS equipment and sharing his knowledge on the detail of experiments, Carlos R. López-Barrón from ExxonMobil chemical company for performing FT-rheology experiments.

I would like to thank my current and former group members for their continued support: Dr. Shu Wang, Dr. Vivek Yadav, Dr. Guozhen Yang, Dr. Brian Rohde, Tyler

Cooksey, Jialin Qiu, Tzu-Han Li, Minjie Shen, Josiah Hanson, Dr. Xuejian Chen, Dr. Hongda Cao, Dr. Fahimeh Khakzad and Rosalie Berg. This dissertation would not have been possible without their intellectual contributions. Especially thanks to Dr. Shu Wang who have shared all her knowledge regarding the project of sustainable thermoplastic elastomers when I first joined this group.

Last but not least, I would like to express my dearest thanks to my family for their support and encouragement. Thanks to my parents, Min Zhang, Yunzhi Ding, my parents in law, Yuzhen Zheng, Wenying Zhang who have always been there for me. My deepest thanks go to my husband, Lingfeng Zhang and my lovely son, Leon who give me such a warm family. This dissertation would not have been possible without their warm love, continued patience and endless support.

STRUCTURE-PROPERTY RELATIONSHIPS IN SUSTAINABLE THERMOPLASTIC ELASTOMERS

An Abstract

of

A Dissertation

Presented to

the Faculty of the Department of Chemical & Biomolecular Engineering

University of Houston

In Partial Fulfillment

of the Requirements for the Degree

Doctor of Philosophy

in Chemical Engineering

by

Wenyue Ding

August 2019

Abstract

Thermoplastic elastomers (TPEs), predominantly composed of ABA triblock copolymers containing glassy polystyrene endblocks and rubbery polydiene midblocks, are widely used in electronics, adhesives and automotive components. Sustainable TPEs derived from renewable resources can be attractive alternatives to petroleum-based TPEs when sustainability requirements are met without compromising material performance. Vegetable oils and their fatty acids are promising replacements for petroleum sources as polymer feedstocks due to their abundance, lack of toxicity and ease of functionalization. However, fatty acid-derived TPEs exhibit inferior mechanical properties to petroleum-based products due to lack of entanglements, stemming from the presence of long alkyl chains on the fatty acids. To facilitate the adoption of polymers derived from vegetable oils and fatty acids, we aim to develop approaches to enhance the mechanical properties of this class of materials.

In this study, two approaches were evaluated as means to enhance the mechanical properties of sustainable TPEs with fatty acid-derived midblocks: incorporation of hydrogen bonds or ionic interactions. In the first approach, the hydrogen bond-containing comonomer acrylamide was incorporated into midblock. The triblock copolymers exhibited not only greatly improved mechanical properties, but also accessible processing temperatures. In the second approach, ionic interactions were introduced into midblock by neutralizing the comonomer methacrylic acid. The tensile strength and modulus were significantly enhanced by the incorporation of ionic interactions and the strain at break was improved at low degrees of neutralization.

In addition, the fatty acid-derived triblock copolymers exhibited a closed packed spherical (CPS) morphology under oscillatory shear, attributed to the presence of the higher dispersity midblock. The presence of CPS morphology in the bulk block copolymers has rarely been reported, which motivated the investigation of the kinetics and mechanisms through *in-situ* small-angle X-ray scattering and Fourier transform-rheology. The orientation of CPS layers was found to be affected by the strain amplitudes. For the first time, we observed shear deordering at high strain amplitude for the sphere-forming block copolymers in the bulk.

Finally, to expand the library of renewable building blocks for TPEs, a rosin-derived polymer possessing a high glass transition temperature was evaluated as the endblocks in sustainable TPEs. The triblock copolymers exhibited elastomeric behavior at room temperature and accessible order-disorder transitions, appropriate for thermoplastic elastomer applications.

Table of Contents

List of Figures

List of Schemes

List of Tables

Chapter 1 Introduction

Polymers play a vital and ubiquitous role in everyday life. Due to their broad range of properties, the applications range from daily necessities such as clothing, packaging and toys to more sophisticated applications such as medicine, electronics and automotive components.[1] The vast majority of the polymers are sourced from petroleum with six percent of the oil produced worldwide being used for their production every year.[2] The well-known concerns of oil depletion and potential environmental hazards have motivated researchers to develop sustainable polymers.[3, 4] Many efforts have been made on replacing fossil raw materials with renewable alternatives, leading to a variety of renewable polymers developed in laboratory research.[2] However, for renewable polymers to find commercial applications, not only favorable economics are required but also material properties comparable to their petroleum based counterparts, such as thermal resistance, mechanical strength, processability and compatibility. Such tough criteria prevent most of studied renewable polymers from finding commercial applications. Therefore, it is crucial to understand the structure-property relationships in these sustainable polymers and seek potential opportunities to enhance their performance.

Elastomers or rubbers are polymers with generally low Young's modulus and high failure strain. They find a variety of applications in automotive parts, medicine, adhesives and consumer goods with a market size valued at more than 70 billion USD at 2017.[5] Conventional elastomers are crosslinked polymers produced by vulcanization that present particular challenges of lack of processability and recyclability. Thermoplastic elastomers (TPEs), on the other hand, have both advantages of conventional crosslinked elastomers (e.g., softness, flexibility and resilience) and thermoplastics (e.g.,

processability and recyclability). Due to their unique properties, the market demand has kept increasing in recent years, and the market value is anticipated to reach $24 billion in 2019.[6] Nonetheless, the commercial TPEs on the market are exclusively sourced from petroleum. Due to above-mentioned concerns of oil depletion and environmental hazards, there is an emerging need to find bioderived building blocks to develop sustainable TPEs with desirable physical properties.

Enormous efforts have focused on the development of sustainable TPEs. A diverse collection of renewable building blocks has been created and spans an assortment of feedstocks, including (but not limited to) fatty acids,[7] essential oils,[8] plant sugars,[9, 10] rosin,[11] lignin[12] and turpentine[13]. However, the creation of such a library of building blocks is only the first step towards the development of sustainable TPEs. The widespread adoption of sustainable TPEs requires both sustainability and promising material performance, especially mechanical properties. Unfortunately, the majority of the sustainable TPEs reported so far exhibited inferior mechanical properties to petroleum-based products.[7, 11, 14, 15] Such a phenomenon is ascribed to the lack of entanglements in the sustainable TPEs stemming from the presence of bulky moieties in the renewable components.[7, 16, 17] Thus, developing methods to overcome this common issue in sustainable TPEs becomes imperative.

In this study, we aim to overcome the lack of entanglements in fatty acid-derived sustainable TPEs and enhance their mechanical properties by incorporating supramolecular networks. Two types of networks were evaluated: networks through hydrogen bonds and ionic bonds. Then we explored the kinetics and mechanism of shear alignment of fatty acid-derived TPEs forming a closed packed spherical morphology. The

formation of a closed packed spherical morphology by a bulk block copolymer has rarely been reported in literature, and in this study is observed due to the presence of a higher dispersity midblock. Finally, we evaluated rosin derived polymer with a high glass transition temperature as a building block for sustainable TPEs.

1.1 Block copolymer-based thermoplastic elastomers

Block copolymers (BCPs), which consist of two or more chemically distinct homopolymers tethered to each other, can phase separate at nanometer scales when the strength of repulsive interaction between blocks is sufficiently large. Based on the composition of each blocks and the strength of interaction, several types of morphologies can be achieved: spheres, cylinders, gyroids and lamellae. BCPs can be classified based on the number of blocks (e.g., diblock, triblock and multiblock) and the architecture of polymer (linear, star, comb and bottle brush). Among them, ABA triblock copolymers in which A represents glassy endblocks and B the rubbery midblock has been proven to be desirable for application as TPEs. At low temperatures (typically room temperature), the glassy endblocks self-assemble into spherical or cylindrical domains, dispersed into the rubbery midblock matrix. The dispersed glassy domains act as physical crosslinkers that firmly bound the rubbery matrix together, which gives the material elastomeric behavior (Figure 1.1). When heated above the order-disorder transition temperature (T_{ODT}), the phase separated domains disappear such that the triblock copolymers become disordered and behave like liquid which is convenient for processing. The most commonly used commercial TPEs are styrenic block copolymers such as poly(styrene-*b*-butadiene-*b*-styrene) (SBS) or poly(styrene-*b*-isoprene-*b*-styrene) (SIS).

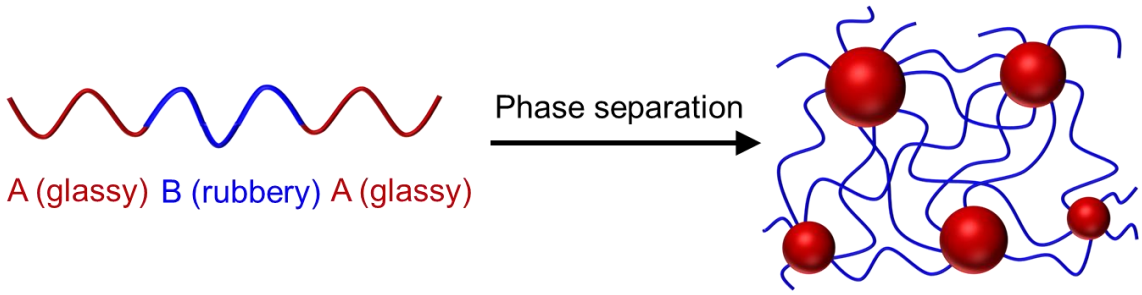

Figure 1.1 Physical crosslinked network formed by microphase separation in ABA triblock copolymers

The overall molecular weights and composition of each block play important roles in the properties of ABA triblock copolymers. There is always a tradeoff between material performance and processability. For example, higher molecular weight BCPs gives better mechanical properties, but also results in higher processing temperatures and melt viscosities that pose challenges in processing. Thus, for commercial TPEs, the molecular weights of the polystyrene (PS) blocks are generally in the range of 10 kg/mol to 15 kg/mol, while the polydiene midblocks have molecular weights from 50 kg/mol to 70 kg/mol.[18] The PS fraction is about 20~30%, at which the equilibrium morphology of the SBS or SIS triblock copolymer is PS spheres or cylinders dispersed in the soft matrix.[18] Such molecular design gives SBS and SIS superior mechanical properties. They have tensile strengths up to about 30 MPa and elongation at break of up to 800%, comparable to the mechanical properties of vulcanized rubbers.[18]

However, the diene-based TPEs have a major drawback. They have poor oxidative stability and UV resistance due to the unsaturated midblocks.[19-21] This drawback could be overcome by the hydrogenation of the midblock, but this adds to the cost. Several researchers developed saturated TPEs with poly(alkyl acrylate) center blocks and short-chain poly(alkyl methacrylate) end blocks which are potential substitutes for traditional diene-based TPEs.[22-24] Unfortunately, they are found to be

inferior to the diene-besed TPEs with regards to mechanical properties. The cause of this deficiency was traced to the high molecular weight between entanglements of the polyacrylates compared to the polydienes.[22] Although the mechanical properties are not comparable to the diene-based TPEs, the stability has been improved and they find application in pressure-sensitive adhesives.[25]

1.2 Thermodynamics and phase behaviors

The physical properties and mechanical performance of BCPs are highly related to their phase behavior. In order to design a BCP-based TPE with desirable properties (e.g., accessible order-disorder transition temperatures, high tensile strength and strain at break), it is crucial to understand the thermodynamics and therefore its phase behaviors.

The phase behavior of bulk BCPs is determined by three factors: the overall degree of polymerization N, the composition f and segment-segment interaction parameter χ. Both N and f can be tuned by design of synthetic protocols while χ is determined by the choice of block components. Smaller χ values indicate more favorable interactions between components. For most combinations of components, χ decreases with increasing temperature that $\chi = \alpha T^{-1} + \beta$, where α and β are constants. In the system with upper critical solution temperature, at equilibrium, the block copolymer chains will adopt minimum free energy configurations. At low temperature, the large interaction parameter χ favors a reduction in monomer-monomer contact by inducing local compositional ordering, which is microphase separation.[26] On the other hand, at high temperatures, when χ is small enough that entropic factors will dominate, a disordered phase is favored.[26]

The value of χ can be either theoretically calculated using the solubility parameter method or experimentally determined. Numerous experimental methods have been developed on the determination of χ including small angle neutron scattering or cloud point measurements on polymer blends, the PVT methods of pure components to determine solubility parameters, and order-disorder transition temperature measurements on block copolymers. Among them, cloud point measurements have been proven to be not only effective but also relatively straightforward to carry out.

The determination of χ by cloud point measurements is based on Flory-Huggins theory. The free energy of mixing of two homopolymers A and B is given by[27, 28]

$$\frac{\Delta G_m}{kT} = \frac{\phi_A ln\phi_A}{v_{mon,A}N_{mon,A}} + \frac{\phi_B ln\phi_B}{v_{mon,B}N_{mon,B}} + \chi\frac{\phi_A\phi_B}{v_{ref}}, \qquad \text{Equation 1.1}$$

where ΔG_m is the free energy change on mixing per unit volume, k is the Boltzmann constant, T is the absolute temperature, ϕ_i is the volume fraction of each blend component (i=A or B), $v_{mon,i}$ is the volume of each monomer on chain i, v_{ref} is the reference volume (100 Å^3), $N_{mon,i}$ is the number of monomer repeat units in chain i, and χ is the Flory-Huggins interaction parameter (based on the reference volume v_{ref}).

The binodal curve can be constructed by deriving expressions for the chemical potentials of each component in the blend using Flory Huggins theory (Equation 1.1) and equating the chemical potentials for each component in phases I and II:

$$ln\frac{\phi_A^I}{\phi_A^{II}} + (\phi_A^{II} - \phi_A^I)\left(1 - \frac{N_{w,A}}{N_{w,B}}\right) + \chi N_{w,A}[(1-\phi_A^I)^2 - (1-\phi_A^{II})^2] = 0 \text{ and} \qquad \text{Equation 1.2}$$

$$ln\frac{1-\phi_A^I}{1-\phi_A^{II}} + (\phi_A^I - \phi_A^{II})\left(1 - \frac{N_{w,B}}{N_{w,A}}\right) + \chi N_{w,B}[(\phi_A^I)^2 - (\phi_A^{II})^2] = 0. \qquad \text{Equation 1.3}$$

Simultaneously solving Equation 1.2 and Equation 1.3 leads to the determination of ϕ_A^I and ϕ_A^{II} as a function of χ. Finally, χ(T) relationship can be determined by comparing the cloud points with the binodal curve.

In recent years, many efforts have been made on developing BCP phase diagrams. Various theoretical phase diagrams for different types of BCPs (e.g., symmetric,[29] nonsymmetric,[30] polydisperse,[31] monodisperse,[32] linear, star[33-37] and graft[38, 39]) have been determined using self-consistent field theory. The most common morphologies for linear block copolymers include bcc spheres (S), hexagonally closed packed spheres (S_{cp}), cylinders (C), gyroid(G) and lamellar (L). Such theoretical phase diagrams along with the Flory-Huggins interaction parameter χ, function as essential tools allowing the design of block copolymers with desirable morphologies.

1.3 Sustainable triblock copolymer-based thermoplastic elastomers

In the past few decades, interest in renewable polymers has witnessed continuous growth in both academia and industry. A variety of biobased feedstocks have been developed for renewable TPEs, Recently, enormous research efforts have focused on sustainable triblock copolymer-based TPEs. For example, fatty acid or vegetable oil-derived polyacrylates,[7, 40] plant-based poly(δ-decalactone)[41, 42] plant-oil derived polymyrcene,[9] amino acid-derived polyesters,[43] and mint-derived poly(menthide)[8, 44] were found to be appropriate replacements for the rubbery midblock due to their low T_g. The development of sustainable glassy endblocks has emphasized lactide and lactone derivatives.[10, 45-49] Some other studies include glassy endblocks composed of tulip-derived poly(α-methylene-γ-butyrolactone),[50] bicyclic sugar-derived poly(methacrylic isosorbide),[51] salicylic acid-derived poly(acetylsalicylic ethyl methacrylate),[12] terpene-

derived poly(α-methyl-*p*-methylstyrene),[13] and glucose-derived poly(glucose-6-acrylate-1,2,3,4-tetraacetate).[52]

Plant oils and their fatty acids are a particularly attractive source, due to their low toxicity, biodegradability, availability and relatively low price.[53-59] The carbon-carbon double bond in the vegetable oils enables the epoxidation that opens up opportunities for a variety of functionalization and subsequent polymerization. Vegetable oils can firstly be epoxidized then followed by polymerization result in epoxy resins.[60, 61] Also, the epoxidized vegetable oils can not only be converted to polyols for polyurethanes but also can be acrylated through a ring-opening reaction with acrylic acid, leading to polyacrylates.[62-67] Furthermore, vegetable oils can be functionalized with cyclic structures, and then polymerized through ring-opening metathesis polymerization (ROMP).[68-71] The vegetable oils can be hydrolyzed to be fatty acids. The carboxylic acid end-group of a fatty acid can be converted to a hydroxyl end-group[72, 73] and subsequently converted to an acrylate or methacrylate group,[74] convenient for controlled radical polymerization techniques.

Rosin, comprised of abietic acid and many other isomers, with an annual production of more than 1 million tons, has been widely used in adhesives, coatings, inks, detergents, lubricants, fuel additives, and food additives.[75] These hydrocarbon rich diterpene resin acids provide high glass transition temperature, hydrophobicity and rigidity to polymeric materials. Recently, a variety of rosin-derived polymeric materials have been developed, including amphiphilic block copolymers for application as inter-cellular carriers,[76] and cationically modified rosin acids as biomaterials.[77-80] Two notable studies investigated thermoplastic elastomers derived from rosin: copolymers developed

from rosin and fatty acids were grafted to cellulose,[81] and polynorbornene derivatives containing rosin-based moieties were synthesized through ring-opening metathesis polymerization and used as the end-blocks of ABA triblock copolymers.[16] To our knowledge, no prior studies have utilized controlled radical polymerization to prepare well-defined ABA triblock copolymers incorporating pendant rosin-containing polymers as the glassy blocks.

1.4 Lack of entanglements in sustainable TPEs

However, a common issue with bioderived polymers is that they usually contain bulky moieties as side-chain that results in high entanglement molecular weight which attributes to poor mechanical performance. For example, our group has previously reported replacing the polydiene midblock in conventional TPEs with sustainable polyacrylates derived from fatty acids.[7] The thermal, rheological, and mechanical properties of the polymers were tunable through variation of the length of the alkyl side-chain of the polyacrylate.[7] However, their tensile strength and strain at break were found to be inferior to commercial TPEs.[7] These undesirable mechanical properties are attributed to lack of entanglement in the rubbery matrix due to the high entanglement molecular weight (M_e) of polymers with long alkyl side-chains (e.g., M_e of poly(lauryl methacrylate) is 225 kg/mol[23]). Other studies on sustainable TPEs with poor mechanical performance also have utilized polymers with bulky moieties and resulting high M_e, such as glucose-derived poly(glucose-6-acrylate-1,2,3,4-tetraacetate),[52] salicylic acid-derived poly(acetylsalicylic ethyl methacrylate),[14] rosin derived poly(dehydroabietic ethyl methacrylate)[11] and dehydroabietic-containing polynorbornene.[16] Thus, it is highly

important to develop a method to overcome the lack of entanglements in these materials for the broad application of sustainable polymers.

1.5 Supramolecular networks

The elastomeric properties of traditional ABA triblock copolymers rely exclusively on the thermodynamic incompatibility between different segments to form physically crosslinked networks. Incorporation of additional crosslinks (covalent or noncovalent) to the ABA triblock copolymer system, either in soft B matrix or hard A domains, has been proven to enhance the mechanical properties. Wang et al. incorporated covalent crosslinks, using click chemistry, into soybean oil-derived ABA triblock copolymers.[15] By carefully controlling the coupling density, the triblock copolymers remained soluble in organic solvents and showed improved tensile strength. However, polymers with covalent crosslinks usually exhibit poor processibility, which prevent their use for certain applications.

By contrast, supramolecular networks that introduce dynamic interactions to polymer system through reversible crosslinks are more attractive. The dynamic nature of the bonds not only is beneficial to enhance mechanical properties but also enables additional features such as stimuli responsibility and shape memory properties.[82-85] Various types of supramolecular interactions, such as ionic interaction,[86-88] hydrogen bonding, [89-91] π-π stacking[92-95] and metal-ligand coordination[96, 97], have been incorporated into TPEs to prepare advanced materials. In this study, we are particularly interested in using ionic interaction and hydrogen bonding.

Hydrogen bonds have been widely used in enhancing the mechanical properties of TPEs. Yang and coworkers prepared triblock copolymers containing a polynorbornene

midblock that exhibited improved mechanical properties with the incorporation of a secondary amide group.[89] Hayashi et al. improved the mechanical properties of TPEs containing a poly(butyl acrylate) midblock through incorporation of acrylamide.[90, 91] Additionally, hydrogen bonds can be incorporated into endblocks to reinforce the hard domains.[98] Many questions remain, however, on the morphological, thermal, and mechanical behavior of ABA triblock copolymers which contain a transient network.

The presence of hydrogen bonding has been examined in a limited number of studies on biobased polymers, such as in nanocomposites composed of soybean oil and cellulose nanocrystals,[99] shape-memory materials synthesized from soybean amide methacrylate,[100] self-healing and thermoreversible rubber synthesized from vegetable oil-derived fatty dimer acid,[101] nanosheets derived from conjugated linoleic acid,[102] high performance polyimide containing biobased adenine,[103] and nanofibers derived from rice flour.[104] To our knowledge, the incorporation of hydrogen bonding has not been previously examined as a means of improving mechanical behavior in biobased thermoplastic elastomers with bulky constituents such as those derived from vegetable oil feedstocks.

Ionic interactions, as another type of dynamic interactions, have also been incorporated into TPEs for enhancement of mechanical properties. The incorporation of ionic interaction to endblocks has mainly focused on using sulfonated polystyrene. Storey and coworkers prepared ionomer based poly(styrene-block-isobutylene-block-styrene) by partially sulfonating the aromatic blocks.[105] The sulfonated ionomers exhibit higher mechanical properties than those of the unsulfonated parents. Ghosh et al. sulfonated the maleated SEBS block copolymer and neutralized by different metal acetates to form

ionomers containing both carboxylate and sulfonate anions on the same polymer backbone.[106, 107] The tensile strength, tear strength, hardness, and thermal stability increase with increasing degree of neutralization, but the elongation at break decrease. In one study, instead of using sulfonated polystyrene as endblocks, Long prepared ABA triblock copolymer through NMP with the phosphonium ion in endblocks.[88] The storage modulus increased as the mole percentage of ions was increased.

However, only a few studies incorporated ionic interactions into soft midblock. In one noticeable study, Wang incorporated 2 wt% of imidazole into B block of ABA triblock copolymer and evaluated the influence of different level of ionic crosslinking in B block on the mechanical properties.[86] They found the tensile stress and elastic recovery were significantly enhanced though the elongation at break was sacrificed. Similarly, the same group also prepared BAB triblock copolymers with imidazole containing elastic B block as the end blocks.[87] Even though the block sequence was reversed, typical stress-strain behavior for thermoplastic elastomers was observed, which might be attributed to the presence of ionic association in the B block. To the best of our knowledge, no prior studies have incorporated acid based ionic interactions (e.g., neutralized methacrylic acid) to the midblock of an ABA triblock copolymer.

1.6 Overview of the thesis

In the following chapters the dissertation is organized as outlined below.

Chapter 2 describes the experimental methods used in this study. Detailed information on chemicals used, synthesis techniques and characterization procedures will be discussed.

Chapter 3 discusses the enhancement of mechanical properties of fatty acid derived TPEs through incorporation of supramolecular network by hydrogen bonds. The effects of hydrogen bonds content on physical properties are evaluated.

Chapter 4 investigates the enhancement of mechanical properties of fatty acid derived TPEs through incorporation of supramolecular network by ionic interactions. The effects of degree of neutralization and total acid content on the physical properties of TPEs are studied.

Chapter 5 presents the shear alignment of fatty acid derived ABA triblock copolymer with closed packed spherical morphology. The in-situ SAXS and FT-rheology were used to monitor the kinetics of the alignment process. The effect of strain amplitudes on the kinetics and final orientation are discussed.

Chapter 6 discusses the development of sustainable TPEs with rosin derived endblocks. The morphological, thermal and mechanical properties of the triblock copolymers are characterized.

Chapter 7 gives a summary and conclusions of this research. An outlook of the challenges and future work is also discussed.

Chapter 2 Experimental Methods

This chapter describes synthesis and characterization methods for the development of sustainable thermoplastic elastomers. Atom transfer radical polymerization (ATRP) was used for the synthesis of rosin derived sustainable TPE poly(dehydroabietic ethyl methacrylate-*b*-*n*-butyl acylate-*b*-dehydroabietic ethyl methacrylate) (DnBD) and the fully (meth)acrylate-based TPE poly(methyl methacrylate-*b*-*n*-butyl acylate-*b*-methyl methacrylate) (MnBM). Reversible addition fragmentation chain transfer (RAFT) polymerization was used for the preparation of fatty-acid derived polymers, including poly(lauryl acrylate-*co*-acrylamide) (PLAM) copolymers, poly(styrene-*b*-(lauryl acrylate-*co*-acrylamide)-*b*-styrene) (SLAS) triblock copolymers, poly(lauryl methacrylate-co-tert butyl methacrylate) (PLtB) copolymers and poly(methyl methacrylate-*b*-(lauryl methacrylate-*co*-*tert* butyl methacrylate)-*b*-methyl methacrylate) (MLtM) triblock copolymers.

The structure of the polymers was characterized by proton nuclear magnetic resonance (^{1}H-NMR) and gel permeation chromatography (GPC). The thermal properties were measured by differential scanning calorimeter (DSC) and thermogravimetric analysis (TGA). The master curves and order-disorder transition temperature were characterized with rheology. The morphology was probed by small angle x-ray scattering (SAXS). The mechanical properties of the triblock copolymers were characterized through tensile testing. Specific details pertaining to the synthesis and characterization methods are presented here.

2.1 Polymer synthesis

2.1.1 Synthesis of poly(dehydroabietic ethyl methacrylate) (PDAEMA)

Dehydroabietic acid was purified by repeated recrystallization of ethanolamine salt.[108] Dehydroabietic acid (100 g) was dissolved in 250 mL of ethanol, and the solution was heated up to 70 °C. Ethanolamine (18 g) was then added to the solution, and stirred for several minutes followed by addition of 250 mL of deionized water. The solution was slowly cooled down to room temperature and filtered to collect the ethanolamine salt. The ethanolamine salt was recrystallized in an ethanol/water mixture (5/5 v/v) 5 times and acidified by diluted hydrochloride to afford white crystals. The product was then dried under vacuum at 80 °C overnight. Dehydroabietic ethyl methacrylate (DAEMA) was synthesized according to reported procedures,[75] with slight modification, shown in Scheme 2.1. Dehydroabietic acid (10.00 g, 33.3 mmol) was dissolved in 60 mL of DCM; then, 10 mL of oxalyl chloride (8.45 g, 66.6 mmol) and two drops of dry DMF were added. The reaction was stirred at 0 °C under N_2 for 3h. Excess oxalyl chloride and DCM were removed using a rotary evaporator, and the prepared dehydroabietic chloride was dissolved in 60 mL of dichloromethane. 2-HEMA (4.80 g, 36.9 mmol) and trimethylamine (5.00 g, 49.4 mmol) were subsequently added dropwise at 0 °C. The reaction mixture was gently warmed to room temperature and stirred under N_2 for 48 h, and then neutralizing through washing with 5% sodium bicarbonate solution followed by drying over anhydrous sodium sulfate and evaporated to dryness, forming a white powder. The product was further purified by silica gel chromatography (ethyl acetate/hexane: 1/9 v/v) to afford a white powder.

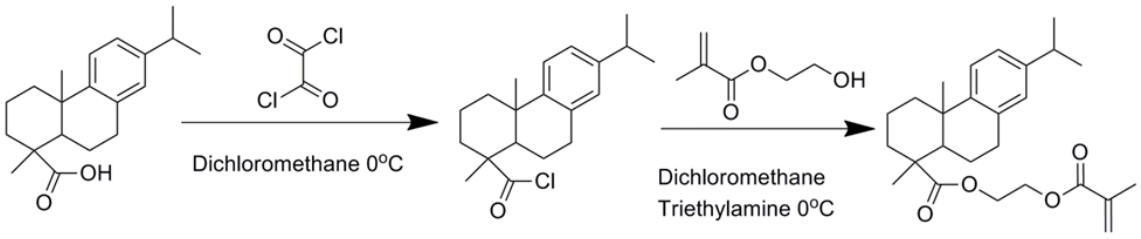

Scheme 2.1 Synthesis of DAEMA monomer

PDAEMA homopolymer was synthesized by atom transfer radical polymerization (ATRP) following a reported procedure.[75] In a nitrogen glove box, CuBr, DAEMA, Me_6Tren, EBriB and THF were added to a pressure vessel. Once sealed, the vessel was taken out of glovebox and heated in an oil bath at 90 °C for 16 h. The polymerization was stopped by diluting the reaction mixture with THF. The crude product was passed through a neutral alumina column, concentrated by rotary evaporator, precipitated in methanol three times and dried under vacuum at room temperature overnight.

2.1.2 Synthesis of poly(dehydroabietic ethyl methacrylate-b-n-butyl acylate-b-dehydroabietic ethyl methacrylate) (DnBD) triblock copolymer

The DnBD triblock copolymers were synthesized through two-steps ATRP (Scheme 2.2). Poly(*n*-butyl acrylate) (PnBA) was firstly synthesized as a macroinitiator following reported procedures.[109] In a nitrogen glovebox, diethyl meso-2,5-dibromoadipate, *n*-butyl acrylate and $NiBr_2(PPh_3)_2$ were added to a pressure vessel. Once sealed, the vessel was taken out of glovebox and heated in an oil bath at 85 ℃ for polymerization. After reaction for 17 h, the contents in the pressure vessel were dissolved in THF, passed through a neutral alumina column to remove the metal complex, concentrated by rotary evaporator, and then precipitated in cold methanol. The precipitant was collected and dried under vacuum at room temperature overnight.

PnBA was used as the macroinitiator to produce the triblock copolymer, DnBD. A typical procedure for synthesis of the triblock copolymers is described as follows. In the glovebox, PnBA (1.0 g) and DMF (4.0 g) were added to a pressure vessel in a nitrogen glove box. The mixture was stirred for 30 min to form a homogenous solution. CuCl (2.6 mg), PMDETA (4.5 mg) and DAEMA (1.5 g) were added to the pressure vessel subsequently. Once sealed, the vessel was taken out of the glovebox and heated in an oil bath at 90 °C for 8 h. The reaction mixture was quenched by diluting with THF, passed through a neutral alumina column, concentrated using rotary evaporator and precipitated into methanol three times. DnBD was collected and dried under vacuum at 110 °C overnight. DnBD triblock copolymers are referred to as DnBD*X*, where *X* is the vol% PDAEMA in the polymer.

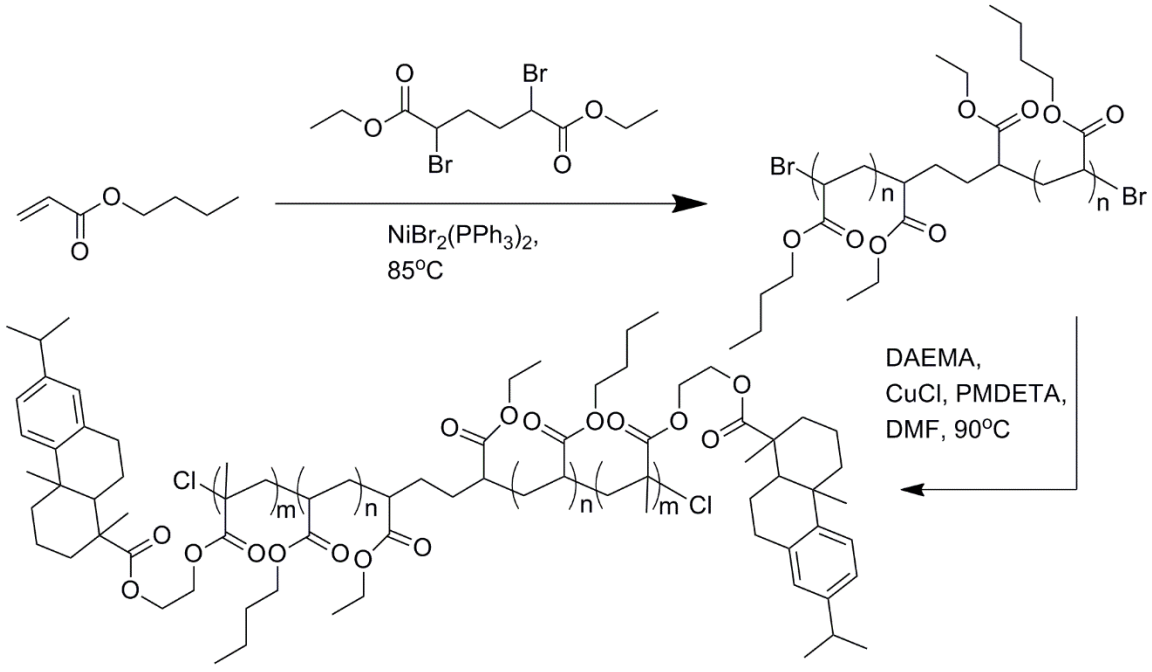

Scheme 2.2 Synthesis of DnBD triblock copolymer

2.1.3 Synthesis of poly(methyl methacrylate-b-n-butyl acylate-b-methyl methacrylate) (MnBM) triblock copolymer

The MnBM triblock copolymers were synthesized by two-steps ATRP. The PnBA was firstly prepared by a difunctional initiator as previously described. Then, PnBA was used as the macroinitiator to produce the triblock copolymer, MnBM. In the glovebox, PnBA (1.0 g) and toluene (4.0 mL) were added to a pressure vessel with a stir bar in a nitrogen glove box. The mixture was stirred for 30 min to form a homogenous solution. CuCl (2.6 mg), dNbpy (22.6 mg) and methyl methacrylate (1.11 g) were added to the pressure vessel subsequently. Once sealed, the vessel was taken out of the glovebox and heated in an oil bath at 85 °C for 24 h. The reaction mixture was quenched by diluting with THF, passed through a neutral alumina column, concentrated using rotary evaporator and precipitated into methanol three times. MnBM was collected and dried under vacuum at 110 °C overnight. MnBM triblock copolymers are referred to as MnBMX, where X is the vol% methyl methacrylate in the polymer.

2.1.4 Synthesis of Poly(styrene-b-(lauryl acrylate-co-acrylamide)-b-styrene) (SLAS)Triblock Copolymers

The SLAS triblock copolymers were synthesized through two-steps RAFT polymerization (Scheme 2.3). Firstly, the midblock poly(lauryl acrylate-*co*-acrylamide) **(**PLAM**)** copolymers were synthesized by reversible addition-fragmentation chain transfer (RAFT) polymerization. The chain transfer agent 1,4-bis(thiobenzoylthiomethyl)benzene (BTBTMB) was synthesized according to literature procedures.[110] Briefly, phenylmagnesium bromide was firstly prepared by reaction between bromobenzene and magnesium turnings, and then reacted with carbon disulfide

and α,α-dibromoxylene, followed by purification to yield the product. Our full synthetic procedures have been previously reported.[111] 2,2'-Azobis(2-methylpropionitrile) (AIBN) was recrystallized in reagent alcohol prior to use, and lauryl acrylate (LA) was passed through a silica gel column to remove monomethyl ether hydroquinone inhibitor. Acrylamide (AM) and 1,4-dioxane were used as received. As an example, a copolymer containing 4 wt% polyacrylamide was prepared as follows: in a round bottom flask, lauryl acrylate (20 g, 0.083 mol), acrylamide (0.84g, 0.012 mol), BTBTMB (0.07 g, 0.17 mmol), AIBN (5.6 mg, 0.03 mmol) and 1,4-dioxane (40 mL) were added. The flask was then sealed with a rubber septum, purged with argon for 30 min and immersed into an oil bath at 70°C. After stirring for 2 days, the reaction was quenched with water and the PLAM copolymer was precipitated into methanol three times followed by drying in a vacuum oven at 40 °C overnight. PLAM copolymers with different acrylamide content were synthesized by changing the feed ratio of LA and AM. PLAM copolymers are referred to as PLAM*X*, where *X* is the weight percent of polyacrylamide in the polymer.

Then, the SLAS triblock copolymers were synthesized by chain extension of PLAM copolymers. Styrene was passed through a basic aluminum oxide column to remove 4-tert-butylcatechol inhibitor. Toluene was purified using a SG Waters solvent purification system. A typical procedure is as follows: in a round bottom flask, PLAM copolymer (2 g, 0.023 mmol), styrene (0.7 g, 6.7 mol), AIBN (1mg, 0.006 mmol) and toluene (6ml) were added. The flask was then sealed with a rubber septum, purged with argon for 30 min and immersed into an oil bath at 70°C. After stirring for 2 days, the reaction was quenched with water and the SLAS triblock copolymer was precipitated into methanol three times followed by drying in a vacuum oven at 100°C overnight. SLAS

triblock copolymers with different polystyrene content were synthesized by changing the feed ratio of PLAM and styrene. SLAS triblock copolymers are referred to as SLAS*X*-*Y*, where *X* is the weight percent of polyacrylamide in the midblock, and *Y* is the volume percent of polystyrene in polymer.

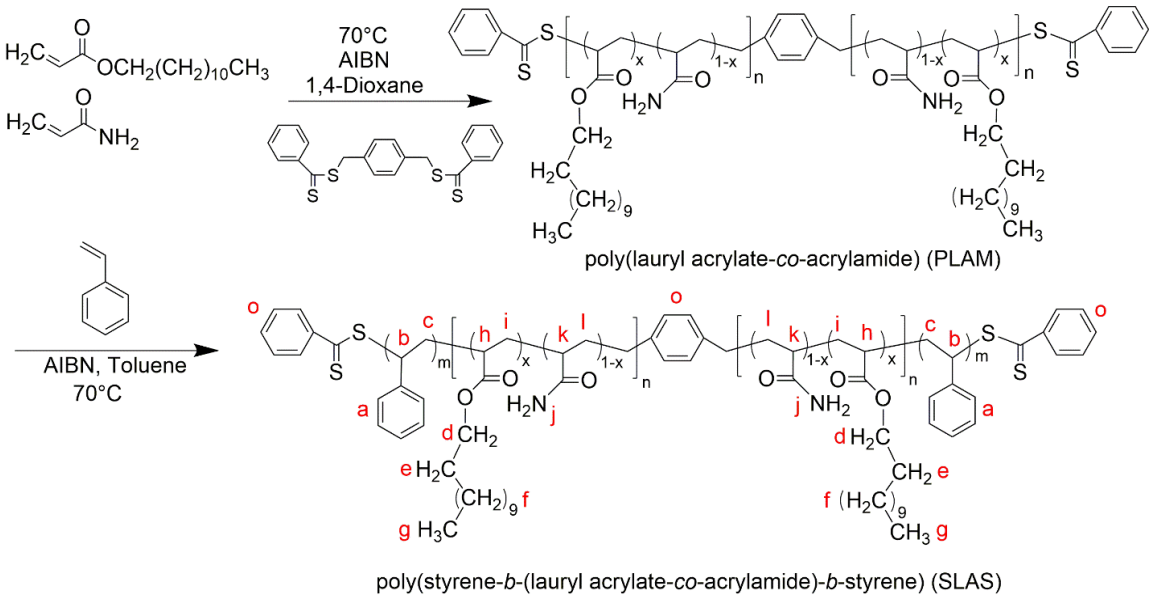

Scheme 2.3 Synthesis of SLAS triblock copolymers. Assignment of NMR peaks is indicated in red.

2.1.5 Synthesis and Characterization of Poly(styrene-b-(lauryl acrylate-co-methyl acrylate)-b-styrene) (SLMS) Triblock Copolymer

A poly(lauryl acrylate-co-methyl acrylate) (PLM) copolymer was synthesized by reversible addition-fragmentation chain-transfer (RAFT) polymerization using BTBTMB as chain transfer agent, The synthesis procedure is similar to that of poly(styrene-b-(lauryl acrylate-co-methyl acrylate)-b-styrene) copolymers. Methyl acrylate was passed through a basic aluminum oxide column to remove monomethyl ether hydroquinone inhibitor. A copolymer containing 3.5 vol % poly(methyl acrylate) was prepared as follows: in a round bottom flask, lauryl acrylate (20 g, 0.083 mol), methyl acrylate (0.9 g,

0.010 mol), BTBTMB (0.07 g, 0.17 mmol), AIBN (5.6 mg, 0.03 mmol) and 1,4-dioxane (40 mL) were added. The flask was then sealed with a rubber septum, purged with argon for 30 min and immersed into an oil bath at 70°C. After stirring for 2 days, the reaction was quenched with water and the PLM copolymer was precipitated into methanol three times followed by drying in a vacuum oven at 40°C overnight. Then, PLM copolymer was chain extended with styrene to synthesize the poly(styrene-*b*-(lauryl acrylate-*co*-methyl acrylate)-*b*-styrene) (SLMS) triblock copolymer. PLM copolymer (5 g, 0.065 mmol), styrene (0.7 g, 6.7 mol), AIBN (1mg, 0.006 mmol) and toluene (15 ml) were added. The flask was then sealed with a rubber septum, purged with argon for 30 min and immersed into an oil bath at 70°C. After stirring for 2 days, the reaction was quenched with water and the SLMS triblock copolymer was precipitated into methanol three times followed by drying in a vacuum oven at 100°C overnight. The SLMS triblock copolymer is referred to as SLMS3-21, with 3 vol% poly(methyl acrylate) in the midblock, and 21 vol% polystyrene in triblock copolymer.

2.1.6 Synthesis of Low Molecular Weight Poly(lauryl acrylate-co-acrylamide) and Polystyrene

Low molecular weight poly(lauryl acrylate-*co*-acrylamide) copolymers (PLAMX-L, *X* is the weight percent of polyacrylamide in the polymer) and polystyrene (PS-L) were synthesized for cloud point measurements. A typical procedure for PLAMX-L is as follows: In a round bottom flask, 2-(dodecylthiocarbonothioylthio)-2-methylpropionic acid (0.158 g, 0.43 mmol), lauryl acrylate (1 g, 4.16 mmol), acrylamide (0.04 g, 0.51 mmol), AIBN (3.6 mg, 0.021 mmol) and 1,4-dioxane (2 ml) were added. The flask was then sealed with a rubber septum, purged with argon for 30 min and immersed into an oil

bath at 70°C. After stirring for 16 hours, the reaction was quenched with water and the PLAM-L copolymer was precipitated into methanol three times followed by drying in a vacuum oven at 40°C overnight. PS-L was synthesized as follows: in a round bottom flask, 2-(dodecylthiocarbonothioylthio)-2-methylpropionic acid (0.158 g, 0.43 mmol), polystyrene (1.5 g, 14.4 mmol) and AIBN (3.6 mg, 0.021 mmol) were added. The flask was then sealed with a rubber septum, purged with argon for 30 min and immersed into an oil bath at 90°C. After stirring for 4 hours, the reaction was quenched with water and the PS-L copolymer was precipitated into methanol three times followed by drying in a vacuum oven at 100°C overnight.

2.1.7 Synthesis of Poly(lauryl methacrylate-co-methacrylic acid)(PLMA) Copolymers

The PLMA copolymers were synthesized by hydrolysis of poly(lauryl methacrylate-*co*-*tert* butyl methacrylate) (PLtB) copolymers with trifluoroacetic acid (Scheme 2.4). Fistly, PLtB copolymers were synthesized by reversible addition-fragmentation chain-transfer (RAFT) polymerization using chain transfer agent 4-cyano-4-[(dodecylsulfanylthiocarbonyl)sulfanyl]pentanoic acid. Lauryl methacrylate and *tert*-butyl methacrylate were passed through a basic aluminum oxide column to remove monomethyl ether hydroquinone inhibitor. As an example, a copolymer containing 10 mol% poly(*tert*-butyl methacrylate) was prepared as follows: in a round bottom flask, lauryl methacrylate (40 g, 0.16 mol), *tert*-butyl methacrylate (2.4 g, 0.017 mol), 4-cyano-4-[(dodecylsulfanylthiocarbonyl)sulfanyl]pentanoic acid (126 mg, 0.31 mmol), AIBN (10.4 mg, 0.06 mmol) and 1,4-dioxane (26 mL) were added. The flask was then sealed with a rubber septum, purged with argon for 30 min and immersed into an oil bath at 70°C. After stirring for 16 hours, the reaction was quenched by cooling with cold water

and the PLtB copolymers were precipitated into methanol three times followed by drying in a vacuum oven at 40 °C overnight. PLtB copolymers with different *tert*-butyl methacrylate content were synthesized by changing the feed ratio of lauryl methacrylate and *tert*-butyl methacrylate. PLtB copolymers are referred to as PLtB*X*, where *X* is the molar percent of poly(*tert*-butyl methacrylate) in the copolymer.

The PLtB copolymers were further hydrolyzed with trifluoroacetic acid to be PLMA copolymers. In a round bottom flask, PLtB copolymers (36g) were dissolved in 280 mL dichloromethane. Under vigorous stirring, 20 mL trifluoroacetic acid was added dropwise into the solution and the reaction was carried out at room temperature for 36 hours. The solution was then concentrated and precipitated into methanol followed by drying in a vacuum oven at 40°C overnight. PLMA copolymers are referred to as PLMA*X*, where *X* is the molar percent of poly(methacrylic acid) in the copolymer.

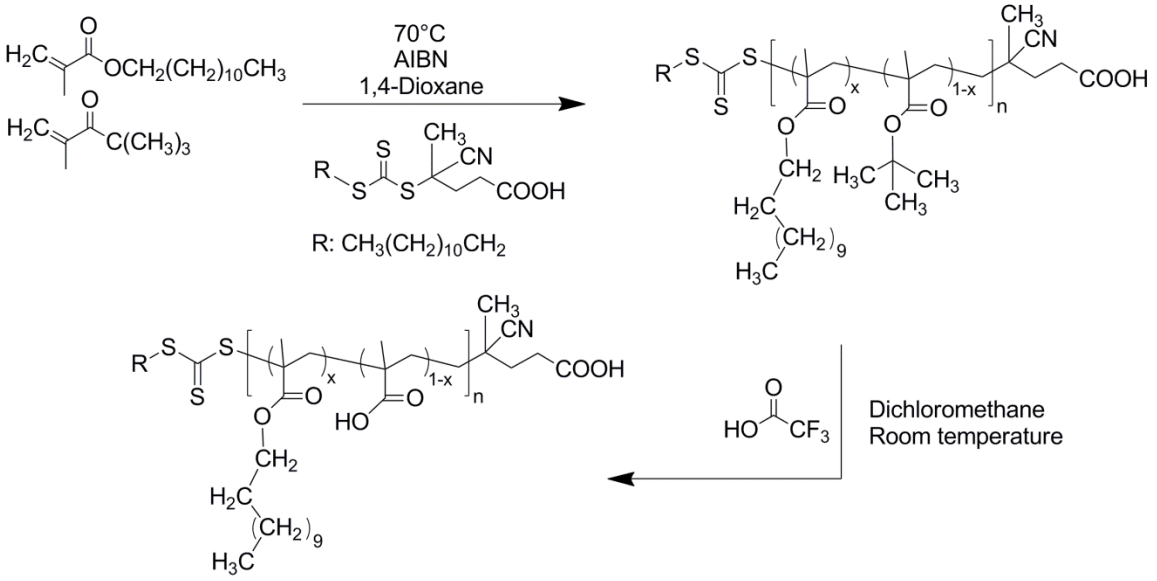

Scheme 2.4 Synthesis of PLMA copolymers

2.1.8 Synthesis of Poly(methyl methacrylate-b-(lauryl methacrylate-co-methacrylic acid)-b-methyl methacrylate)(MLAM) Triblock Copolymers

The MLAM triblock copolymers were synthesized by hydrolysis of poly(methyl methacrylate-*b*-(lauryl methacrylate-*co*-*tert* butyl methacrylate)-*b*-methyl methacrylate) (MLtM) triblock copolymers. The MLtM were synthesized through two-steps RAFT polymerization (Scheme 2.5). Firstly, the midblock poly(lauryl methacrylate-*co*-*tert*-butyl methacrylate) copolymers were synthesized using difunctional RAFT agent ethane-1,2-diyl bis(4-cyano-4-(((dodecylthio)carbonothioyl)thio)pentanoate). The difunctional RAFT agent was synthesized according to literature procedures. As an example, a copolymer containing 10 mol% poly(*tert*-butyl methacrylate) was prepared as follows: in a round bottom flask, lauryl methacrylate (40 g, 0.16 mol), *tert*-butyl methacrylate (2.4 g, 0.017 mol), difunctional RAFT agent (264 mg, 0.31 mmol), AIBN (10.4 mg, 0.06 mmol) and 1,4-dioxane (26 mL) were added. The flask was then sealed with a rubber septum, purged with argon for 30 min and immersed into an oil bath at 70°C. After stirring for 16 hours, the reaction was quenched by cooling with cold water and the difunctional PLtB copolymers were precipitated into methanol three times followed by drying in a vacuum oven at 40 °C overnight.

Then, the MLtM triblock copolymers were synthesized by chain extension of difunctional PLtB midblock with methyl methacrylate. Methyl methacrylate was passed through a basic alumina oxide column to remove monomethyl ether hydroquinone inhibitor. A typical procedure is as follows: in a round bottom flask, methyl methacrylate (16 g, 0.159 mol), difunctional PLtB copolymer (38 g, 0.37 mmol), AIBN (12 mg, 0.07 mmol) and 1,4-dioxane (120 mL) were added. The flask was then sealed with a rubber

septum, purged with argon for 30 min and immersed into an oil bath at 70°C. After stirring for 20 hours, the reaction was quenched by cooling with cold water and the copolymers were precipitated into methanol three times followed by drying in a vacuum oven at 100 °C overnight. MLtM copolymers are referred to as MLtM*X*, where *X* is the molar percent of poly(*tert*-butyl methacrylate) in the midblock.

The MLtM copolymers were further hydrolyzed with trifluoroacetic acid to be MLAM copolymers. In a round bottom flask, MLtM copolymers (42 g) were dissolved in 280 mL dichloromethane (BDH, ACS grade). Under vigorous stirring, 20 mL trifluoroacetic acid (98%) was added dropwise into the solution and the reaction was carried out at room temperature for 36 hours. The solution was then concentrated and precipitated in to methanol followed by drying in a vacuum oven at 100 °C overnight. MLAM copolymers are referred to as MLAM*X*, where *X* is the molar percent of poly(methacrylic acid) in the midblock.

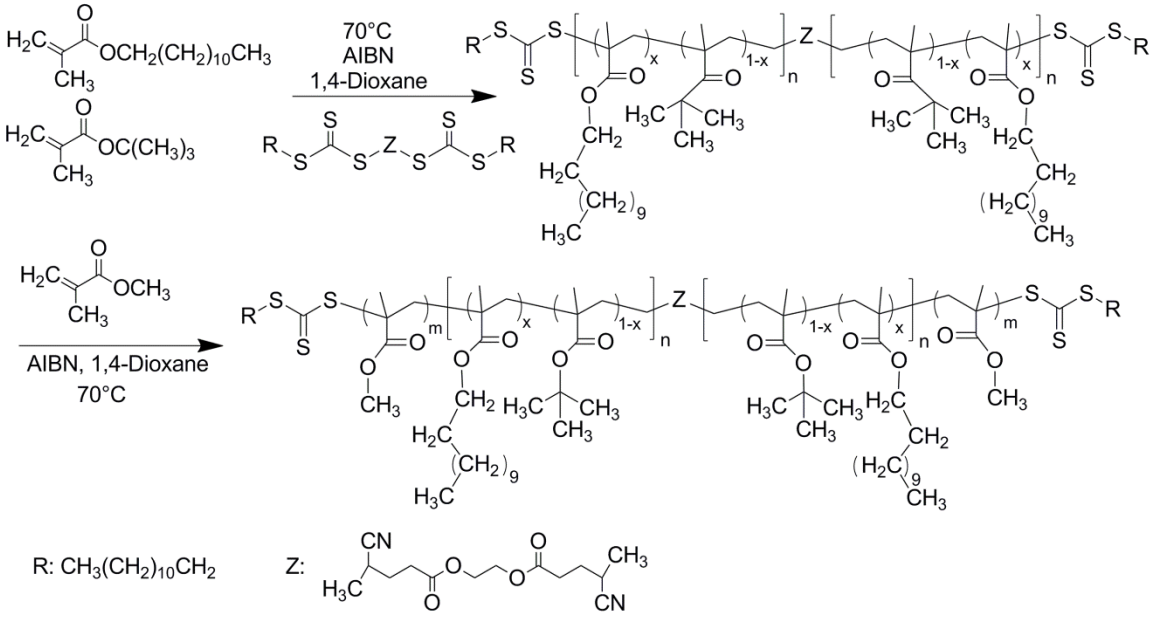

Scheme 2.5 Synthesis of MLtM triblock copolymers

2.1.9 Neutralization of PLAM copolymers and MLAM triblock copolymers

The PLAM copolymers and MLAM triblock copolymers were neutralized with NaOH with different degrees of neutralization. As an example, the PLAM10 copolymer with 50% degree of neutralization was prepared as follow: in a round bottom flask, PLAM10 copolymer (6 g) was dissolved in 20 ml THF. 1.3 mL of NaOH/methanol solution (39 mg/mL) were added to the flask under vigorous stirring. The neutralization was then carried out at room temperature for 24h. After that, the mixture was poured into a Teflon mold, left in fume hood for 24h and dried in vacuum oven at 40 °C overnight.

2.2 Polymer characterizations

2.2.1 Nuclear Magnetic Resonance (NMR)

^{1}H NMR experiments were performed on JEOL ECA-400 instrument using deuterated chloroform (99.96 atom % D) as the solvent. Chemical shifts were referenced to the solvent proton resonance 7.24 ppm.

^{13}C NMR experiments were performed on JEOL ECA-600 II instrument using deuterated chloroform ((99.96 atom % D) as the solvent. The relaxation delay was set to be 10s and nuclear overhauser effect (NOE) was turned off in order to get quantitative ^{13}C NMR spectra.

2.2.2 Gel Permeation Chromatography

Number-average molecular weight (M_n) and molecular weight distribution (the dispersity, Đ) were measured by a Viscotek gel permeation chromatography (GPC) instrument, with two Agilent ResiPore columns, using THF (OmniSolv, HPLC grade) as the mobile phase at 30 °C. The flow rate was 1 mL/min, and the injection volume was

100 μL. A triple detection system, including light scattering, a viscometer, and refractometer, was employed to characterize the absolute molecular weight.

2.2.3 Density measurement

The density of PDAEMA was measured using a density gradient column which was constructed in-house. The polymer was dissolved in DCM and cast on a microscope slide. The sample was air-dried for several hours and then dried under vacuum at 120 °C overnight to remove all solvent and air from within the sample. Two solutions were prepared: 1) an aqueous sodium chloride solution (24 wt% sodium chloride) and 2) a methanol/water solution (35% vol% methanol). A tall graduated glass column was placed in a water bath maintained at 23 °C. A density gradient of the two solutions was created within the column. The prepared column was stabilized in the water bath overnight prior to use. Calibration beads of known density were placed in the column to generate a density-height calibration curve. Finally, the degassed polymer thin film (around 0.5 mm) was placed in the column and the density was determined using density-height calibration curve, after equilibration for 1-2 days. Measurements on three separate specimens were taken to ensure reproducibility. The density of PDAEMA was determined to be 1.1224 ± 0.0003 g/mL.

The density of PLAM copolymers were measured using a density gradient column which was constructed in-house. The polymer was put on a microscope slide, and then heated in a vacuum oven at 40 °C to remove any air bubbles. Two solutions were prepared: 1) methanol/ethylene glycol (40/60 by volume) and 2) methanol/water (90/10 by volume). A tall graduated glass column was placed in a water bath maintained at 23 °C. A density gradient of the two solutions was created within the column. The

prepared column was stabilized in the water bath overnight prior to use. Calibration beads of known density were placed in the column to generate a density-height calibration curve. Finally, the polymer was frozen by liquid nitrogen, sliced into small pieces while still below its glass transition temperature, and placed in the column. The density was determined using density-height calibration curve, after equilibration for 1-2 days. Measurements on three separate specimens were taken to ensure reproducibility. The density of PLAM0, PLAM4 and PLAM8 were measured to be 0.9384 ± 0.0004, 0.9477 ± 0.0008, and 0.9595 ± 0.0004 g/mL, respectively.

2.2.4 Thermal characterization

The glass transition temperature (T_g) was characterized with a TA Instruments Q2000 differential scanning calorimeter (DSC), calibrated with an indium standard, using a nitrogen flow rate of 50 mL/min. The sample was placed in the calorimeter (using a Tzero aluminum pan) and successive heating-cooling-heating ramps were carried out at a rate of 10 °C/min from -70 °C to 200 °C. The T_g was determined from the second heating ramp.

The thermal degradation properties were probed by thermogravimetric analysis (TGA), using a TA Instruments Q500 analyzer. The sample was heated from 25 °C to 600 °C at a rate of 10 °C/min in a nitrogen environment (the balance nitrogen purge flow was 40 mL/min and the sample purge flow was 60 mL/min).

2.2.5 Fourier-Transform Infrared Spectroscopy

Fourier-transform infrared spectroscopy (FTIR) spectra of PLAM copolymers at various temperatures were obtained using a Thermo Scientific Nicolet 4700 spectrometer, with a heating cell. Thin films of polymers were prepared by solvent casting from 1%

(w/v) solution in dichloromethane (J.T. Baker, OmniSolv, HPLC grade) onto potassium bromide (KBr) windows (32 mm diameter, 3 mm thickness). The sample was air-dried for an hour and then transferred to vacuum oven to remove residual solvent. After drying, the sample was mounted to a heating cell and the spectra were recorded with 64 scans at a resolution of 4 cm^{-1} in transmission mode from 23 to 170 °C.

2.2.6 Rheological Properties

The viscoelastic behavior of PLAM, PLtB and PLMA copolymers was evaluated using a TA instruments DHR-2 rheometer with 25 mm diameter parallel plates, and a sample thickness of 1 mm. The linear viscoelastic region was first determined through measurement of the storage (G') and loss (G'') moduli in a sweep from 1% to 10% strain at a frequency (ω) of 10 rad/s. The moduli were then measured at a strain within the linear region, over a range of frequencies (ω = 0.1 – 100 rad/s), measured every 10 °C. time temperature superposition at a reference temperature of 30 °C was performed using TA Instruments TRIOS software to generate master curves.

The order disorder transition temperatures of DnBD, MnBM, SLAS triblock copolymers was evaluated using a TA instruments DHR-2 rheometer with 25 mm diameter parallel plates, and a sample thickness of 1 mm. The linear viscoelastic region was first determined through measurement of the storage (G') and loss (G'') moduli in a sweep from 1% to 10% strain at a frequency (ω) of 10 rad/s. The ω dependencies of G', and G'' were characterized at various temperatures at a chosen value of strain within the linear region. Then G' and tan δ (G''/G') were plotted as a function of temperature at ω = 1 rad/s.

2.2.7 Cloud Point Measurements

The cloud point measurements were conducted to characterize the Flory-Huggins interaction parameter of PS/PLAMX-L binary blends following previously reported procedures.[112] Sample films of PS-L/PLAMX-L blends were cast on microscope slides from a solution in dichloromethane (10 wt%) followed by drying in a vacuum oven at 150 °C for 4 h. The films were covered by a microscope cover glass and sealed using 3M Scotch-Weld Epoxy Adhesive to avoid the thermal degradation of the polymers at elevated temperatures. The cloud point temperatures were determined through observing the optical character of the sample in a microscope (Olympus BX51TRF) equipped with a heating cell (Instec HCS302-01). The sample was first heated to a temperature at which the blend was homogeneous, and then the sample was cooled down slowly by 2 °C increments and stabilized at each temperature for 10 min before observation of the sample with the microscope. The temperature at which the sample started showing inhomogeneity was identified as the cloud point temperature.

2.2.8 Small Angle X-ray Scattering

The morphology of was probed using a Rigaku S-MAX 3000 small-angle X-ray scattering (SAXS) instrument, equipped with CMF optic incident beam ($\lambda = 0.154$ nm), 3 pinhole collimations, a 2-dimensional multiwire area detector with 1024 × 1024 pixels. The sample to detector distance was 3 m. The two-dimensional scattering patterns were azimuthally integrated to a one-dimensional profile of intensity versus scattering vector, $q = 4\pi \sin(\theta/2)/\lambda$ [θ is the scattering angle; λ is the wavelength]. For SLAS triblock copolymer, SAXS data fitting was performed with SasView using combined functions of SphereModel and HardsphereStructure. The effect of size distribution of hard spheres

was also incorporated into curve fitting by enabling the polydispersity function in SasView. The size distribution was characterized using $\mathrm{PD} = \sigma / R_{\mathrm{sp}}$, where σ is the standard deviation and R_{sp} is the hard sphere radius.

2.2.8 Mechanical testing

Tensile testing was conducted using an Instron 5966 universal testing system with a 100 N load cell at a grip speed of 10 mm/min. Dog bone-shaped testing bars (following ASTM D638, bar type 5, thickness 1.5 mm) were prepared by compression molding on a Carver Hotpress at an applied load of 4200 lbs at 180 °C. Pneumatic grips (maximum 2 kN) were used to affix the sample in the testing frame, at a compressed air pressure of 35 psi. The measurements were repeated with 5 test specimens.

Chapter 3 Improving Mechanical Properties of Fatty Acid-Derived Triblock Copolymers by Incorporation of Hydrogen Bonds

In this chapter, we explore the presence of hydrogen bonding in the long-chain polyacrylate midblock of a thermoplastic elastomeric triblock copolymer as a method of improving its mechanical behavior. Poly(styrene-*b*-(lauryl acrylate)-*b*-styrene) triblock copolymers, previously reported by our group to exhibit low tensile strength and elongation at break due to the lack of entanglements in the poly(lauryl acrylate midblock,[111] were modified through the addition of acrylamide to the midblock, which undergoes hydrogen bonding. Poly(styrene-*b*-(lauryl acrylate-*co*-acrylamide)-*b*-styrene) **(**SLAS) triblock copolymers, containing a poly(lauryl acrylate-*co*-acrylamide) random copolymer as the midblock and polystyrene endblocks, were synthesized. The extent of hydrogen bonding was quantified with Fourier-transform infrared spectroscopy. The morphological, thermal and mechanical properties of SLAS triblock copolymers were explored. The impact of the formation of a transient network on the polymer physical properties was evaluated.

3.1 Synthesis of poly(styrene-b-(lauryl acrylate-co-acrylamide)-b-styrene) triblock copolymers

Poly(styrene-*b*-(lauryl acrylate-*co*-acrylamide)-*b*-styrene) **(**SLAS) triblock copolymers were synthesized following a previously reported procedure with modification.[111] First, the PLAM random copolymers were synthesized using a bifunctional chain transfer agent, BTBTMB. Next, the PLAM random copolymers were chain extended with polystyrene to form SLAS triblock copolymers. Three series of SLAS triblock copolymers were synthesized (Table 3.1), each containing a different

midblock acrylamide (AM) content (0, 4 and 8 wt% AM). Within each series, the vol% polystyrene (PS) in the triblock copolymer was varied (from 14-33 vol%). All SLAS triblock copolymers contained midblocks of similar molecular weight (around 80-85 kg/mol).

Table 3.1 Molecular characteristics of SLAS triblock copolymers

Polymer Name	Midblock[a]	M_n (PS-PLAM-PS) (kg/mol)[b]	Đ[c]	vol% PS[d]	N of midblock[e]	N of each endblock[f]
SLAS0-17	PLAM0	7.9-81.8-7.9	1.61	17	1450	120
SLAS0-24	PLAM0	12.8-81.8-12.8	1.57	24	1450	210
SLAS0-31	PLAM0	20.3-81.8-20.3	1.65	31	1450	320
SLAS4-16	PLAM4	9.3-84.5-9.3	1.69	16	1480	150
SLAS4-23	PLAM4	14.1-84.5-14.1	1.67	23	1480	220
SLAS4-33	PLAM4	22.3-84.5-22.3	1.58	33	1480	350
SLAS8-14	PLAM8	6.8-79.6-6.8	1.59	14	1380	110
SLAS8-23	PLAM8	10.8-79.6-10.8	1.71	23	1380	170
SLAS8-30	PLAM8	18.7-79.6-18.7	1.61	30	1380	300
SLMS3-21	PLM3	11.4-77.4-11.4	1.75	21	1340	160

[a] Midblock characteristics: PLAM0: M_n = 81.8 kg/mol, Đ = 1.31, wt% AM = 0%, dn/dc = 0.067 mL/g; PLAM4: M_n = 84.5 kg/mol, Đ = 1.32, wt% AM = 4%, dn/dc = 0.067 mL/g; PLAM8: M_n = 79.6 kg/mol, Đ = 1.28, wt% AM = 8%, dn/dc = 0.068 mL/g. PLM3: M_n = 77.4 kg/mol, Đ = 1.35, wt% methyl acrylate = 3%, dn/dc = 0.068 mL/g.

[b] Midblock number-average molecular weight M_n characterized with GPC with light scattering, endblock M_n characterized using overall M_n (GPC) and block copolymer composition (NMR).

[c] Triblock copolymer dispersity Đ characterized with GPC with light scattering

[d] Triblock copolymer composition characterized by NMR along with the density of PLAM (characterized by density gradient column) and PS (1.04 g/mL[113]), calculated using Equation 3.2

[e] Number of repeat units, N, of the midblock, based on v_{ref} = 100 Å^3

[f] Number of repeat units, N, of each PS endblock, based on v_{ref} = 100 Å^3

The compositions of PLAM copolymers were examined with ^{1}H NMR (Figure 3.1). Peaks corresponding to the backbone (-CH- at 2.25 ppm, -CH_2- at 1.87 and 1.59 ppm) and side chains (-OCH_2- at 4.00 ppm, -CH_2-CH_2- at 1.59 and 1.26 ppm, and -CH_3 at 0.87 ppm) indicate the incorporation of lauryl acrylate (LA) in the midblock. Peaks corresponding to the backbone (-CH- at 2.25 ppm, -CH_2- at 1.87 and 1.59 ppm) and side chains (-NH_2 at 6.04 and 5.31 ppm) confirm the successful incorporation of AM. The wt% AM in the midblock was calculated from the areas of peaks d (4.00 ppm) and j (6.04 and 5.31 ppm) by Equation 3.1 (peak labels provided in Scheme 2.3):

$$wt\ \%AM = \frac{A_j \times 71.08}{A_d \times 240.38 + A_j \times 71.08} \times 100, \qquad \text{Equation 3.1}$$

in which A_j and A_g are the integration of peaks corresponding to -NH_2- in acrylamide and -CH_3- in lauryl acrylate. GPC analysis characterized the midblock M_n and Đ (Table 1). We note that although the LA monomer was only 90% pure as received, the impurities present did not interfere with the polymerization and were removed following precipitation of the polymer.

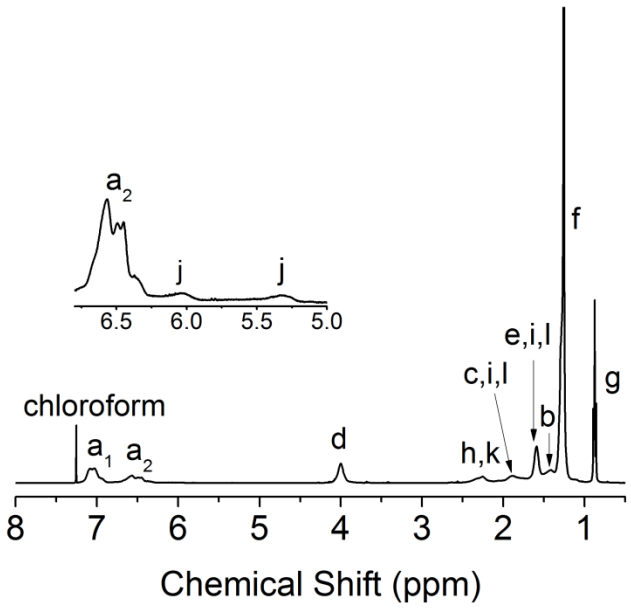

Figure 3.1 ^{1}H NMR data obtained from SLAS8-23. Chemical structure and peak labeling are shown in Scheme 2.3 .

Aliquots were obtained during the copolymerization of LA and AM to examine M_n and Đ as a function of LA conversion (data obtained on PLAM8 shown in Figure 3.2). M_n increased linearly with LA conversion and Đ was around 1.2-1.3, confirming the reaction was well controlled (Figure 3.2a). Dashed line indicates theoretical M_n. The wt% AM was constant throughout the reaction and consistent with the feed composition (dashed line, Figure 3.2b), indicating comparable reactivities of LA and AM and lack of composition drift, similar to the previously reported case for copolymerization of butyl acrylate and AM, which form a random copolymer.[91] Furthermore, differential scanning calorimetry analysis revealed that the presence of AM did not impact the melting temperature of PLAM.

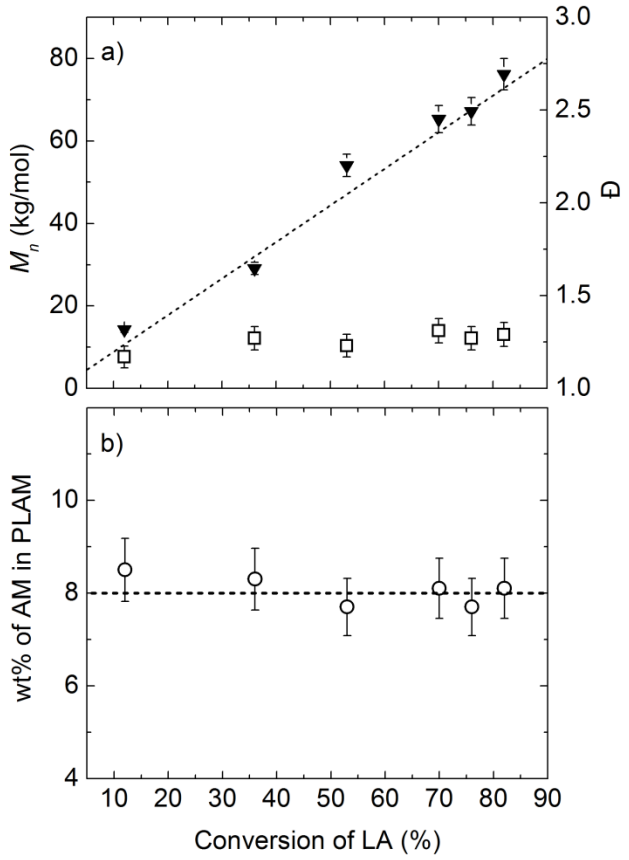

Figure 3.2 a) M_n (▼) and Đ (□) vs. conversion for polymerization of PLAM8. b) Wt% of AM in the PLAM8 copolymer as a function of conversion of LA.

Following chain extension of PLAM copolymers with PS, ^{1}H NMR confirmed incorporation of PS endblocks in SLAS triblock copolymers, with peaks at 7.04 and 6.58 ppm corresponding to the aromatic =CH (Figure 3.1). The vol% PS in the triblock copolymers was calculated from the areas of peaks a (7.04 and 6.58 ppm), d (4.00 ppm) and j (6.04 and 5.31 ppm) using Equation 3.2 (peak labels in Scheme 2.3):

$$vol\%\ PS = \frac{2}{5} \times \frac{\rho_{PLAM}}{\rho_{PS}} \times \frac{A_a \times 104.15}{A_d \times 240.38 + A_j \times 71.04}, \qquad \text{Equation 3.2}$$

in which ρ_{PLAM} is the density of PLAM copolymer (measured by density gradient column, reported in main text) , ρ_{PS} is the density of polystyrene, 1.04 g/ml, A_a, A_d and A_j are the integration of peaks a, d and j. The endblock M_n was determined through knowledge of the midblock M_n and vol% PS in the triblock copolymer using Equation 3.3:

$$M_{n,PS} = \frac{2}{5} \times M_{n,PLAM} \times \frac{A_a \times 104.15}{A_d \times 240.38 + A_j \times 71.04}, \qquad \text{Equation 3.3}$$

in which A_a is the integration of peak corresponding to aromatic ring in styrene, $M_{n,PLAM}$ is the molecular weight of PLAM midblock determined by GPC. All SLAS triblock copolymer characteristics are summarized in Table 3.1. In all cases, GPC data for SLAS triblock copolymers show trimodal distributions, and dispersity values higher than 1.5 (Table 3.1, Figure 3.3 and Figure 3.4a). The presence of a weak low molecular weight shoulder that overlaps with the peak associated with the PLAM midblock might indicates the presence of a small fraction of unreacted midblock. In order to probe this further, fractional precipitation was carried with a selective solvent (acetone/THF, 6/1, v/v), which is a good solvent for the PLAM midblock and a poor solvent for the PS endblocks. The fractionation procedure isolated the main triblock copolymer peak (Figure 3.4b). The isolated triblock copolymer did not exhibit a significant low molecular weight shoulder. Thus, we conclude the fraction of unreacted PLAM is very small. The more pronounced high molecular weight shoulder is most likely due to chain coupling.[14, 114, 115] Bimolecular termination is a commonly reported issue in RAFT polymerization of styrene due to its low propagation rate (k_p).[115-117] To confirm the presence of chain coupling, a kinetic study was performed upon chain extension of PLAM4 with styrene. A pseudo-first order kinetic plot is shown in Figure 3.4a. The deviation from linearity of $\ln([M]_0/[M])$ vs time was observed after 50% conversion, indicating a reduced radical concentration over time

due to bimolecular radical-radical termination.[118] Figure 3.4b shows the evolution of the GPC traces during the chain extension of PLAM4 with styrene. The higher molecular weight shoulder became more and more pronounced during the course of reaction, indicating a significant extent of bimolecular termination, consistent with the deviation from linearity of $\ln([M]_0/[M])$ vs time.

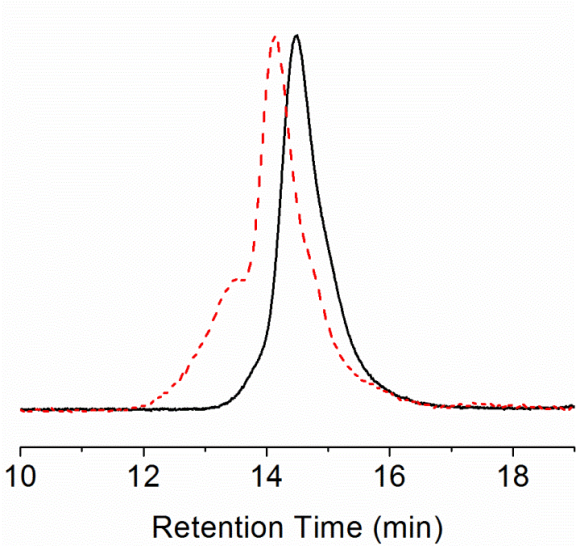

Figure 3.3 GPC data obtained from PLAM4 (black solid curve) and SLAS4-16 (red dashed curve).

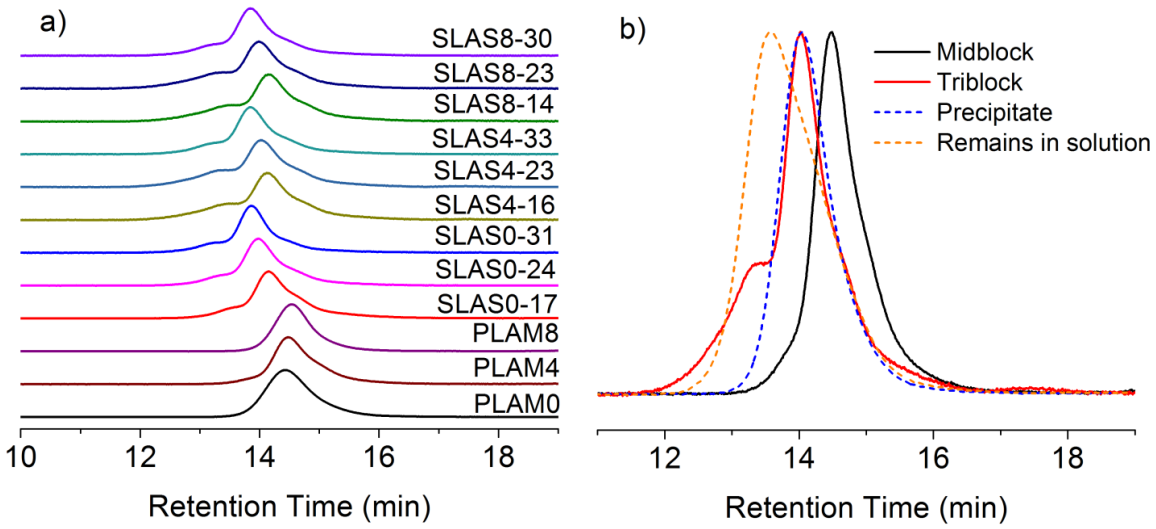

Figure 3.4 a) GPC data obtained from PLAM copolymers and SLAS triblock copolymers. b) GPC results from fractionation of triblock copolymer SLAS4-16 with acetone/THF mixture (6/1, v/v).

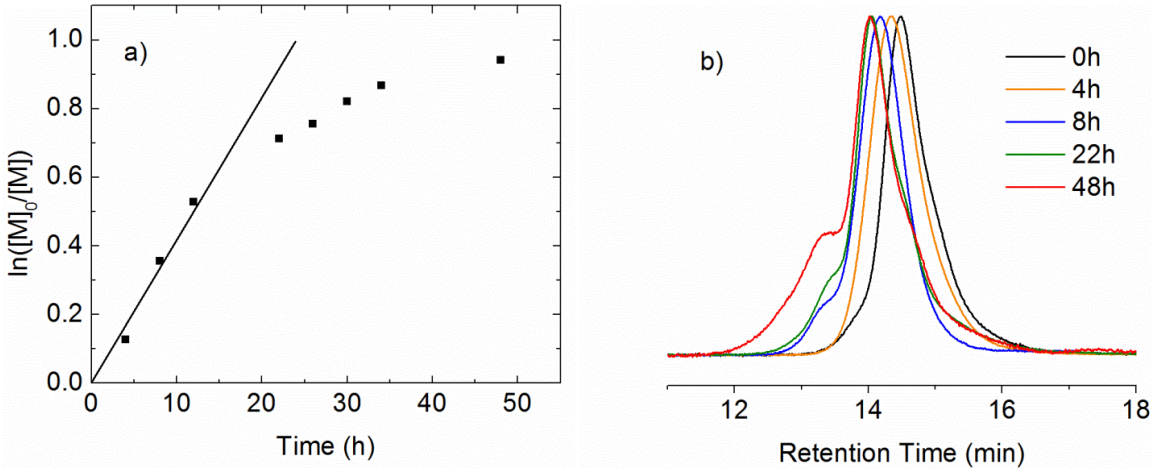

Figure 3.5 a) Pseudo-first order kinetic plots of chain extension of PLAM4 with styrene and b) GPC traces showing the evolution of the molecular weight distribution with reaction time.

The thermal properties of SLAS triblock copolymers were characterized with differential scanning calorimetry. The glass transition temperature (T_g) of the PS midblock and melting temperature (T_m) of the PLAM midblock are presented in Table 3.2 and Figure 3.6 (the resolution of the DSC experiment was not sufficient to observe the T_g of the PLAM midblock). The incorporation of acrylamide did not impact the T_g

and T_m of the blocks of the SLAS triblock copolymers. Furthermore, we anticipate little impact of the higher dispersity of the block copolymer on the thermal properties. Prior studies have shown that the glass transition temperature is not affected by higher dispersity.[119] The T_g values of the PS endblocks are consistent with that of homopolymer PS (after accounting for depression in T_g at low molecular weight[120]), and the T_m values of the PLAM midblocks are consistent with our prior characterization of poly(lauryl acrylate) homopolymer.[7]

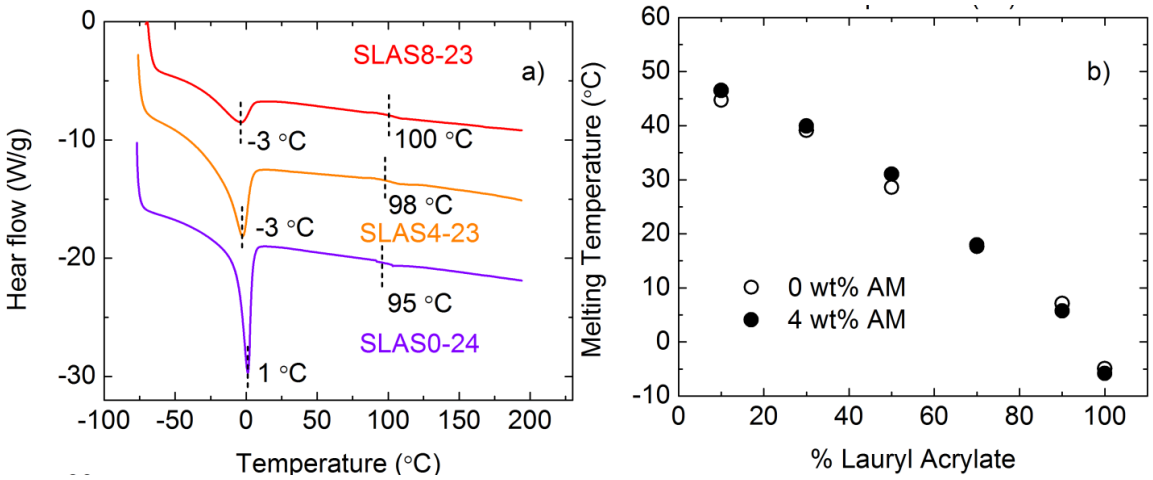

Figure 3.6 a) Representative DSC curves from SLAS triblock copolymers and b) melting temperature as a function of weight percentage of lauryl acrylate in the copolymer of poly(lauryl acrylate-*co*-stearyl acrylate-*co*-acrylamide).

Table 3.2 T_g and T_m of SLAS triblock copolymer

Polymer Name	T_g of PS (°C)	T_m of PLAM (°C)
SLAS0-17	87	-1
SLAS0-24	95	1
SLAS0-31	93	-2
SLAS4-16	89	-2
SLAS4-23	98	-3
SLAS4-33	97	-2
SLAS8-14	86	-4
SLAS8-23	100	-3
SLAS8-30	97	2

3.2 Quantification of extent of hydrogen bonding

FTIR spectroscopy was used to assess the state of hydrogen bonding (quantifying presence of bonded and free hydrogen bonding groups) in both PLAM copolymers (i.e., the midblocks of the SLAS triblock copolymers) and SLAS triblock copolymers. FTIR spectra were obtained as a function of temperature on PLAM copolymers of varying AM content (Figure 3.7a) and peak deconvolution was used to identify peaks associated with various chemical groups (Figure 3.7b). Peaks associated with carbonyl groups were observed at 1735, 1716, 1693, and 1671 cm^{-1}, corresponding to free carbonyl groups on LA repeat units, hydrogen bonded carbonyl groups on LA repeat units, free carbonyl groups on AM repeat units, and hydrogen bonded carbonyl groups on AM repeat units, respectively. Furthermore, a peak at 1615 cm^{-1} was identified as the amide II band (major contribution from N-H in plane bending).

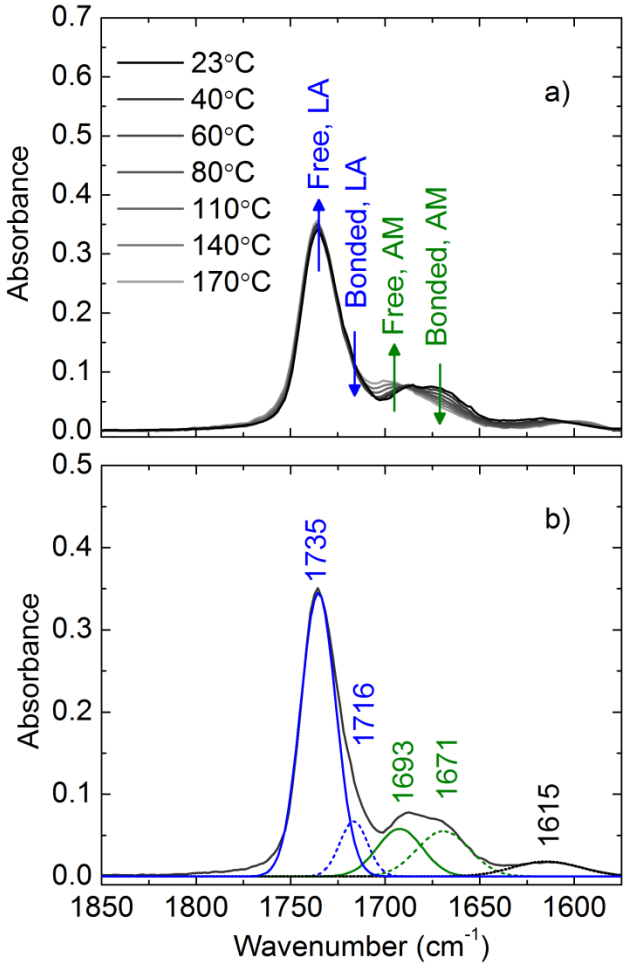

Figure 3.7 a) Temperature-dependent FTIR spectra obtained from PLAM4. b) Deconvolution of FTIR spectrum of PLAM4 at 40 °C.

Spectra were obtained at various temperatures (Figure 4 in the main text) in order to measure the molar absorptivity ratio between bonded and free carbonyl bands, calculated using Equation 3.4 (ref. [121]) (relevant peak areas are reported in Table 3.3):

$$k_{\mathrm{m}} = \frac{a_{\mathrm{HB,m}}}{a_{\mathrm{F,m}}} = \frac{A_{\mathrm{HB,m}}^{T_2} - A_{\mathrm{HB,m}}^{T_1}}{A_{\mathrm{F,m}}^{T_1} - A_{\mathrm{F,m}}^{T_2}}, \qquad \text{Equation 3.4}$$

where k_{m} is molar absorptivity ratio of species m (m is either LA or AM), $a_{\mathrm{HB,m}}$ and $a_{\mathrm{F,m}}$ are the molar absorptivities of hydrogen bonded and free carbonyl groups of species m, $A_{\mathrm{HB,m}}^{T_1}$ and $A_{\mathrm{F,m}}^{T_2}$ are the peak areas of the hydrogen bonded carbonyl groups of species

m at temperatures T_1 and T_2, and $A_{\mathrm{F,m}}^{T_1}$ and $A_{\mathrm{F,m}}^{T_2}$ are the peak areas of the free carbonyl groups of species m at temperatures T_1 and T_2. A plot of $A_{\mathrm{F,m}}$ vs. $A_{\mathrm{HB,m}}$ was constructed from data obtained at various temperatures, and k_{m} was quantified (i.e., the slope of this plot was taken as $-k_{\mathrm{m}}$, Figure 3.8). Thus, k_{LA} and k_{AM} were determined to be 1.57 and 1.34, respectively.

Table 3.3 Peak area differences at $a_{\mathrm{HB,AM}}$, $a_{\mathrm{F,AM}}$, $a_{\mathrm{HB,LA}}$and $a_{\mathrm{F,LA}}$ various temperatures for PLAM4 (a are defined in Equation 3.4)

Temperature (°C)	$a_{\mathrm{F,LA}}$	$a_{\mathrm{HB,LA}}$	$a_{\mathrm{F,AM}}$	$a_{\mathrm{HB,AM}}$
40	8.05	1.30	1.45	2.09
50	8.12	1.16	1.57	1.92
60	8.15	1.07	1.61	1.86
70	8.15	0.92	1.70	1.77
80	8.19	0.88	1.80	1.59
90	8.24	0.80	1.84	1.57
100	8.28	0.72	1.93	1.41
110	8.41	0.59	1.97	1.29
120	8.47	0.50	2.03	1.22
130	8.53	0.44	2.16	1.13
140	8.65	0.31	2.26	1.07

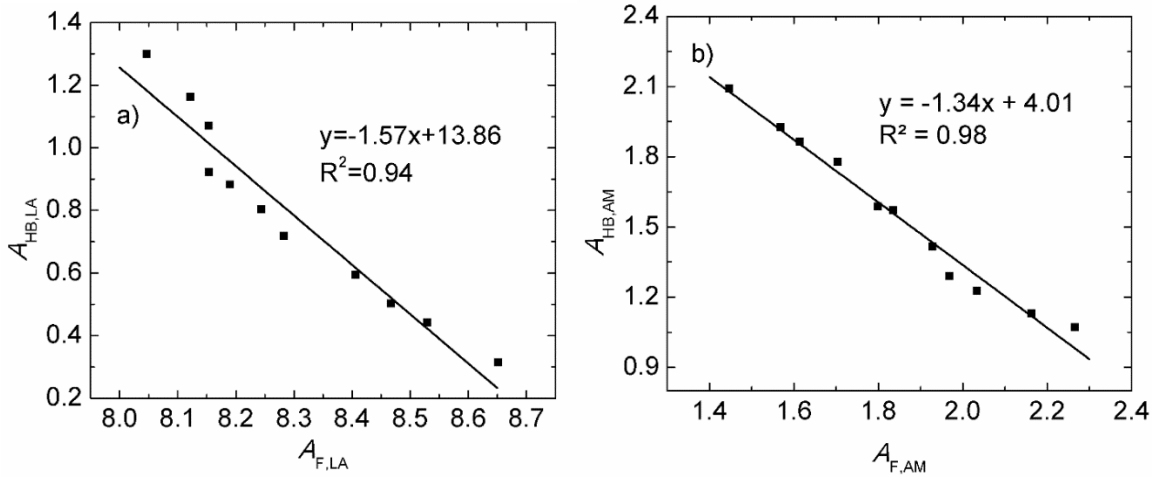

Figure 3.8 Area of hydrogen bonded carbonyl band vs. area of free carbonyl band for a) LA and b) AM at various temperatures. The slopes provided the molar absorptivity ratios for LA and AM (the slope is $-k_m$).

The peak area $A_{\mathrm{HB,m}}$ was adjusted by k_{m} (Equation 3.5), and the fraction of hydrogen bonded carbonyl groups of species *m*, total number of active hydrogen bonded groups per chain, and dynamic crosslinking density were determined using Equation 3.6 - Equation 3.9

$$A'_{\mathrm{HB,m}}(T) = \frac{A_{\mathrm{HB,m}}(T)}{k_{\mathrm{m}}}, \qquad \text{Equation 3.5}$$

$$A'_{\mathrm{total,m}}(T) = A'_{\mathrm{HB,m}}(T) + A_{\mathrm{F,m}}(T), \qquad \text{Equation 3.6}$$

$$f_{\mathrm{HB,m}}(T) = \frac{A'_{\mathrm{HB,m}}(T)}{A'_{\mathrm{Total,m}}(T)}, \qquad \text{Equation 3.7}$$

$$N_{\mathrm{HB}}(T) = N_{\mathrm{AM}} f_{\mathrm{HB,AM}}(T) + N_{\mathrm{LA}} f_{\mathrm{HB,LA}}(T) \text{ and} \qquad \text{Equation 3.8}$$

$$\nu(T) = \frac{\rho_{PLAM}(T)[N_{\mathrm{HB}}(T) + 1]}{M_{n,PLAM}}, \qquad \text{Equation 3.9}$$

where $A'_{\mathrm{HB,m}}(T)$ is the adjusted area of hydrogen bonded carbonyl band for species *m*, $A'_{\mathrm{total,m}}(T)$ is the adjusted total area of carbonyl band for species *m*, $f_{\mathrm{HB,m}}(T)$ is the fraction of hydrogen bonded carbonyl group for species *m*, $N_{\mathrm{HB}}(T)$ is the total number of active hydrogen bonds per chain, N_{AM} and N_{LA} are the number of AM and LA repeat units per chain, ν(T) is the crosslink density and $\rho_{PLAM}(T)$ is the density of PLAM copolymer. The temperature-dependent density of PLAM copolymers were estimated using thermal expansion coefficient of poly(lauryl methacrylate)[122], $\rho(\mathrm{T}) = \rho(25℃)/[1 + 6.8 \times 10^{-4}(T - 25)]$. The temperature-dependent densities were found to have a small effect on of value of crosslink density. The areas of carbonyl bands ($A'_{\mathrm{HB,m}}$, $A_{\mathrm{F,m}}$ and $A'_{\mathrm{total,m}}$), $f_{\mathrm{HB,m}}$, N_{HB} and ν are plotted as a function of *T* in Figure 3.9 and Figure 3.10.

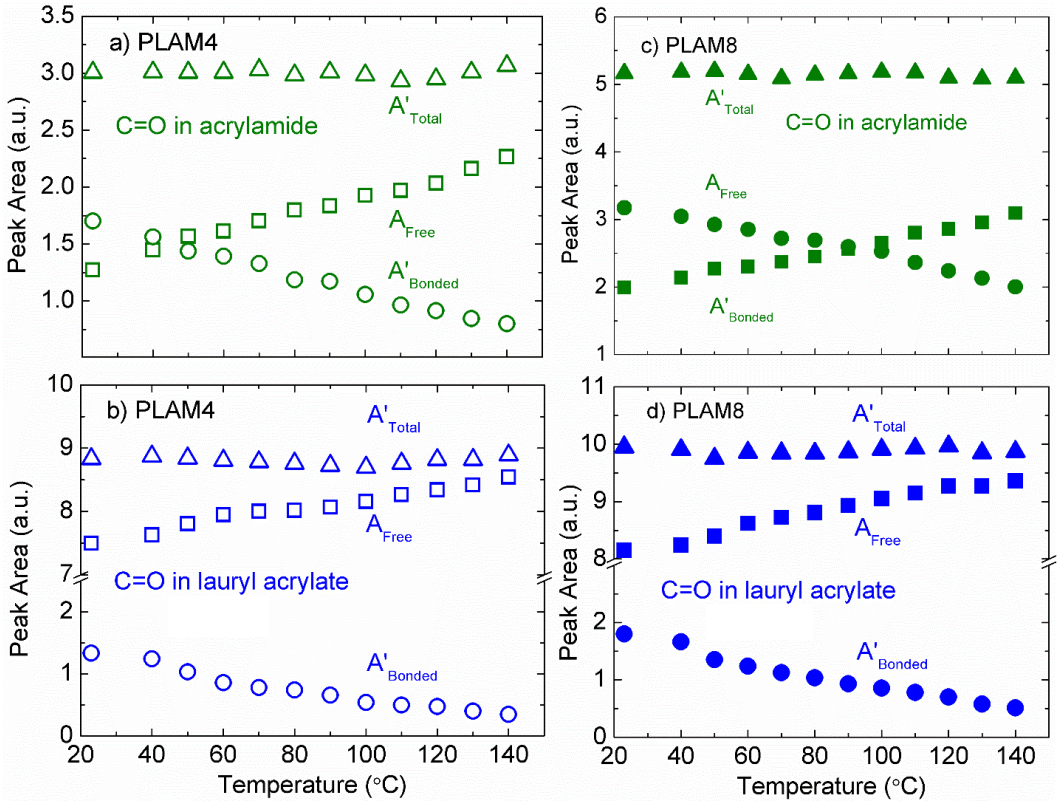

Figure 3.9 Areas of FTIR peaks associated with carbonyl bonds in a) AM and b) LA obtained from PLAM4. Areas of FTIR peaks associated with carbonyl bonds in c) AM and d) LA obtained from PLAM8.

For both AM and LA repeat units, the adjusted total area of the carbonyl band ($A'_{\mathrm{total,m}}$) was constant over the full temperature range (Figure 3.9). An increase in the area of the peaks associated with free carbonyl groups ($A_{\mathrm{F,m}}$) with increasing temperature was accompanied by a decrease in the area associated with hydrogen bonded groups ($A'_{\mathrm{HB,m}}$) (Figure 3.9). The quantified fraction of hydrogen bonded repeat units ($f_{\mathrm{HB,m}}$), shown in Figure 3.10a, thus decreased with increasing temperature for both LA and AM repeat units, indicating conversion of carbonyl groups from hydrogen bonded to free as temperature increased. AM repeat units showed a significantly higher fraction of hydrogen bonded groups as compared to LA repeat units at all temperatures (Figure

3.10a). The total number of active hydrogen bonded groups (N_{HB}) and crosslinked density (ν) also decreased with increasing temperature (Figure 3.10 b and c).

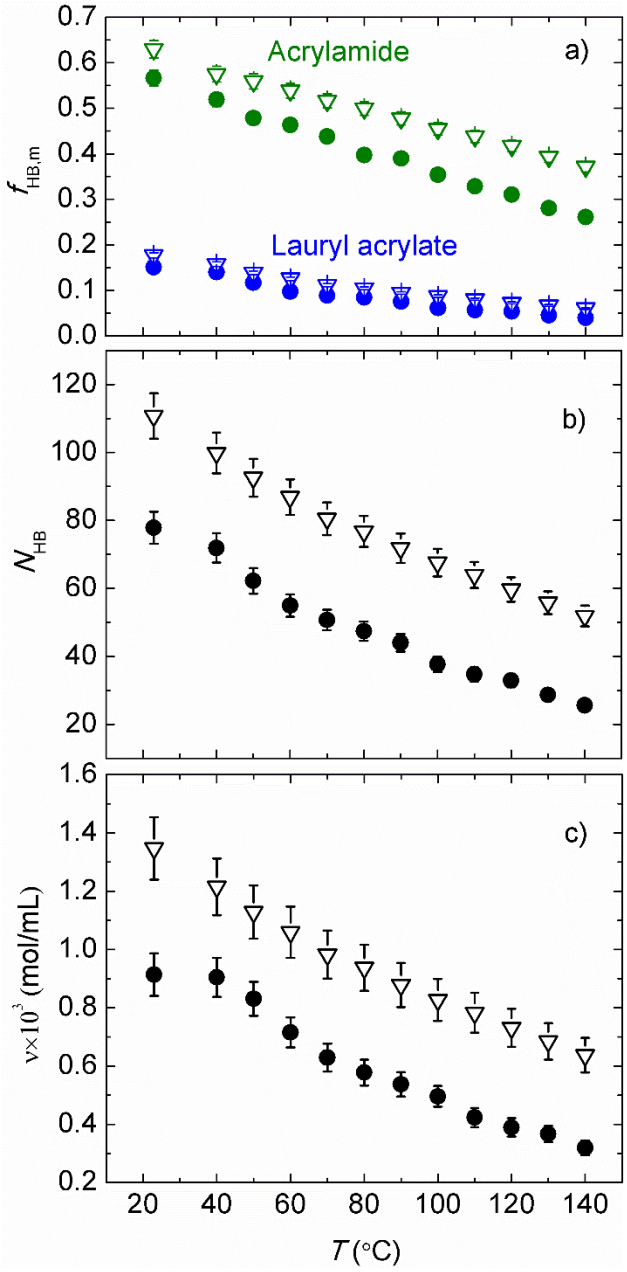

Figure 3.10 a) Fraction of hydrogen bonded carbonyl groups of LA (blue symbols) and AM (green sumbols) repeat units, b) total number of active hydrogen bonds per chain, and c) dynamic crosslink density as function of temperature for PLAM4 (●) and PLAM8 (▽).

The effect of the AM content in PLAM on the fraction of hydrogen bonded carbonyl groups was also examined (Figure 3.11). An increase in AM content resulted in a larger fraction of hydrogen bonded carbonyl groups (Figure 3.10a), larger total number of hydrogen bonds per chain (Figure 3.10b), and larger crosslink density (Figure 3.10c).

FTIR data were also obtained for the triblock copolymer SLAS8-14 to evaluate the effect of the triblock copolymer architecture on the fraction of hydrogen bonds. Spectra obtained from PLAM8 and the triblock copolymer SLAS8-14 were directly compared (Figure 3.11b), as SLAS8-14 contains the midblock PLAM8. The spectra overlap well with each other, indicating chain extension to triblock copolymer did not have great impact on the dynamic crosslink density. Thus, the temperature dependency of dynamic crosslink density of SLAS triblock copolymers is anticipated to be same as that of PLAM copolymers. At low temperatures, the high crosslink density indicates the formation of a transient network. At elevated temperatures, the decrease in crosslink density is anticipated to be beneficial for melt processing.

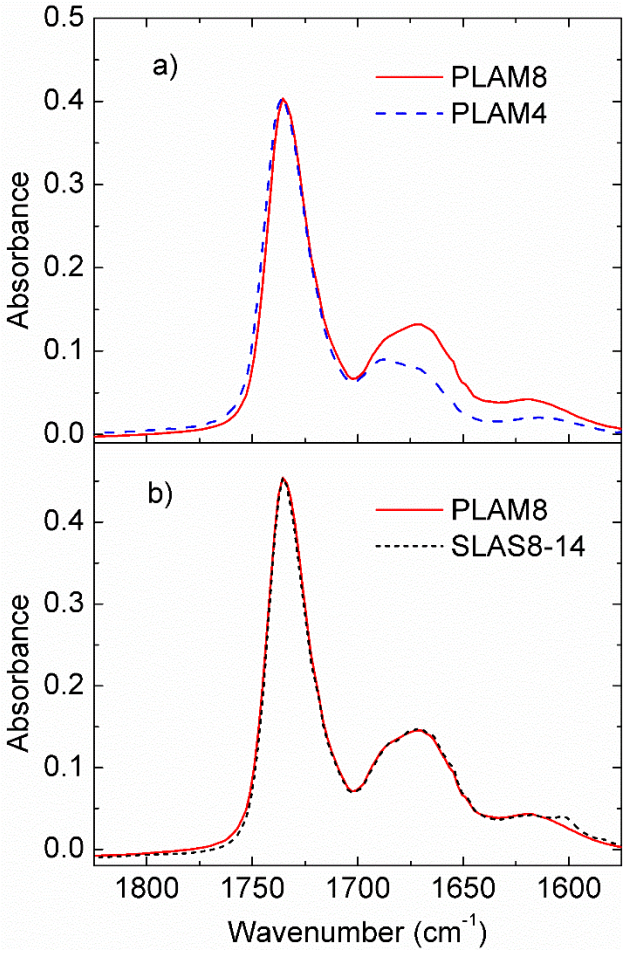

Figure 3.11 Comparison of FTIR spectra obtained from a) PLAM4 and PLAM8 (containing different AM content) and b) PLAM8 and SLAS8-14 (SLAS8-14 contains PLAM8 as the midblock). The absorbance of the peaks are normalized to the absorbance of carbonyl group of LA repeat unite at 1735 cm^{-1}.

3.3 Impact of hydrogen bonding on the viscoelastic behavior of PLAM copolymers

The presence of hydrogen bonding in the PLAM copolymers (i.e., the midblocks of the SLAS triblock copolymers) is anticipated to impact their rheological properties. The frequency (ω)-dependent dynamic moduli (G', G'') were characterized at various temperatures, and time-temperature superposition was employed to extend the range of accessible frequencies (Figure 3.12). Time-temperature superposition was effective for all samples across the accessible temperature range (PLAM0: 30°C; PLAM4: 30-70°C;

PLAM8: 30-90°C), indicating a single relaxation mechanism of dynamic moduli (shift factors are shown in Figure 3.13). We first examine the behavior of poly(lauryl acrylate) (labeled PLAM0), which does not contain AM and therefore should not undergo hydrogen bonding. The dynamic moduli of PLAM0 showed characteristic liquid behavior in the terminal region, with slopes of 2 and 1 for *G'* and *G"* vs. ω (on a log-log plot), respectively, throughout the measured temperature range. With the addition of AM to the midblock, the curves shifted to lower frequency. Both PLAM4 and PLAM8, containing 4 and 8 wt% AM in the midblock, respectively, showed a rubbery region at high frequencies (with *G'* and *G"* superimposed), and then transitioned to the terminal flow region at lower frequencies. The relaxation of PLAM8 to the terminal flow region occurred at a lower frequency than that of PLAM4, and both occurred at a lower frequency than PLAM0. In the rubbery region, the dynamic moduli of PLAM8 were greater than that of PLAM4, attributed to the higher crosslinking density characterized with FTIR (facilitated by the presence of AM groups which undergo hydrogen bonding). In the terminal flow region, the power law exponents of *G'* and *G"* for PLAM4 and PLAM8 deviated from that typically observed. The exponent for *G'* decreased from 1 to 0.97 and 0.91 for PLAM4 and PLAM8, respectively. Similarly, the exponent for *G*' decreased from 2 to 1.7 and 1.33 for PLAM4 and PLAM8, respectively. Similar deviation of power law exponents in the terminal flow region has been previously observed in poly(*n*-butyl acrylate) in the presence of different types of hydrogen bonding.[84]

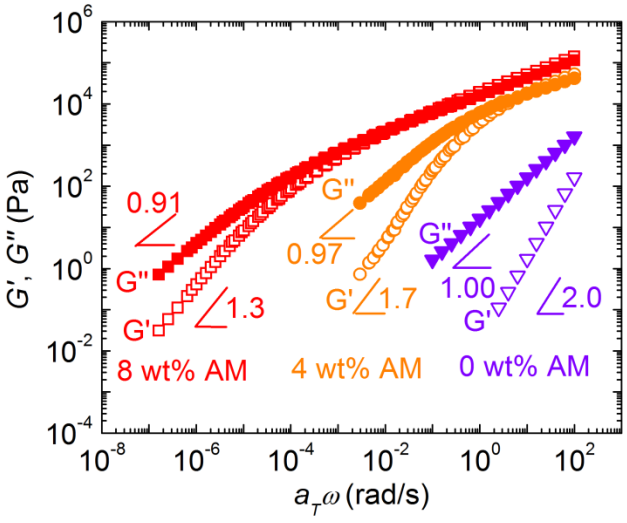

Figure 3.12 Storage (*G'*, open symbols) and loss (*G''*, closed symbols) moduli as functions of frequency for PLAMX copolymers with a reference temperature of 30 °C.

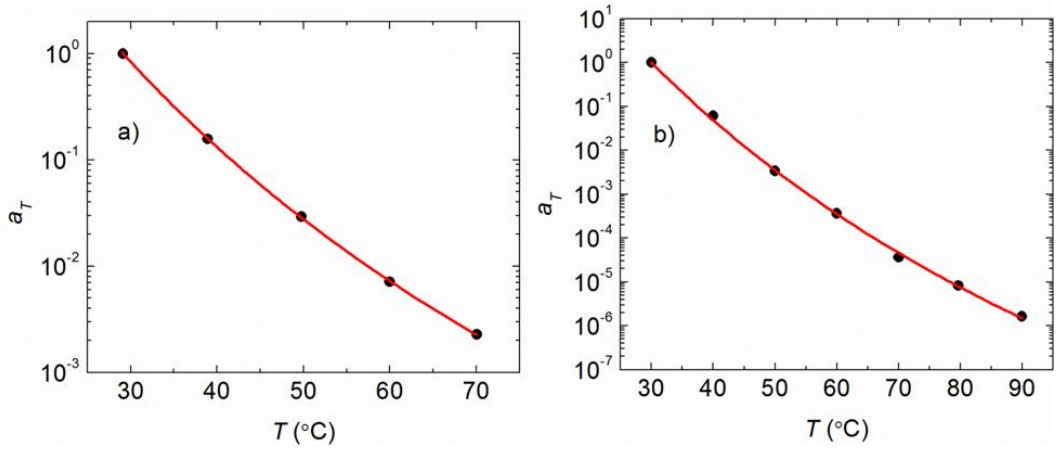

Figure 3.13 Shift factor a_T (●) as a function of temperature for a) PLAM4 and b) PLAM8. Red curves show the fit of the WLF equation to the data.

3.4 Impact of acrylamide content on thermodynamic interactions and order-disorder transition of SLAS triblock copolymers

The order-disorder transition temperature (T_{ODT}) of the SLAS triblock copolymers was characterized through observation of the temperature-dependence of *G'* (measured at ω = 1 rad/s). Rheology data obtained from SLAS triblock copolymers with PS content in the range of 14-17 vol% are shown in Figure 3.14. At low temperatures (< 100 °C),

increasing the AM content increased *G'*, due to higher crosslink density (Figure 3.14a). For both SLAS0-17 and SLAS4-16 (containing 0 and 4 wt% AM, respectively), an initial decrease of *G'* is observed, corresponding to the first maximum of tan δ in Figure 3.14b, attributed to the glass transition (T_g) of the PS block. The feature is less distinguishable in the data obtained from SLAS8-14 (containing 8 wt% AM), likely due to the proximity of the T_{ODT} and T_g. As the temperature was increased, a drastic decrease in *G'* was observed, a signature of T_{ODT}. T_{ODT}, determined from the intersection of two extrapolated lines (shown in Figure 3.14a), showed a drastic decrease with increasing AM content in the midblock (Table 3.4). SLAS triblock copolymers with 23 vol% PS did not undergo a T_{ODT} in the measurable temperature range (up to 270 °C) (Figure 3.15).

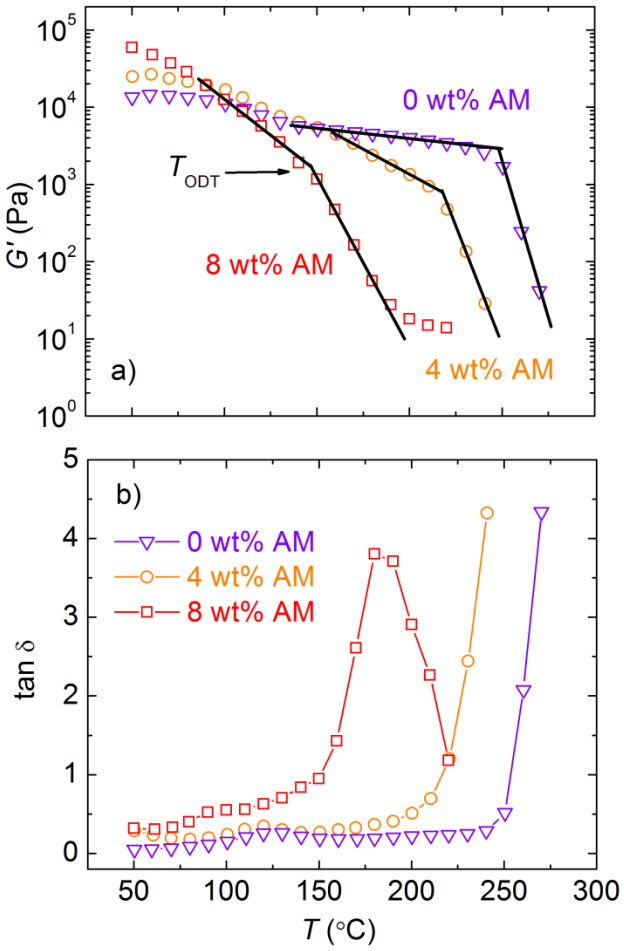

Figure 3.14 *G'* (log scale) (a) and tan δ (b) obtained at ω = 1 rad/s as functions of temperature for SLASX-Y triblock copolymers containing similar vol% PS (Y = 14-17).

Table 3.4 Flory-Huggins interaction parameter χ between poly(lauryl acrylate-co-acrylamide) and polystyrene (v_{ref} = 100 Å^3) predicted from the T_{ODT} and theoretical block copolymer phase diagram

Triblock copolymer	wt% AM in midblock	T_{ODT} (°C)[a]	Theoretical χN at T_{ODT}[b]	Theoretical χ at T_{ODT}[b]
SLAS0-17	0	248±1	37	0.022±0.0011
SLAS4-16	4	216±1	38	0.021±0.0010
SLAS8-14	8	148±3	42	0.026±0.0013

[a] Measured with rheology

[b] χN and χ determined from the theoretical phase diagram from Matsen et al [31], using the values of N and vol% PS reported in Table 3.1

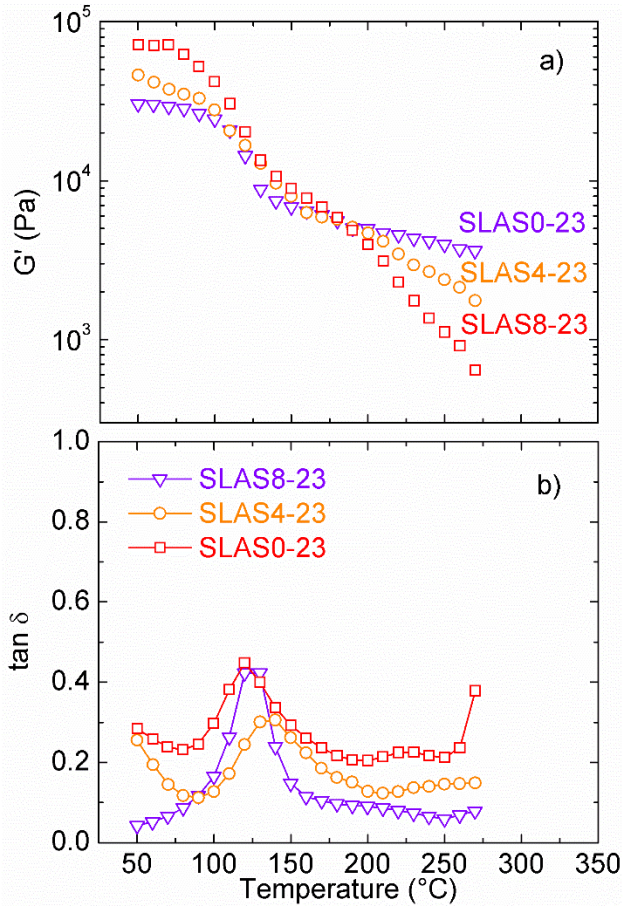

Figure 3.15 a) *G'* (log scale) vs. temperature for SLAS0-23, SLAS4-23 and SLAS8-23 and b) tan δ vs. temperature for SLAS0-23, SLAS4-23 and SLAS8-23.

To understand the decrease in T_{ODT} with increasing AM content, the Flory-Huggins interaction parameter χ between the midblock (a random copolymer of AM and LA) and PS was characterized. The interaction strength of a block copolymer is defined by χN, where N is the total number of repeat units of the triblock copolymer. χN at the order-disorder transition (ODT) depends on the block copolymer composition (vol% of each block), and can be determined from a theoretical phase diagram (such as Matsen et al.[31, 32], applicable to a triblock copolymer). Recall from the previous discussion that all the SLAS triblock copolymers exhibited high dispersities; increase in dispersity is anticipated to decrease χN at the order-disorder transition (ODT).[123] In this study, a phase diagram for a triblock copolymer containing a higher dispersity block (reported in ref.[31])

was employed to determine χN at the ODT. With known values of N, χ at T_{ODT} was thus determined for each block copolymer (Table 3.4 and open symbols in Figure 3.16). In the series of SLAS triblock copolymers with comparable vol% PS (14-17 vol%) and N (Table 3.1), similar values were predicted for χ at the ODT (Table 3.4). However, the drastic differences in the measured T_{ODT} of these polymers indicate the temperature dependence of χ varies with varying AM content in the midblock.

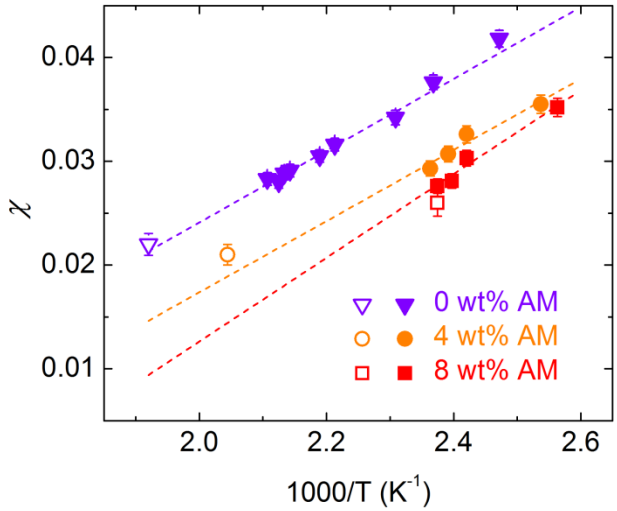

Figure 3.16 χ as a function of 1/T for PS/PLAMX. Closed symbols designate values obtained from cloud point measurements on binary blends; open symbols designate values obtained from the order-disorder transition temperature of the triblock copolymers.

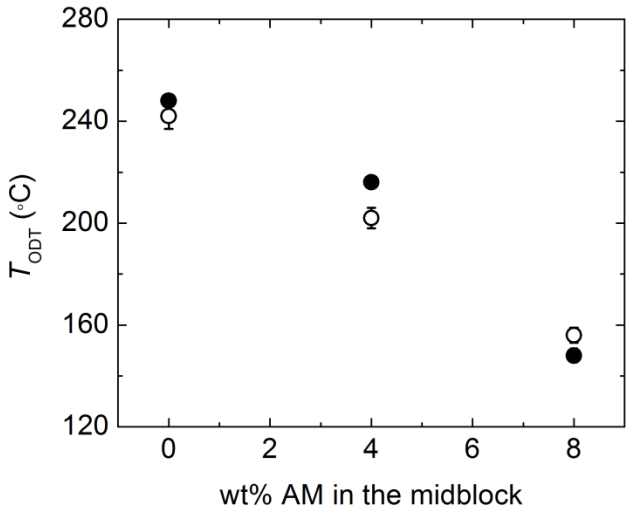

Figure 3.17 T_{ODT} as a function of wt% AM in the midblock. a) Measured using rheology (●).b) Predicted from theoretical block copolymer phase diagram [31] and measured $\chi(T)$ behavior (○).

To explore this further, cloud point measurements were employed to characterize χ between PLAM (the midblock of the triblock copolymer) and PS (the endblocks of the triblock copolymer). The low molecular weight polymers PLAM*X*-L (where X is the wt% of acrylamide) and PS-L were synthesized (Table 3.5). Four PS-L/PLAM4-L blends and four PS-L/PLAM8-L blends were prepared at various compositions. Cloud point temperatures for each blend were determined using optical microscopy (Table 3.6). Theoretical binodal curve were generated with Flory-Huggins Theory, following previously reported procedures (Figure 3.18).[112] Finally, comparing the cloud point data and theoretical binodal curves provided relationships between χ and T (Table 3.6). χ as a function of $1/T$ for PS/PLAM0 (taken from ref. [112]), PS/PLAM4 and PS/PLAM8 are shown in Figure 3.16. As the AM content increased in the PLAMX copolymer, a distinct decrease in χ was observed. This trend is consistent with the experimental observation of decreasing T_{ODT} in the SLAS triblock copolymers with increasing AM content in the midblock (Figure 3.17).

Table 3.5 Molecular characteristics of low molecular weight PS and PLAM-L

Sample	M_n (kg/mol)	M_w (kg/mol)	Đ	N_w
PS	3.1	3.5	1.11	56
PLAM4-L	3.9	4.1	1.06	72
PLAM8-L	4.5	4.9	1.08	84

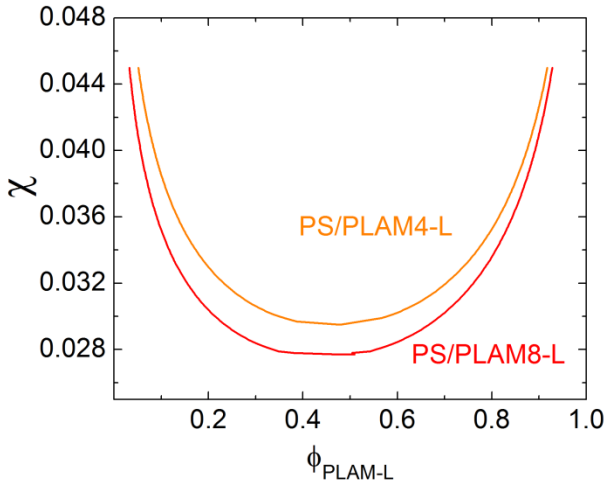

Figure 3.18 Theoretical binodal curves predicted from Flory-Huggins theory for blends PS/PLAM4-L and PS/PLAM8-L following reported procedure in ref [112].

Table 3.6 PS/PLAM4-L and PS/PLAM8-L blend characteristics and results of cloud point measurements[a]

Blend	Φ_{PLAM-L}	T_{cp} (°C)	χ
PS/PLAM4-L	0.298	145	0.0307±0.0008
	0.549	150	0.0293±0.0007
	0.725	140	0.0326±0.0008
	0.804	121	0.0355±0.0009
PS/PLAM8-L	0.313	144	0.0281±0.0007
	0.500	148	0.0276±0.0007
	0.707	140	0.0303±0.0008
	0.833	117	0.0352±0.0009

[a] Φ_{PLAM-L} is volume fraction of PLAM-L in the blend, T_{cp} is cloud point temperature.

This result was further confirmed with predictions of χ with a combination of solubility parameter theory and random copolymer theory. Solubility parameter theory was employed to predict $\chi(T)$. SLAS triblock copolymers contain three components: poly(lauryl acrylate) (PLA), polyacrylamide (PAM) and polystyrene (PS). Group contribution methods[124] were used to calculate solubility parameters (δ) for poly(lauryl acrylate) (PLA), polyacrylamide (PAM) and polystyrene (PS). The results are listed in Table 3.7. The interaction parameter χ_{12} between polymer 1 and polymer 2 were then calculated for each pair of polymers (PLA/PAM, PAM/PS, PLA/PS) using Equation 3.10:

$$\chi_{1,2} = \frac{v_{ref}}{kT}(\delta_1 - \delta_2)^2, \qquad \text{Equation 3.10}$$

where v_{ref} is the reference volume, 100Å^3, k is the Boltzmann constant, T is temperature, and δ_1 and δ_2 are solubility parameters for components 1 and 2. Results are tabulated in Table 3.7 and Table 3.8. The interaction between PLA and PAM was determined to be most repulsive (highest χ), while the interaction between PLA and PS was the most favorable. In the ordered state of the SLAS triblock copolymers, the most repulsive pair (PLA and PAM) are in the same phase, which is unfavorable. This unfavorable interaction can be minimized through transition to the disordered state in which all three components are in the same phase such that PLA and PAM can both interact with PS. Thus, SLAS triblock copolymers with higher PAM content exhibited lower T_{ODT} in order to minimize unfavorable interactions.

Table 3.7 Solubility parameters calculated from group contribution methods

Component	PLAc	PAM	PS
δ (MPa$^{1/2}$)	17.4	25.9	19.0

Table 3.8 Segmental χ parameters between each polymer pair

Polymer pair:	PLAc\PAM	PS\PAM	PLAc\PS
$\chi_{1,2}$	523/T	345/T	18.5/T

We also quantified χ between the midblock PLAM (a random copolymer of AM and LA) and endblock PS using random copolymer theory (Equation 3.11)

$$\chi = \chi_{PLA,PS} f_{PLA} + \chi_{PAM,PS} f_{PAM} - \chi_{PLA,PAM} f_{PLA} f_{PAM}, \qquad \text{Equation 3.11}$$

where $\chi_{PLA,PS}, \chi_{PAM,PS}$,and $\chi_{PLA,PAM}$ are the interaction parameters for PLA/PS, PAM/PS and PLA/PAM, respectively (listed in Table 3.8), and f_{PLA} and f_{PAM} are the mole fractions of PLA and PAM in the midblock, respectively. At a given temperature, χ decreases with increasing AM content in the midblock (Table 3.9), consistent with experimental observations of T_{ODT} in this triblock copolymer series.

Table 3.9 χ between poly(lauryl acrylate-co-acrylamide) and polystyrene, determined from solubility parameter and random copolymer theories

Triblock copolymer	wt% AM in midblock	χ
SLAS0-17	0	18.5/T
SLAS4-16	4	2.24/T
SLAS8-14	8	0.84/T

3.5 Disordered spherical morphology of SLAS triblock copolymers

Small angle X-ray scattering (SAXS) was used to characterize the morphology of SLAS triblock copolymers. The 1D azimuthal integrated SAXS profiles exhibited a primary peak with broad higher order peaks (Figure 3.19 and Figure 3.20). The higher order peak locations were not consistent with traditional equilibrium block copolymer phases (such as ordered lamellae, spheres, cylinders, or a gyroid phase, Figure 3.21), but were characteristic of a disordered spherical morphology that has been previously reported by our group[125] for poly(styrene-*b*-lauryl acrylate-*b*-styrene) triblock copolymers (i.e., SLAS triblock copolymers with 0 wt% AM).

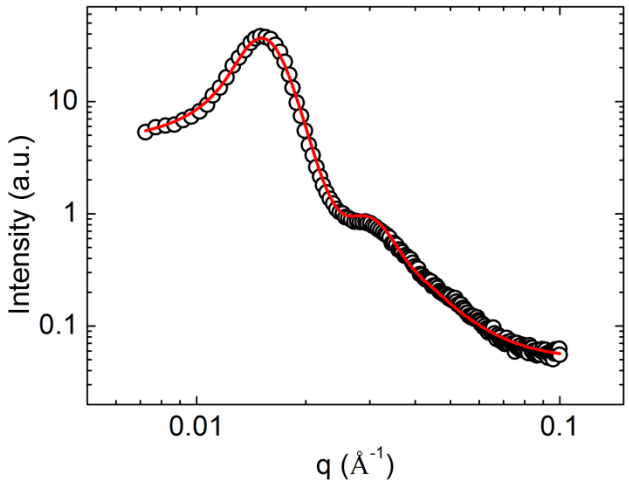

Figure 3.19 1D SAXS data obtained from SLAS4-23 (○) and Percus-Yevick hard-sphere model fit (red solid curve).

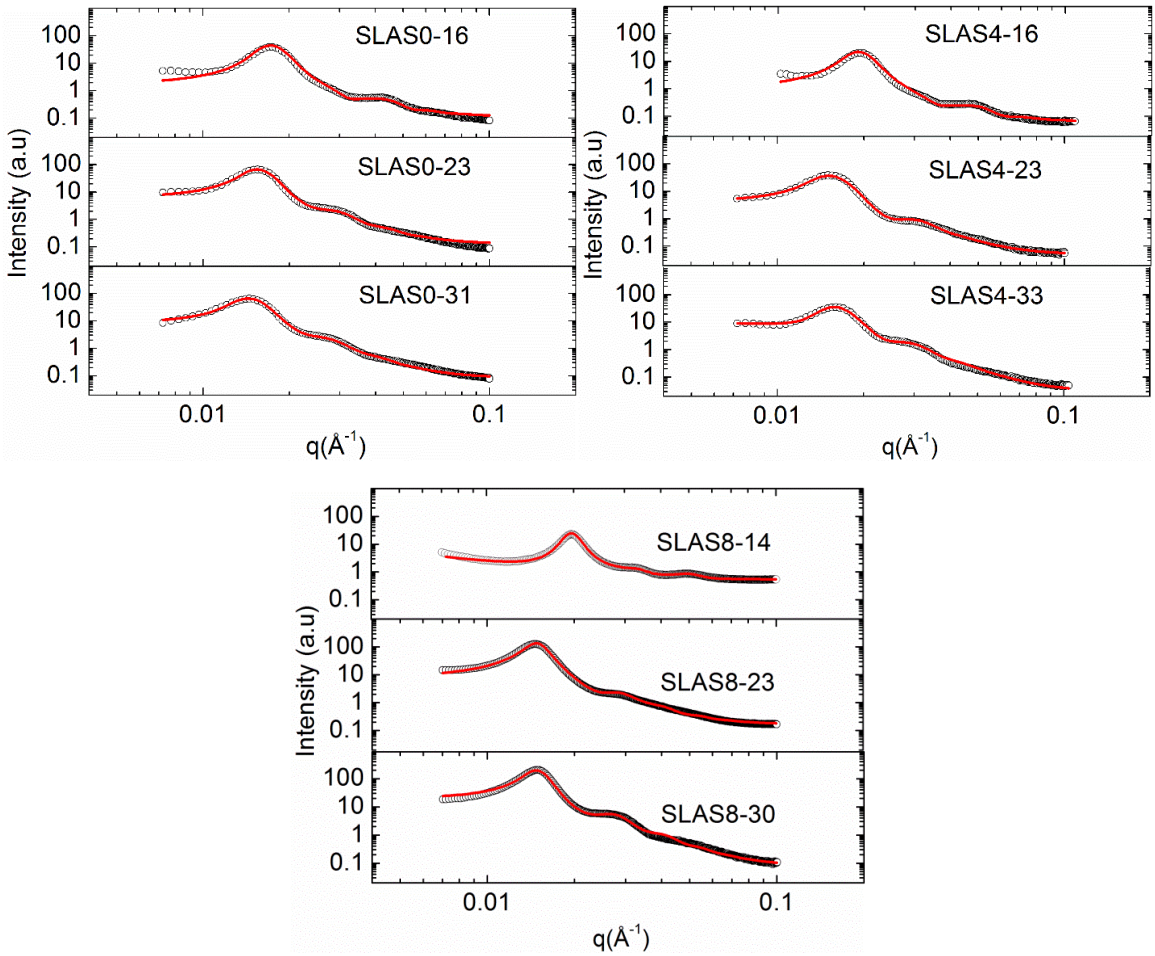

Figure 3.20 1D SAXS data obtained from SLAS triblock copolymers (○), including fit of the Percus – Yevick hard-sphere model (red solid curves).

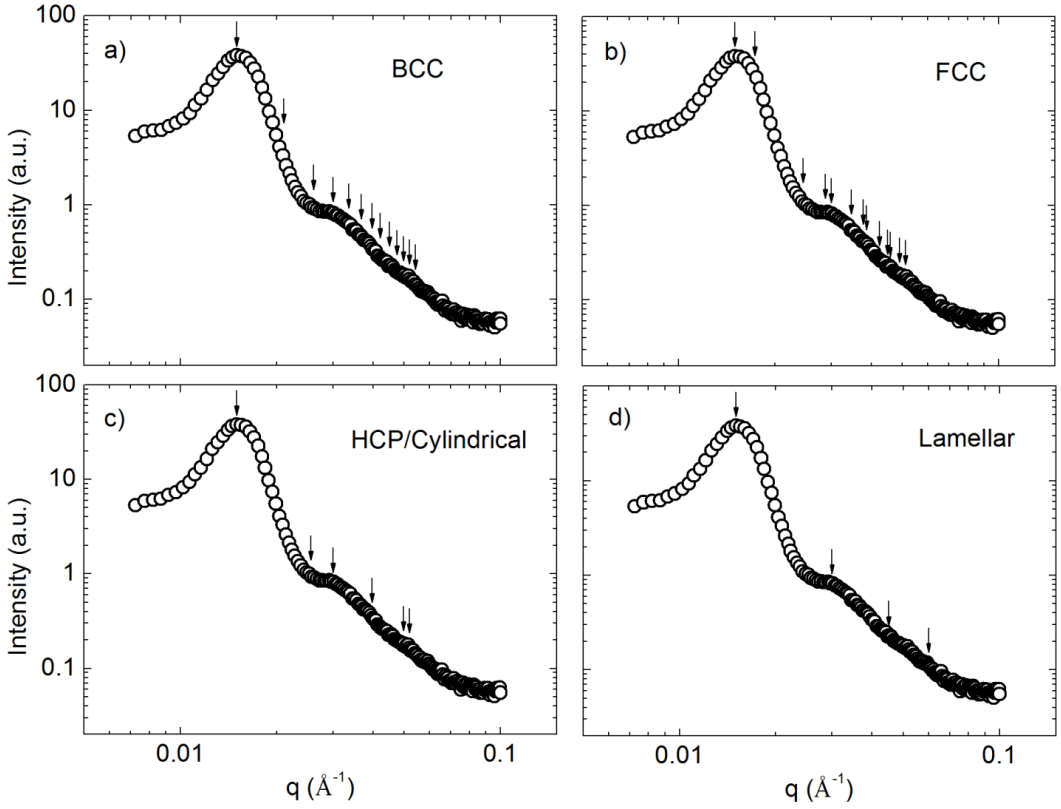

Figure 3.21 1D SAXS pattern for SLAS4-23 with predictions for commonly observed block copolymer morphologies for a) body-centered cubic (BCC) spheres, b) face-centered cubic (FCC) spheres, c) hexagonally closed packed (HCP) spheres or cylinders and d) lamellae.

The data in Figure 3.19 and Figure 3.20 were fit with the Percus–Yevick structure factor for hard spheres (Equation 3.12-Equation 3.14), which assumes the presence of spherical PS domains (modeled as hard spheres) with average sphere radius $R_{sp,}$ and radius of interaction R_{hs} ($R_{hs} > R_{sp}$).

$$I(q) = KN_sP(q)S(q), \qquad \text{Equation 3.12}$$

$$P(q) = \left\{ v_{sp} \frac{3}{(qR_{sp})^3} \left[sin(qR_{sp}) - qR_{sp}cos(qR_{sp}) \right] \right\}^2, \text{and} \qquad \text{Equation 3.13}$$

$$S(q) = \left[1 + 24\eta \frac{G(2qR_{hs})}{2qR_{hs}} \right]^{-1}, \qquad \text{Equation 3.14}$$

where K is a constant that is a function of the type of radiation used and the sample properties, N_s is the number of scatters, $P(q)$ is the spherical form factor and $S(q)$ is the hard sphere structure factor with Percus–Yevick closure, v_{sp} is the volume of sphere, R_{sp} is the hard sphere radius, R_{hs} is the interaction radius with $R_{hs} > R_{sp}$, η is the volume fraction of hard sphere interaction. $G(2qR_{hs})$ is a function defined in ref. [126] The SAXS data were well-described with the Percus–Yevick model, revealing the disordered sphere morphology of SLAS triblock copolymers. The R_{sp}, R_{hs}, and PD values ($PD = \sigma/R_{sp}$, where σ is the standard deviation of the hard sphere radius) extracted from data fitting are summarized in Figure 3.22 and Table 3.10. R_{sp} and R_{hs} increased with increasing PS content, indicating the formation of larger domains, due to increased molecular weight of the PS block.[127, 128] The PD values also increased with increasing PS content, indicating the presence of broader size distributions. In each series of triblock copolymers with the same vol% PS, yet differing AM content, the R_{sp} and R_{hs} values differed by less than 1 nm, indicating that the AM content had little effect on the SLAS triblock copolymer morphology. One exception is the observation of a decrease in PD in the SLAS8 series compared to triblock copolymers with lower AM content (Figure 3.22). It also worth noting that the SLAS triblock copolymers exhibited spherical morphologies even at high vol% of PS (30-33%), which is in contrast to prior studies on monodisperse triblock copolymers that mostly exhibited cylindrical morphologies within the same block composition range.[29, 32, 129] Matsen has shown increasing the dispersity shifts the boundary of spherical domains to larger volume fractions and lower χN, thus broadening the phase window .[31]

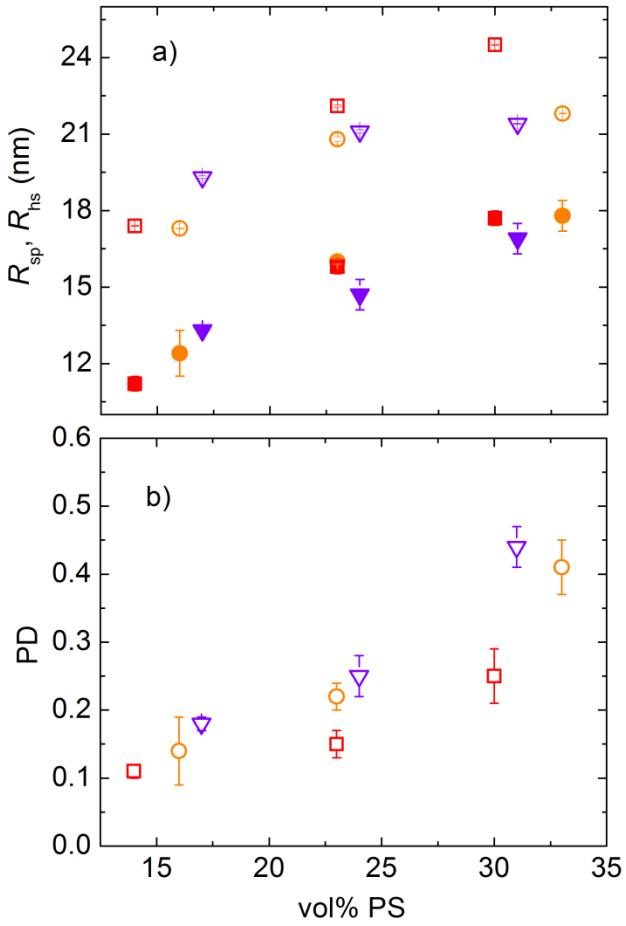

Figure 3.22 a) R_{sp} (closed symbols), R_{hs} (open symbols) and b) PD for SLAS triblock copolymers with the following wt% AM in the midblock: 0 (violet ▽), 4 (orange ○), and 8 series (red □).

Table 3.10 Morphological parameters of SLAS triblock copolymers

	R_{sp} (nm)	R_{hs} (nm)	PD
SLAS0-17	13.3±0.1	19.3±0.05	0.18±0.01
SLAS0-24	14.7±0.6	21.1±0.06	0.25±0.03
SLAS0-31	16.9±0.6	21.4±0.01	0.44±0.03
SLAS4-16	12.4±0.9	17.3±0.02	0.14±0.05
SLAS4-23	16.0±0.1	20.8±0.09	0.22±0.02
SLAS4-33	17.8±0.6	21.8±0.01	0.41±0.04
SLAS8-14	11.2±0.3	17.4±0.02	0.11±0.01
SLAS8-23	15.8±0.3	22.1±0.04	0.15±0.04
SLAS8-30	17.7±0.3	24.5±0.02	0.25±0.02

3.6 Presence of AM improves mechanical properties of SLAS triblock copolymers

The mechanical properties of SLAS triblock copolymers were investigated by tensile testing. Representative stress-strain curves for SLAS triblock copolymers containing 23 vol% PS are shown in Figure 3.23. The quantified tensile strength and strain at break for each polymer are summarized in Figure 3.24. The tensile strength increased dramatically with increasing AM content, as well as with increasing vol% PS (Figure 3.24a). The strain at break exhibited a maximum value at intermediate AM content: the strain at break increased from 0 – 4 wt% AM, and then decreased from 4 – 8 wt% AM (Figure 3.24b). The strain at break decreased with increasing vol% PS (Figure 3.24b).

With increasing AM content in the SLAS triblock copolymers, the crosslink density resulting from hydrogen bonds increased (quantified with FTIR, Figure 3.10). It is well understood that the tensile strength of an elastomer increases with increasing crosslink density when in the low crosslink density regime,[130, 131] demonstrated by the observed increase in tensile strength with increasing AM content. The impact of hydrogen bonding interactions on the strain at break is slightly more complex, as SLAS triblock copolymers with intermediate AM content exhibited the highest strain at break. At low AM content, dynamic hydrogen bonds repeatedly associate and dissociate, inducing energy dissipation and thus preventing local concentration of stress in the PS domains, greatly improving the strain at break of the material.[91, 132] However, at high AM content, the increased apparent crosslink density results in poor chain mobility, which results in stress concentration in PS domains and thus lower strain at break.[132]

Increasing the amount of hard block (vol% PS) present in the SLAS triblock copolymers both increased the tensile strength and decreased the strain at break. These behaviors are consistent with prior studies on triblock copolymer based TPEs, [23, 133-136] and are attributed to the increase in volume of filler (i.e., glassy domains) in the TPE.[137]

Our objective for the addition of AM into the midblock of the SLAS triblock copolymer was to incorporate hydrogen bonding interactions and the formation of a transient network into the triblock copolymer matrix. This was motivated by the fact that poly(lauryl acrylate) (PLA) has a high entanglement molecular weight (> 200 kg/mol) and therefore the triblock copolymer matrix is unentangled. However, one unintended consequence of this approach is that AM does not contain the bulky alkyl side-chains of LA, and therefore in addition to providing hydrogen bonding interactions, the presence of AM could reduce the entanglement molecular weight of the copolymer. Therefore, we wanted to probe whether the improvements we observed in the tensile properties with the addition of AM were due to the presence of hydrogen bonding interactions, or simply a reductions in the entanglement molecular weight and increasing the relative "spacing" between alkyl side-chains of the LA repeat units along the polymer backbone. To probe this question, we synthesized a triblock copolymer in which AM was replaced with methyl acrylate (MA), which has a similar molecular size to AM (Figure 3.25). Poly(styrene-*b*-(lauryl acrylate-*co*-methyl acrylate)-*b*-styrene) (SLMS3-21) triblock copolymer, containing 3 wt% of methyl acrylate in the midblock and 21 vol% of PS was synthesized, with molecular characteristics shown in Table 3.1. SLMS3-21 was designed to have comparable molecular weight and PS content to SLAS4-23. Interestingly, the mechanical properties of SLMS3-21 are indistinguishable with the series of SLAS

triblock copolymers containing 0 wt% AM (Figure 3.23 and Figure 3.24). Therefore simply adding a comonomer with a smaller molecular volume was not sufficient to realize improvements in the mechanical properties. We thus concluded that the enhancement in properties with the presence of AM is attributed to the formation of a transient network through hydrogen bonding in the matrix.

We also considered whether polymer dispersity and degree of microphase segregation may offer explanations for the poor mechanical properties observed in SLAS triblock copolymers in the absence of hydrogen bonding (i.e., 0% AM). The mechanical properties of triblock copolymers arise from the formation of a strong physical network, with both hard block chain ends covalently bonded to the middle elastomeric block. For a polydisperse triblock copolymer, the presence of homopolymer and diblock copolymer contamination may have a large impact on mechanical properties, as these molecules do not effectively contribute to the formation of physical network, thus resulting in lower tensile strength.[17] In this study, the SLAS triblock copolymers all exhibit trimodal molecular weight distributions (e.g., see earlier discussion of Figure 3.3). While it is likely that the broad molecular weight distribution diminished the observed mechanical properties, the series of SLAS triblock copolymers with varying AM content presented in this manuscript all have similar molecular weight distributions. In addition, the extent of microphase segregation, domain spacing, and interfacial width also play a role in the mechanical properties of triblock copolymers. Higher extent of microphase separation[138], smaller domain spacing[139, 140] and larger interfacial width[141-143] are expected to contribute to higher modulus and tensile strength. The interfacial width of SLAS triblock copolymers without AM was calculated to be 15 Å, comparable with the reported value

(23 Å) for SBS triblock copolymers. Therefore, the degree of microphase separation is likely not a key factor limiting the performance of the SLAS triblock copolymers. Furthermore, in this study, all the SLAS triblock copolymers, both with and without the AM comonomer, exhibited comparable morphologies. In summary, the variations in modulus and strain at break in the series of SLAS triblock copolymers with varying AM content are not attributed to differences in either dispersity or morphology.

We can therefore conclude that the enhancement of mechanical properties of fatty acid-derived triblock copolymers by incorporation of AM in the triblock copolymer midblock is attributed to the formation of a transient network through hydrogen bonding. The desired mechanical properties can be effectively controlled by varying both wt% AM and vol% PS in the triblock copolymer.

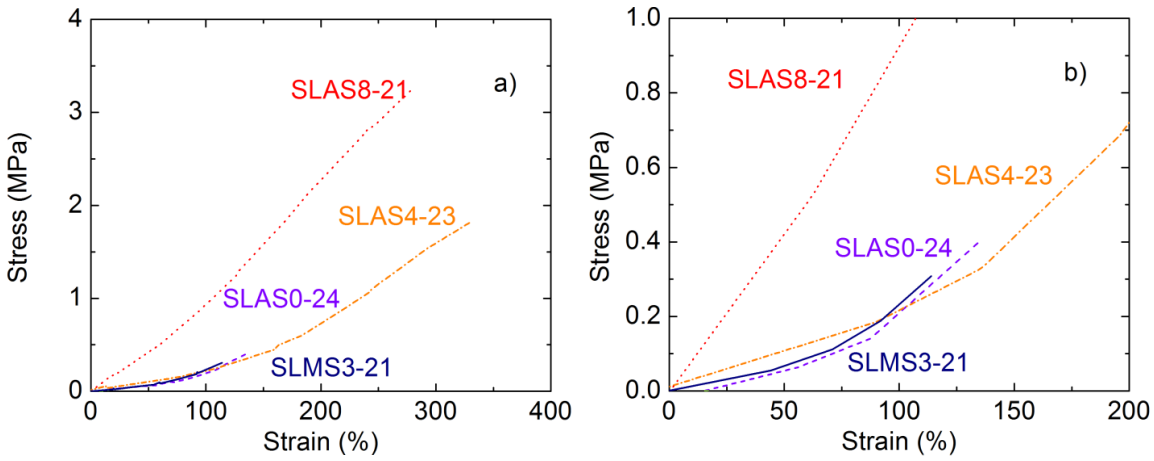

Figure 3.23 (a) Representative tensile stress-strain curves for SLASX-Y triblock copolymers containing similar vol% PS (Y = 23-24). (b) closer view of low strain region.

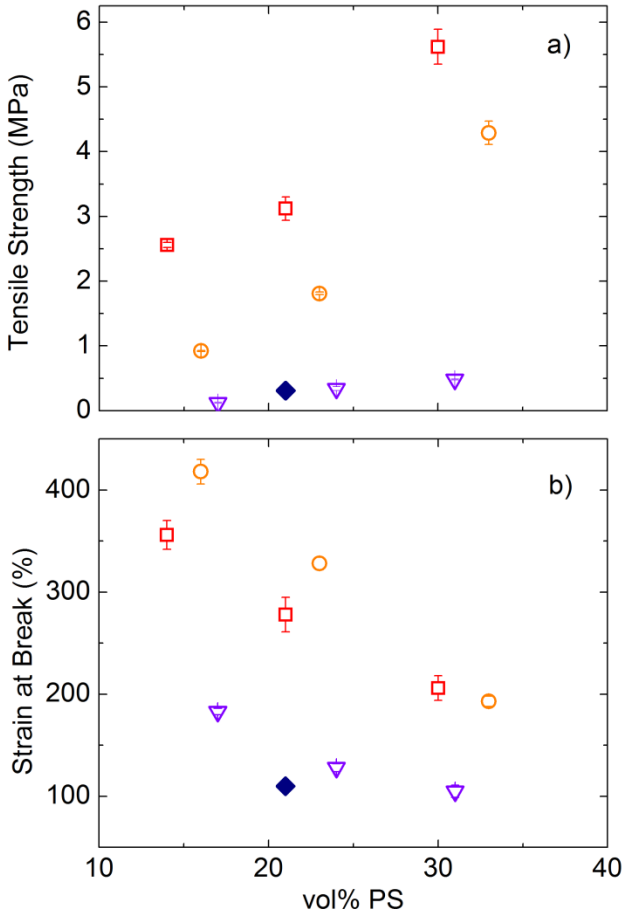

Figure 3.24 a) Tensile strength and b) strain at break for SLAS triblock copolymers.

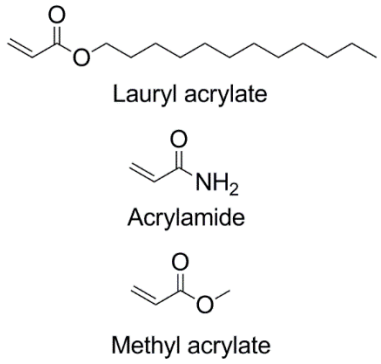

Figure 3.25 Chemical structures of lauryl acrylate, acrylamide and methyl acrylate

3.7 Concluding remarks

The impact of hydrogen bonding on the physical properties of fatty acid-based triblock copolymer thermoplastic elastomers (TPEs) was evaluated. The triblock

copolymers were synthesized by copolymerization of fatty acid-based lauryl acrylate and the hydrogen bonding comonomer acrylamide to form the midblock, followed by chain extension with styrene to form the endblocks. The extent of hydrogen bonding was tunable by controlling the fraction of acrylamide in the midblock. FTIR confirmed the presence of hydrogen bonding at low temperatures, and effective dissociation of hydrogen bonds at elevated temperatures, facilitating melt processing of these polymers. The incorporation of acrylamide greatly reduced the order-disorder transition temperature due to more favorable thermodynamic interactions between the midblock and endblocks. SAXS analyses revealed the presence of a disordered spherical morphology that was unaffected by the presence of hydrogen bonding. The observed triblock copolymer morphology of polystyrene spheres dispersed in the rubbery matrix is appropriate for application as TPEs. Mechanical testing revealed that the incorporation of hydrogen bonding significantly improved the tensile strength and strain at break of the triblock copolymers. Indeed, this work demonstrates the utility of hydrogen bonding to improve the mechanical properties of triblock copolymer thermoplastic elastomers which contain bulky constituents in the midblock (such as the long alkyl side-chains in the fatty acid-based polymers explored in this work).

Chapter 4 Improving Mechanical Properties of Fatty Acid-Derived Triblock Copolymers by Incorporation of Ionic Interactions

In this chapter, the presence of ionic interactions in the long-chain polymethacrylate midblock of a thermoplastic elastomeric triblock copolymer was explored as a method of improving its mechanical properties. Poly(methyl methacrylate-*b*-(lauryl methacrylate-*co*-*tert*-butyl methacrylate)-*b*-methyl methacrylate) (MLtM), which exhibits low tensile strength and elongation at break, was modified by hydrolysis to form poly(methyl methacrylate-*b*-(lauryl methacrylate-*co*-methacrylic acid)-*b*-methyl methacrylate) (MLAM). The methacrylic acid group in the midblock was further neutralized with sodium hydroxide to introduce ionic crosslinks into the system. The rheological properties of the midblocks were measured. The effects of acid content and degree of neutralization on the mechanical properties were evaluated. Finally, the correction between the rheological behavior of the midblock and the mechanical properties of the corresponding triblock copolymers was explored.

4.1 Synthesis of poly(lauryl methacrylate-*co*-methacrylate acid) (PLMA) and neutralized PLMA

The poly(lauryl methacrylate-*co*-*tert*-butyl methacrylate) (PLtB) copolymers were firstly synthesized through RAFT polymerization followed by hydrolysis to form poly(lauryl methacrylate-*co*-methacrylate acid) (PLMA) copolymers. Then, PLMA copolymers were neutralized with sodium hydroxide to create ionically crosslinked copolymers PLMA-Na. Three series of PLMA copolymers were synthesized (Table 4.1), each containing different methacrylic acid content (5, 8 and 10 mol%). Within each series,

the degree of neutralization was varied. All the PLMA copolymers have similar molecular weights (104 – 110 kg/mol) and dispersity (Đ: 1.3-1.4).

Table 4.1 Molecular characteristics of PLtB, PLMA and neutralized PLMA copolymers

Polymer Name	M_n (kg/mol)[a]	Đ[b]	mol% COOH[c]	mol% COONa[d]	τ_b (s)[e]
PLtB5	106	1.33	0	0	
PLMA5			5	0	1
PLMA5-Na1			4	1	2
PLMA5-Na2.5			2.5	2.5	5
PLMA5-Na4			1	4	310
PLMA5-Na5			0	5	604
PLtB8	107	1.29	0	0	
PLMA8			8	0	4
PLMA8-Na0.4			7.6	0.4	5
PLMA8-Na0.8			7.2	0.8	49
PLMA8-Na1.6			6.4	1.6	105
PLMA8-Na2.4			5.6	2.4	1150
PLMA8-Na3.2			4.8	3.2	4.4×10^5
PLtB10	110	1.35	0	0	
PLMA10			10	0	45
PLMA10-Na1			9	1	120
PLMA10-Na2			8	2	7320
PLMA10-Na3			7	3	3.7×10^5
PLMA10-Na4			6	4	6.8×10^7
PLMA10-Na5			5	5	9.5×10^9

[a] Number-average molecular weight (M_n) of PLtB copolymers were characterized with GPC with light scattering. The *dn*/*dc* for all the PLtB copolymers was 0.084 mg/L.

[b] Dispersity Đ was characterized with GPC with light scattering.

[c]The total mol% COOH was quantified by calculating the mol% of tert-butyl methacrylate in PLtB copolymer through ^{13}C NMR. The excessive mol% COOH in the neutralized copolymers was calculated by subtracting mol% of COONa from total mol% COOH.

[d]The mol% COONa was quantified by FTIR.

[e]The relaxation time τ_b was determined through rheology using a reference temperature of 30 °C.

The compositions of PLtB copolymers were firstly evaluated by ^{1}H NMR (Figure 4.1a). However, the peaks from *tert*-butyl methacrylate (tBMA) overlap completely with peaks from lauryl methacrylate, preventing the quantification of composition. Thus, quantitative ^{13}C NMR was employed in this case to obtain the composition of PLtB copolymers (Figure 4.1b). The peak corresponds to side chains (-C(**C**H$_3$)$_3$ at 27.8 ppm, peak 11) confirm the successful incorporation of tBMA. Mol% of tBMA was calculated from areas of peak 11 and peak 10 using Equation 4.1:

$$\text{mol\% tBMA} = \frac{A_{11}/3}{A_{10} + A_{11}/3} \times 100, \qquad \text{Equation 4.1}$$

in which A_{11} and A_{10} are the integration of peaks corresponding to –C(**C**H$_3$)$_3$ in tBMA and –CH$_2$-**C**H$_3$ in lauryl methacrylate. GPC analysis characterized the M_n and Đ (Table 4.1) and Figure 4.2 shows a typical GPC data obtained from PLtB10 copolymers. The GPC data shows monomodal distribution with relatively low dispersity (Đ: 1.2-1.3) indicating the RAFT polymerization of PLtB copolymers was well controlled.

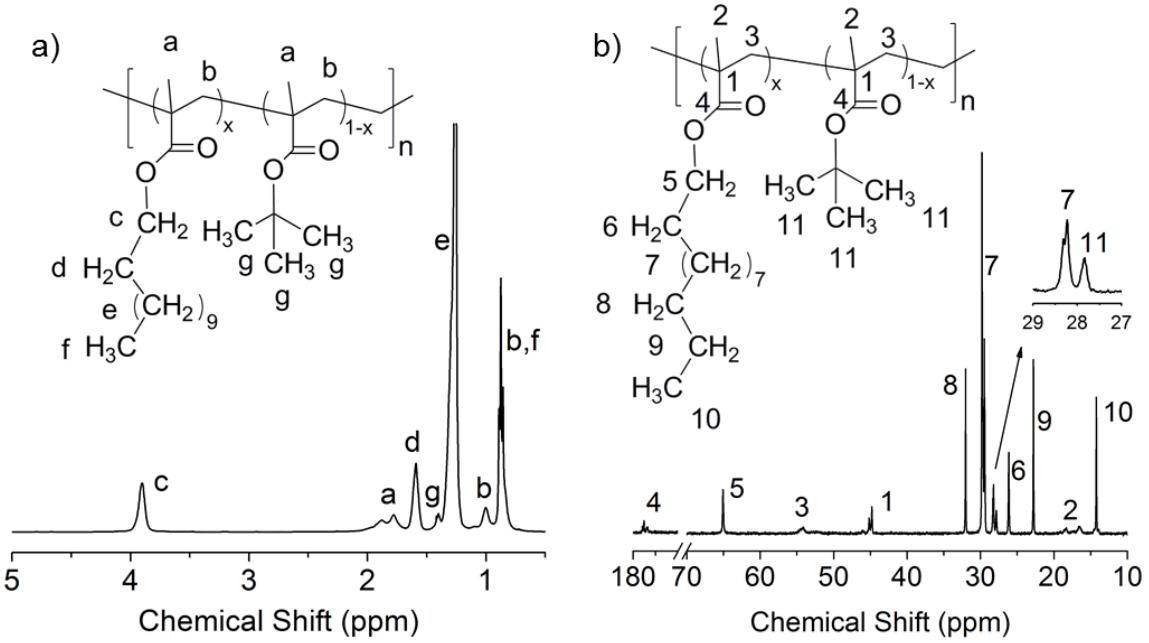

Figure 4.1 a) ^{1}H NMR and b) ^{13}C NMR data obtained from PLtB10

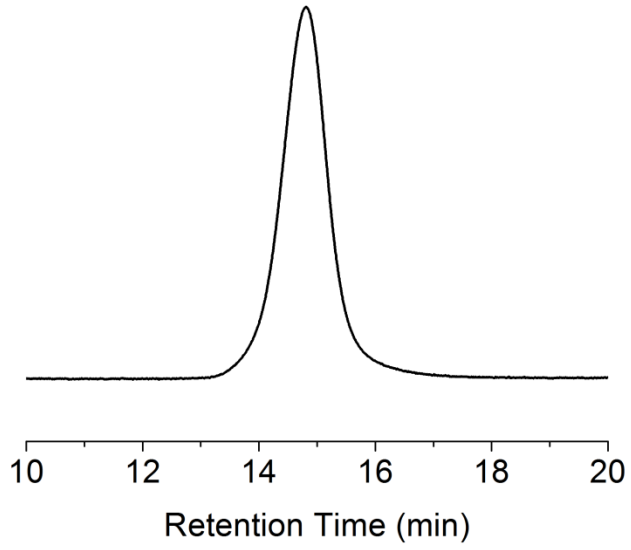

Figure 4.2 GPC data obtained from PLtB10.

The PLtB copolymers were further hydrolyzed with trifluoroacetic acid to form poly(lauryl methacrylate-*co*-methacrylic acid) (PLMA) copolymers. The tBMA was completely hydrolyzed to methacrylic acid as confirmed by ^{13}C NMR (Figure 4.3). The characteristic peak at 27.8 ppm corresponding to $–CH_3$ in the side chain disappeared completely. Thus, the mol% of methacrylic acid in PLMA copolymers was the same as mol% of tBMA in PLtB copolymers.

The PLMA copolymers were further neutralized with sodium hydroxide to form ionically crosslinked copolymers. The degree of neutralization was varied by adding an appropriate amount of NaOH. FTIR spectra were obtained on PLMA8 series (Figure 4.4). Peaks corresponding to C=O stretching of lauryl methacrylate and C=O stretching of methacrylic acid located at 1732 and 1700 cm^{-1} were observed for all the samples. All the peaks are normalized to C=O stretching band of lauryl methacrylate. Upon neutralization, the intensity of peaks corresponding to C=O of methacrylic acid decreased and a new peak corresponding to neutralized acid group COO^- at 1575cm^{-1} was identified, indicating

that part of acid groups in methacrylic acid was successfully neutralized. The mol% Na was calculated from the reduction of peak intensity at 1700 cm^{-1} using Equation 4.2:

$$\text{mol\% Na} = \frac{I_{\text{PLMA}X} - I_{\text{PLMA}X-\text{Na}Y}}{I_{\text{PLMA}X}} \times \text{mol\% PtBMA}, \qquad \text{Equation 4.2}$$

where $I_{\text{PLMA}X}$ and $I_{\text{PLMA}X-\text{Na}Y}$ are the peak intensities of PLMA*X* and neutralized PLMA*X*-Na*Y* at 1700 cm-1, the mol% PtBMA was determined from ^{13}C NMR as describe in previously. The results are tabulated in Table 4.1.

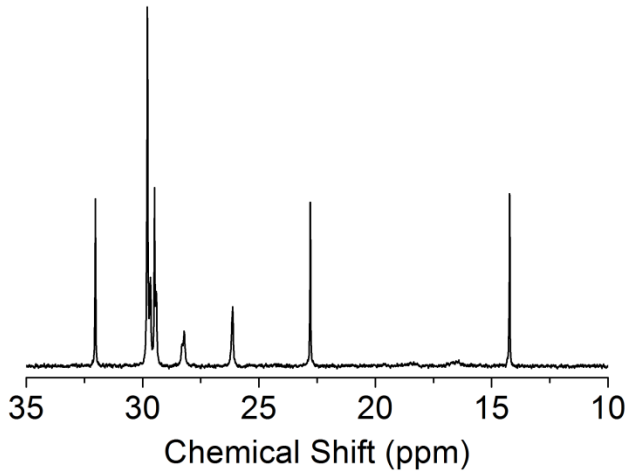

Figure 4.3 ^{13}C NMR obtained from PLMA10.

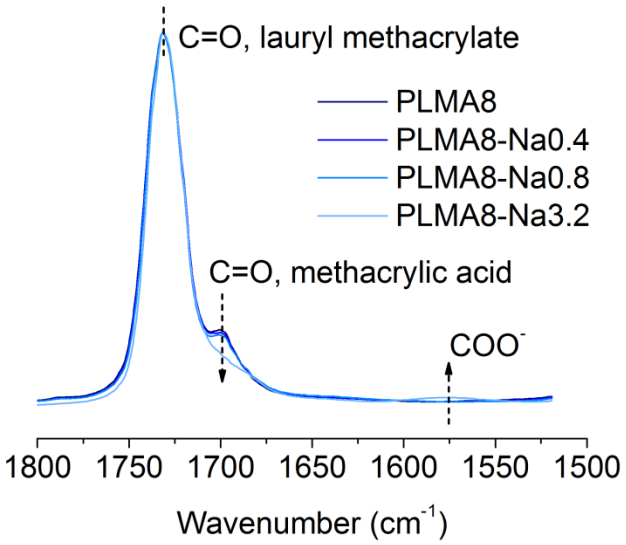

Figure 4.4 FTIR spectra obtained from PLMA8, PLMA8-Na0.4, PLMA8-Na0.8 and PLMA8-Na3.2.

4.2 Synthesis of MLtM, MLAM and neutralized MLAM

Poly(methyl methacrylate-b-(lauryl methacrylate-co-tert butyl methacrylate)-b-methyl methacrylate) (MLtM) was synthesized through two-steps RAFT polymerization using a difunctional chain transfer agent. Firstly, the difunctional midblock PLtB was synthesized followed by chain extension with methyl methacrylate to form MLtM triblock copolymers. Then, MLtM triblock copolymers were hydrolyzed to create MLAM triblock copolymers followed by neutralization with sodium hydroxide to generate ionically crosslinked copolymers MLAM-Na. Three series of MLAM copolymers were synthesized (Table 4.2), each containing different methacrylic acid content (5, 8 and 10 mol%). Within each series, the degree of neutralization was varied. All the triblock copolymers have similar overall molecular weight (125 – 136 kg/mol), wt% of PMMA, and dispersity (Đ: 1.3-1.4).

Table 4.2 Molecular Characteristics of MLtM, MLAM and neutralized MLAM triblock copolymers

Polymer Name	M_n (PMMA-PLtB-PMMA) (kg/mol)[a]	Đ[b]	wt% PMMA	mol% COOH[c]	mol% COONa[d]
MLtM5	15-106-15	1.37	22	0	0
MLAM5				5	0
MLAM5-Na1				4	1
MLAM5-Na2.5				2.5	2.5
MLAM5-Na4				1	4
MLAM5-Na5				0	5
MLtM8	14-107-14	1.41	21	0	0
MLAM8				8	0
MLAM8-Na0.4				7.6	0.4
MLAM8-Na0.8				7.2	0.8
MLAM8-Na1.6				6.4	1.6
MLAM8-Na2.4				5.6	2.4
MLAM8-Na3.2				4.8	3.2
MLtM10	11-103-11	1.39	18	0	0
MLAM10				10	0
MLtM10-Na1				9	1
MLtM10-Na2				8	2
MLtM10-Na3				7	3
MLtM10-Na4				6	4
MLtM10-Na5				5	5

[a] Midblock number-average molecular weight M_n characterized with GPC with light scattering. Difunctional midblock characteristics: PLtB5: M_n = 106 kg/mol, Đ = 1.19, mol% tBMA = 5%; PLtB8: M_n = 107 kg/mol, Đ = 1.21, mol% tBMA = 8%; PLtB10: M_n = 103 kg/mol, Đ = 1.17, mol% tBMA = 10%. Endblock M_n characterized using overall M_n (GPC) and block copolymer composition (NMR).

[b] Triblock copolymer dispersity Đ characterized with GPC with light scattering.

[c] The total mol% COOH was quantified by calculating the mol% of tert-butyl methacrylate in PLtB copolymer through ^{13}C NMR. The excessive mol% COOH in the neutralized copolymers was calculated by subtracting mol% of COONa from total mol% COOH.

[d] The mol% COONa was quantified by FTIR.

The composition and M_n of the difunctional midblock PLtB were characterized using the same methods as discussed in the previous section dealing with monofunctional

PLtB copolymers. The molecular characteristics are shown in Table 4.2. Following chain extension of midblock PLtB with methyl methacrylate, ^{1}H NMR confirmed the incorporation of PMMA endblocks in MLtM triblock copolymers, with peaks at 3.6 ppm corresponding to $–OCH_3$ in the side chain (Figure 4.5). Each endblock M_n was determined through knowledge of the midblock M_n and composition using Equation 4.3 (Table 4.2):

$$M_{n,PMMA} = M_{n,PLtB} \times \frac{A_h/3 \times 100.117}{A_c/2 \times 254.41 + xA_c/2(1-x) \times 140.20}, \quad \text{Equation 4.3}$$

in which A_h and A_c are the integration of peaks h and c, x is the mol% of tBMA characterized through ^{13}C NMR and $M_{n,PLtB}$ is the molecular weight of PLtB midblock determined by GPC. All the MLtM triblock copolymers were characterized by GPC and are summarized in Table 4.2. Upon chain extension, a clear shift of the peak to the left was observed, further confirmed the incorporation of PMMA as endblocks (Figure 4.6). In all cases, the GPC data for MLtM triblock copolymers exhibit a bimodal distribution with a shoulder on the left side, corresponding to larger molecular weight. The appearance of the shoulder is most likely due to bimolecular termination as commonly reported in RAFT polymerization. This general phenomenon is observed at high monomer conversion or when using high molecular weight macro-RAFT agent. In our case, the difunctional midblock has a relatively large molecular weight (>100 kg/mol), thus results in bimolecular termination and the high molecular weight shoulder.

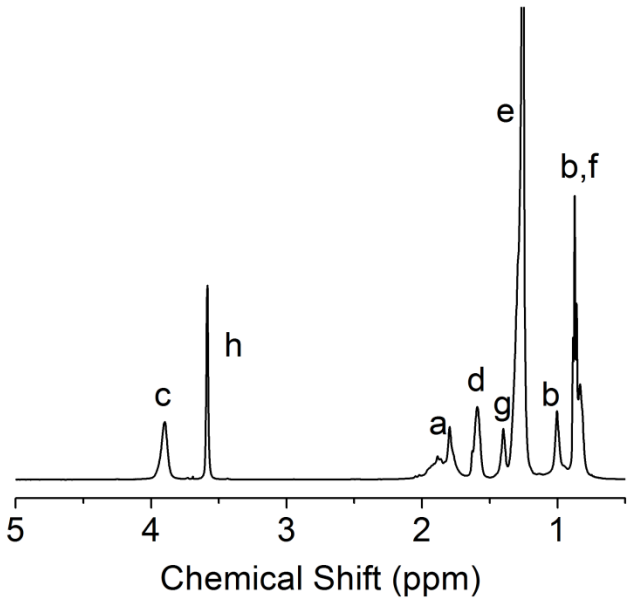

Figure 4.5 ^{1}H NMR data obtained from MLtM10. Chemical structure and peak labeling are shown in Scheme 2.5.

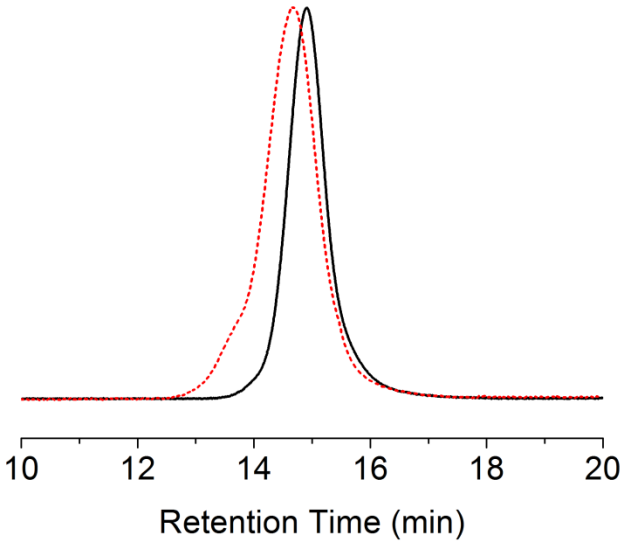

Figure 4.6 GPC data obtained from difunctional PLtB10 (black solid curve) and MLtM (red dashed curve).

4.3 Impact of ionic interactions on the viscoelastic properties of PLMA copolymers

For polymers containing dynamic crosslinks (e.g., hydrogen bonds, ionic interactions), the chain dynamics and the strength of reversible interactions play key roles in the physical properties of the polymers. The dynamic bond lifetime (τ_b), which

quantifies the time scale of the bond reversibility, can be probed by linear rheological properties of the polymers.[144-146] For all the PLtB, PLMA and PLMA-Na copolymers, the frequency (ω)-dependent dynamic moduli (G', G'') were characterized at various temperatures, and time-temperature superposition was employed to extend the range of accessible frequencies using reference temperature at 30 °C (Figure 4.7). Time-temperature superposition was effective for all samples across the accessible temperature range, indicating a single relaxation mechanism of dynamic moduli.

We firstly evaluate the PLtB copolymers, which does not contain dynamic bonds. All the PLtB copolymers exhibited Rouse dynamics at high frequency whereas the slopes of G' and G'' vs ω (on log-log scale) are 1/2 and transitioned to terminal flow region at low frequency. The G'' is higher than G' at all frequencies, characteristic of a viscoelastic liquid. The absence of plateau region of G' indicates the PLtB copolymers remain unentangled, due to ultra-high entanglement molecular weight of poly(lauryl methacrylate) (M_e =225 kg/mol[23]). After hydrolysis, the tert-butyl group was converted to a hydroxyl group which can undergo hydrogen bonding. The formation of the dynamic network by hydrogen bonds in PLMA copolymers resulted in higher moduli as compared to PLtB copolymers. The moduli increased with an increasing percentage of methacrylic acid, due to higher transient crosslink density. Upon neutralization, for most of the case, the shapes of the master curves remained the same that rouse dynamics were observed at high frequencies then transitioned to the terminal flow region. One exception is PLMA5-Na5, in which a plateau region wass observed in the intermediate frequency region, attributed to the formation of a stable physical gel through ion aggregates,[147] likely due to the complete neutralization of this sample.

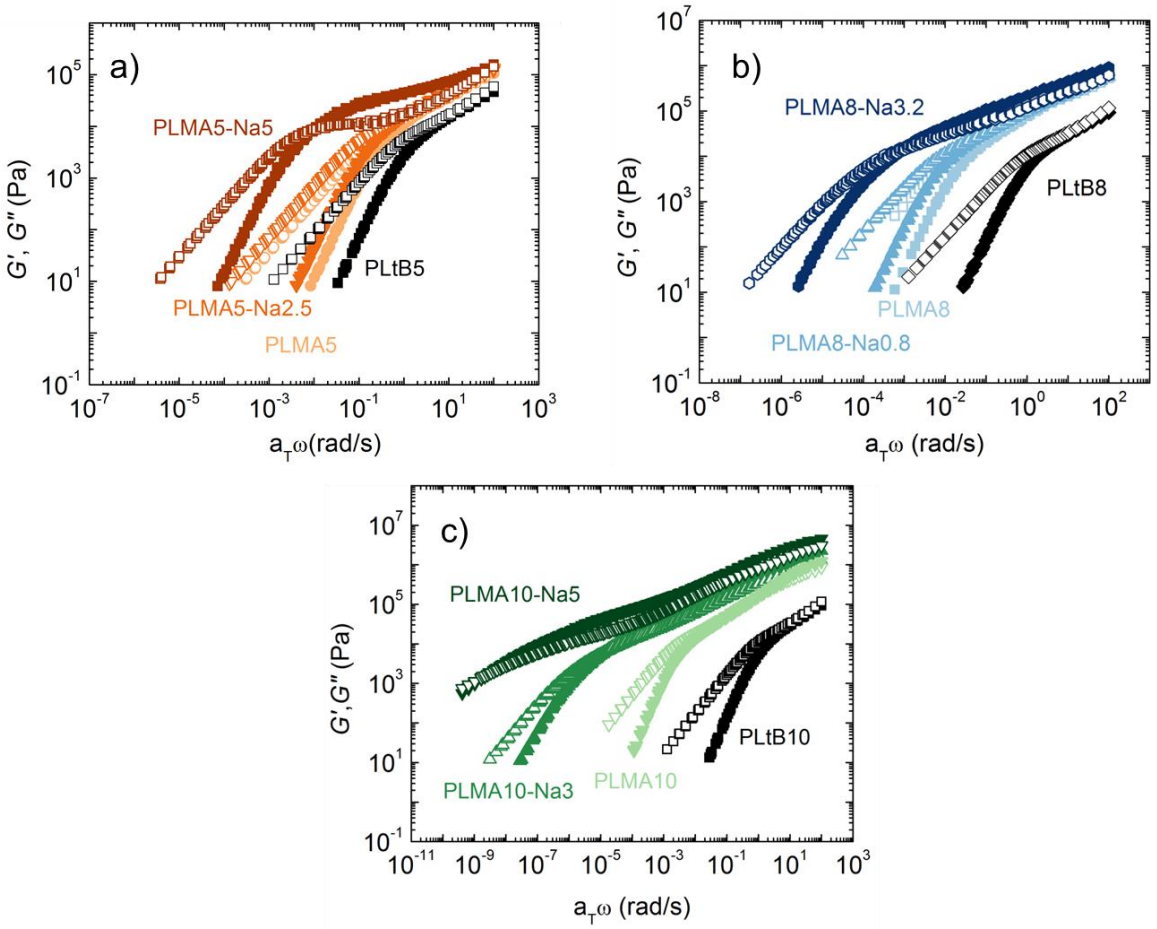

Figure 4.7 Representative master curves for a) PLtB5, PLMA5 and PLMA5-Na*Y*, b) PLtB8, PLMA8 and PLMA8-Na*Y* and c)PLtB10, PLMA10 and PLMA10-Na*Y* triblock copolymers. Reference temperature is 30 °C.

For all the PLMA and PLMA-Na copolymers, *G'* exceeded *G"* at high frequencies and became lower than *G"* at low frequencies. The crossover frequency (ω_{cr}) where *G'* = *G"* can be used to measure dynamic bond lifetime ($\tau_b = 2\pi/\omega_{cr}$).[82, 144, 146] τ_b is the characteristic time scale for the dissociation and association of the dynamic bonds responsible for the network mobility, thus it is crucial for a proper understanding of the dynamic behavior of the material.[148] It is worth noticing that the dynamic bonds will break and reform many times before finally separating, thus τ_b measured from ω_{cr} should be considered as the effective bond lifetime which is greater than the bare bond lifetime.[82] The results are tabulated in Table 4.1. It can be observed that τ_b increased

significantly with increasing ion fraction. In addition, with similar ion fraction, the τ_b also increased with increasing concentration of excess acid groups (i.e., PLMA5-Na1, PLMA8-Na0.8 and PLMA10-Na1). This observation is in accordance with that both ionic bonds and hydrogen bonds act as network crosslinkers, an increasing number of crosslinkers results in slower chain dynamics.

4.4 Presence of ionic interactions improves mechanical properties of MLAM triblock copolymers

The mechanical properties of all the MLtM, MLAM and MLAM-Na triblock copolymers were investigated by tensile testing. Representative stress-strain curves are shown in Figure 4.8. The tensile strength and strain at break for each polymer are tabulated in Table 4.3. The MLtM triblock copolymers exhibited both low tensile strength and strain at break due to lack of entanglements in the midblock. Upon hydrolysis and neutralization, both MLAM and MLAM-Na triblock copolymers showed significantly improved tensile strength and strain at break as compared to the precursor MLtM triblock copolymers. The factors of enhancement of mechanical properties ($F_{\text{Tensile strength}}$ and $F_{\text{Strain at break}}$) were calculated by dividing the tensile strength and strain at break of MLAM and MLAM-Na triblock copolymers by those of MLtM triblock copolymers (Table 4.3). The presence of hydrogen bonds in MLAM triblock copolymers is attributed to the improved mechanical properties. The $F_{\text{Tensile strength}}$ increased with increasing methacrylic acid content due to increased transient crosslink density. A slight enhancement of strain at break is observed at all methacrylic acid contents with $F_{\text{Strain at break}}$ between 1.2-1.5. Upon neutralization, the tensile strength increases significantly with increasing ion content for all three series, except MLAM5-Na5 which will be

discussed in later sections. This observation is in accordance with most of the literature reports.[149, 150] The enhanced strength was attributed to the formation of ionic clusters which can act not only as transient crosslinkers but also as reinforcing fillers. The effect of ion content on strain at break is more complicated. The strain at break remained comparable to that of MLAM precursors at low ion contents, then started decreasing after critical ion contents (> 4%, 3%, and 2% for MLAM5-Na, MLAM8-Na and MLAM10-Na series, correspondingly).

In MLAM and MLAM-Na triblock copolymers, both hydrogen bonds and ionic bonds act as sacrificial bonds (transient crosslinker). Their abilities to quickly associate and dissociate to dissipate energy are critical to the enhancememnt in mechanical properties as compared to MLtM triblock copolymers. Thus, the factors of enhancement of mechanical properties ($F_{\text{Tensile strength}}$ and $F_{\text{Strain at break}}$) are anticipated to correlate with bond dynamics. The $F_{\text{Tensile strength}}$ and $F_{\text{Strain at break}}$ were plotted as a function of midblock relaxation time measured through rheology (Figure 4.9). The $F_{\text{Tensile strength}}$ increases linearly with relaxation time on linear-log plot. The relaxation time increases with increasing number of dynamic bonds and bond strength.[151, 152] Both factors affect tensile strength in a positive way, thus $F_{\text{Tensile strength}}$ increases with relaxation time. $F_{\text{Strain at break}}$ maintained relatively stable at short relaxation times (< 10^3 s) then started dropping at long relaxation times. At short relaxation times, the dynamic bonds can associate and dissociate fast to dissipate energy that induces higher extensibility of the polymer. Thus, $F_{\text{Strain at break}}$ is higher than unity in the short relaxation time region. At long relaxation time, the chain mobility is limited by either an increased number of dynamic bonds or

slow bond dynamics which results in poor energy dissipation. Thus, at long relaxation time, though the tensile strength is improved significantly, the strain at break is sacrificed.

An outlier is identified in Figure 4.9 corresponds to sample MLAM5-Na5, that both $F_{\text{Tensile strength}}$ and $F_{\text{Strain at break}}$ are lower than other samples with similar relaxation time, which is attributed to the full neutralization. Recall from previous sections that the PLMA5-Na5 (the midblock of MLAM5-Na5) showed a plateau region of G' at intermediate frequencies, indicates a formation of a physical network due to the presence of large ion aggregates. These large ion aggregates are more stable than ion clusters or multiplets, thus exhibit slower dynamics. Previous studies have demonstrated that the excess acid can act as a plasticizer that speeds up the ion hoping rate. Therefore, the lack of excess acid in MLAM5 results in a slower ion hoping rate thus reduced mechanical properties.

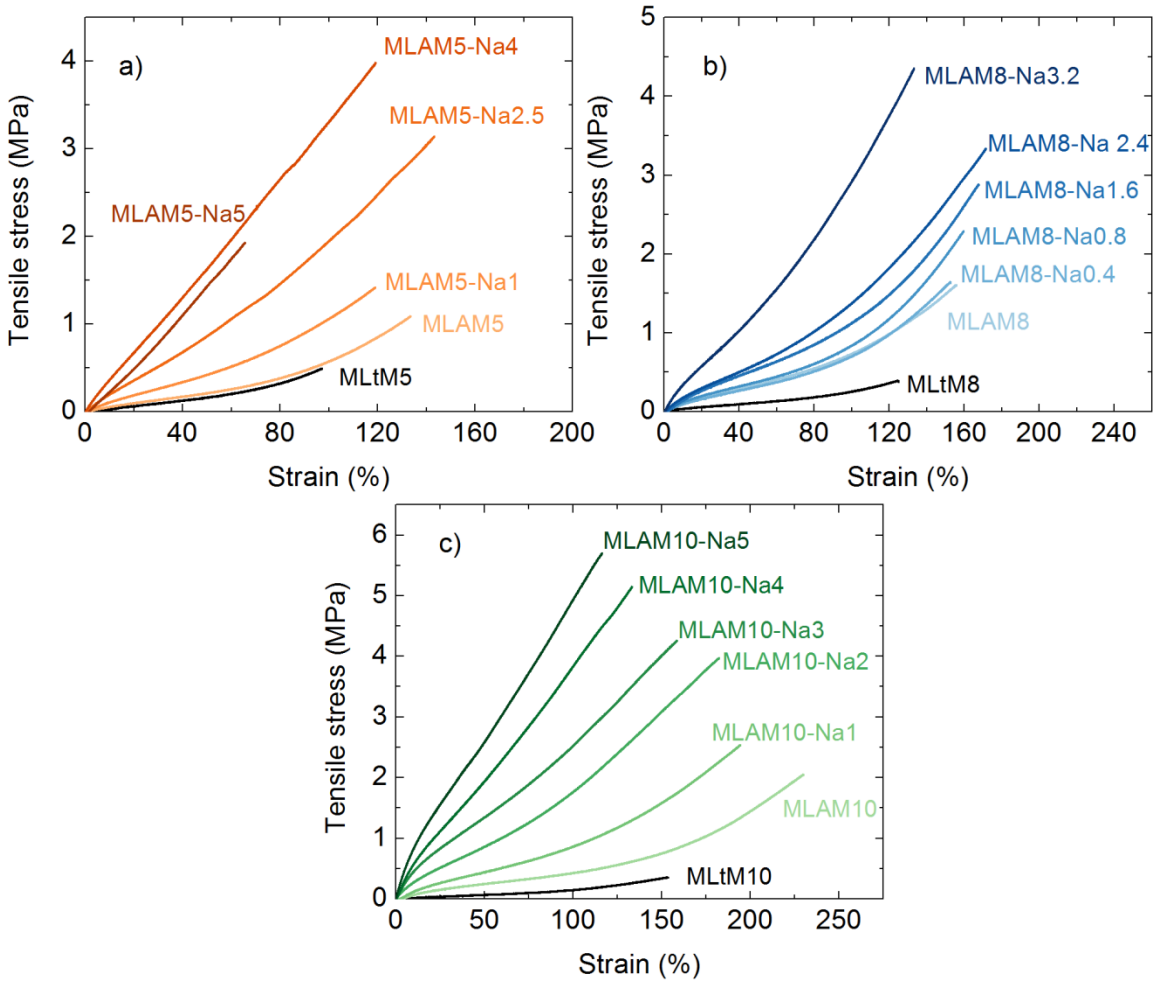

Figure 4.8 Representative stress-strain curves for a) MLtM5, MLAM5 and MLAM5-Na*Y*, b) MLtM8, MLAM8 and MLAM8-Na*Y* and c)MLtM10, MLAM10 and MLAM10-Na*Y* triblock copolymers.

Table 4.3 Mechanical properties of MLtM, MLAM and MLAM-Na triblock copolymers

Polymer Name	Tensile Strength (MPa)	Strain at break (%)	$F_{\text{Tensile strength}}$	$F_{\text{Strain at break}}$
MLtM5	0.46±0.03	96±7	/	/
MLAM5	1.11±0.23	133±8	2.4±0.2	1.4±0.3
MLAM5-Na1	1.41±0.12	142±5	3.1±0.3	1.5±0.1
MLAM5-Na2.5	3.22±0.69	142±23	7.0±1.5	1.5±0.2
MLAM5-Na4	3.7±0.64	115±13	8.0±1.3	1.2±0.1
MLAM5-Na5	1.86±0.17	57±8	4.0±0.4	0.6±0.1
MLtM8	0.39±0.11	125±19	/	/
MLAM8	1.70±0.38	150±16	4.4±1.0	1.2±0.1

Table 4.3 Continued

MLAM8-Na0.4	1.77±0.43	150±13	4.5±1.2	1.2±0.1
MLAM8-Na0.8	2.29±0.26	176±11	5.9±0.8	1.4±0.1
MLAM8-Na1.6	2.85±0.33	180±11	7.8±0.8	1.4±0.1
MLAM8-Na2.4	3.41±0.20	173±9	8.6±0.5	1.4±0.1
MLAM8-Na3.2	4.13±0.30	133±10	10.6±0.8	1.0±0.1
MLtM10	0.35±0.09	150±8	/	/
MLAM10	2.02±0.07	227±15	5.8±0.2	1.5±0.1
MLtM10-Na1	2.54±0.10	189±10	7.3±0.3	1.3±0.1
MLtM10-Na2	3.89±0.24	190±13	11.1±0.7	1.3±0.1
MLtM10-Na3	4.24±0.37	149±11	12.1±1.0	1.0±0.1
MLtM10-Na4	5.08±0.45	133±18	14.5±1.3	0.9±0.1
MLtM10-Na5	5.79±0.34	122±13	16.5±1.0	0.8±0.1

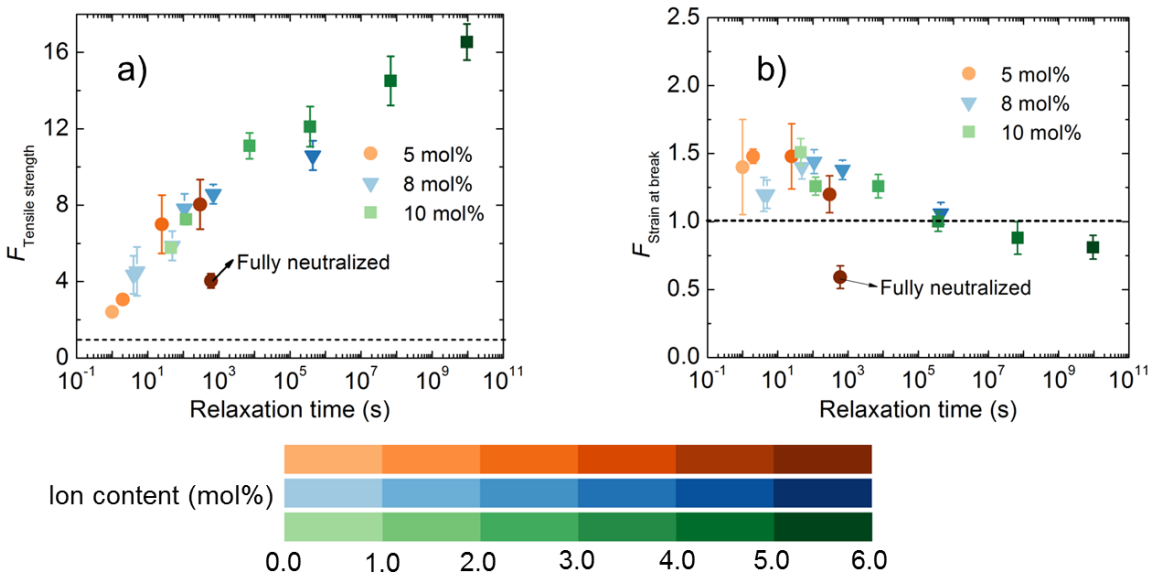

Figure 4.9 Correlation between midblock relaxation time and the factor of enhancement of a) tensile strength and b) strain at break for triblock copolymers.

4.5 Concluding remarks

Ionic bonds were introduced into fatty acid-derived thermoplastic elastomers (TPEs) to enhance their mechanical properties. The comonomer methacrylic acid was neutralized with sodium hydroxide to incorporate ionic interactions into polymers. Both

the effect of acid content and ion content on the rheological properties of the midblock and the mechanical properties of the triblock copolymers were evaluated. Increased relaxation time was observed by increasing ion content and acid content. The mechanical properties were improved significantly by the incorporation of ionic interactions. The factors of enhancement of mechanical properties were correlated with the relaxation time of the midblock. The enhancement of tensile strength increased linearly with the logarithmic of relaxation time and could achieve as high as 16 times compared to its precursor without losing much of extensibility. The strain at break could be enhanced at a low relaxation time region and started dropping at high relaxation times.

Chapter 5 *In-Situ* Shear Alignment of Triblock Copolymers with Closed Packed Spherical Morphology

In this chapter, we present the application of *in-situ* SAXS technique along with FT rheology to study the kinetic pathway of shear alignment process of a fatty acid-derived triblock copolymer with closed packed spherical morphology. The formation of closed packed spherical morphology is highly unanticipated and is attributed to the presence of a higher dispersity midblock.[31, 125] The structural evolution was correlated to the mechanical response of the material under shear. We report the first observation of shear-induced deordering of closed packed spheres in block copolymer melts. Specifically, it was found that at high strain amplitude (γ = 150%), a highly ordered closed packed spherical morphology was achieved at a short time and degenerated to be poorly ordered structure upon shearing. Additionally, we evaluate the effect of strain amplitudes on the orientational behavior of closed packed spherical layers. In medium amplitude oscillatory shear (MAOS) region, a biaxial orientation (parallel and perpendicular) of closed packed spherical layers was observed, while in large amplitude oscillatory shear (LAOS) region, only parallel orientation was observed.

5.1 Introduction

Block copolymers composed of incompatible components have been extensively studied due to their unique properties to self-assemble into microphase-separated morphologies. The self-assembly occurred spontaneously usually leads to a polydomain morphology lacking long-range order. However, many of the practical applications, such as microelectronics[153, 154], functional membranes[155], optical and photovoltaic devices[156-158], require the materials with desirable orientation and macroscopically anisotropic.

Numerous methods have developed to produce well-defined orientation, such as shear alignment[159-161], alignment in electrical field[162, 163] and magnetic field[164, 165], zone annealing[166-168], solvent vapor annealing[169-171] and pattern templated assembly[172-174]. Among them, shear alignment was shown to be a feasible approach to align block copolymer melts and concentrated solutions. There is a large body of works that deals with the shear alignment of block copolymers with spherical[175-177], cylindrical[178-180], gyroid[139, 181, 182] and lamellar[183-186] morphologies. The response of morphology to shear depends on the nature of block copolymers (e.g., architecture, molecular weight and segregation strength) and shear conditions (e.g., temperature, rate of deformation and amplitude of deformation).

The morphological response to shear has been extensively studied and well understood for block copolymers with lamellar and cylindrical morphologies. For both morphologies, three possible orientations can be achieved: parallel, perpendicular and transverse with respect to the shear flow direction.[159, 183, 184, 187-190] Under shear, the microstructure alignment tends to collectively minimize viscous dissipation and chain mixing.[191] In the case of parallel and perpendicular orientations, the concentration gradient between the microdomains is perpendicular to the velocity direction of the shear flow so that the dissimilar chains of blocks do not experience intermixing under flow. Thus, the parallel and perpendicular orientations are more stable than transverse orientation and are commonly encountered in lamellar and cylindrical systems. However, under certain conditions (e.g., high frequency in oscillatory shear[192], presence of liquid crystalline domains on the side chain[180, 193]), the transverse orientation can be achieved.

Relatively few reports have appeared on the shear alignment of sphere-forming block copolymers. The predominant lattice formed by spheres in bulk block copolymers is body-centered cubic (BCC).[175, 194-196] Recently, it has been reported that spherical morphologies can also arrange into complex lattices such as Frank-Kasper σ phase and dodecagonal quasicrystal, which are stabilized by the conformational asymmetry of the block copolymers.[177, 197-200] However, the formation of closely packed lattices (either face-centered cubic (FCC) or hexagonally close-packed (HCP)) by sphere-forming block copolymers is conspicuously absent in the majority of the literature, although the self-consistent mean-field theory has predicted the existence of closed packed spherical morphology in a narrow region in the phase diagram.[32] Huang and coworkers reported the FCC spheres in bulk block copolymers under quiescent condition.[176] Imaizumi and coworkers demonstrated the presence of FCC spheres in a bulk triblock copolymer under extensional flow field upon thermal annealing.[201] The absence of experimental observation of closed packed spherical phase is attributed to the thermal fluctuations thus disrupting the long-range order of closed packed sphere.[202, 203] Also the closed packed spherical phase was shown to be thermodynamically unfavorable, as it is superseded by disordered spherical phase due to the gain in translational entropy.[204] However, the closed packed spherical morphology can be stabilized by alleviating the packing frustrations of the block copolymer melt by various means: addition of solvent[205-207], addition of homopolymer[208, 209] and increase the dispersity[210]. Recently, our group reported the first result of closed packed spherical morphology observed in a neat block copolymer melt under shear.[125] The formation of unanticipated closed packed spherical morphology is attributed to the high dispersity of block copolymer.[125]

In most studies, as well as our previous study on the block copolymer melt forming closed packed spherical morphology, the morphological characterizations of shear alignment of block copolymers were performed ex-situ, making it difficult to study the kinetics involved in the alignment process. The invention of in-situ probe techniques, such as small angle x-ray scattering, small angle neutron scattering and birefringence allows the online monitoring of the morphological change during the alignment process, thus permit the exploration of the kinetic pathway. The majority of the literature demonstrated a monotonic change from an unaligned structure to an aligned structure upon shearing.[175, 185, 207, 211] However, it has been shown in a few studies that shear field can cause non-monotonic changes. Wang et al. found that the orientation of lamellar structure in a concentrated block copolymer solution changed from isotropic to perpendicular and then from perpendicular to disorder.[212, 213] Meins and coworkers reported similar results in a block copolymer melt that the orientation of lamellae change from isotropic to perpendicular, then change from highly ordered perpendicular to less ordered biaxial orientation.[214] These results indicate the existence of intermediate-state, so that one may suspect the "final" orientations reported by ex-situ methods may, in fact, be transient or non-equilibrium states. Thus, it is crucially important to monitor the alignment process in-situ. Moreover, the orientations and degree of order are governed by the shear protocols (e.g., duration, frequencies, temperatures and strain amplitudes), understanding mechanism and kinetics allows optimization of the alignment process and tune of process conditions for targeted application.

Previous in situ shear alignment experiments mainly focused on studying the influence of shear on the structural change through scattering techniques or birefringence,

but only a few studies have associated the morphological change to the underlying mechanical response under nonlinear flow. Recent years, Fourier transform (FT) rheology has been introduced as a tool to quantify the mechanical response to oscillatory shear in the nonlinear region by analysis of higher order harmonics in stress response.[215] The relative intensity of third harmonics ($I_{3/1}$) is shown to be sensitive to the morphological change. Therefore, it is straight forward to use $I_{3/1}$ as a mechanical response parameter to monitor the shear alignment process.[186, 214, 216, 217]

5.2 Experimental methods

5.2.1 Materials

All chemicals are purchased from Sigma Aldrich unless otherwise noted.

5.2.2 Synthesis and characterization of poly(styrene-b-lauryl acrylate-b-styrene) triblock copolymer

The poly(styrene-b-lauryl acrylate-b-styrene) (SAS) triblock copolymer was synthesized through two-steps reversible addition-fragmentation chain transfer (RAFT) polymerization. A detailed description of the synthetic procedures is described elsewhere.[111] Proton nuclear magnetic resonance (^{1}H NMR) was performed on JEOL-500 using deuterated chloroform. The number-average molecular weight (M_n) and dispersity ($Đ$) were measured by a Viscotek gel permeation chromatography (GPC) instrument. The order−disorder transition temperature (T_{ODT}) of the SAS triblock copolymer was probed using a TA Instruments DHR-2 rheometer equipped with 25mm parallel plates. The detailed description of characterizations is described elsewhere.[111] The molecular characteristics of SAS triblock copolymer are summarized in Table 5.1.

Table 5.1 Characteristic of SAS triblock copolymer

M_n of midblock (kg/mol)	57.3
M_n of triblock copolymer (kg/mol)	76.2
$Đ$	1.67
vol% of styrene in triblock copolymer	23%
T_{ODT} (°C)	220.8

5.2.3 Rheological measurement

All the ex-situ rheological measurements were performed on a strain-controlled rheometer (ARES-G2, TA instrument) equipped with cone and partitioned plate geometry (25 mm outer diameter, 10 mm inner diameter and 0.1 rad cone angle) under direct strain oscillation. Sample disks with 25mm diameter and 1mm thickness were prepared by compression molding on a Carver Hotpress at an applied load of 4200 lbs at 230 °C. Two different types of rheological tests were performed at 130 °C: (1) dynamic strain sweeps with strain amplitude ranging from 1% to 1000% were performed at frequencies of 1 and 10 rad/s. (2) dynamic time sweeps at frequency of 10 rad/s with strain amplitudes of 50%, 100% and 150%.

All the measurements were carried out using the transient data collection mode, which allows the record of stress and strain wave-form data. The data were sampled with a density of 128 points/cycle. For dynamic strain sweeps, at each strain amplitude value, 20 cycles of oscillation were performed to generate equilibrated oscillatory shear flow and only the last four cycles were analyzed. For dynamic time sweeps, the stress and strain wave-form data were collected continuously for the first 500 cycles. After that, 4

cycles of oscillation were collected for every 20 cycles. The stress and strain wave-form data were analyzed with "MITlaos" software. The storage (G') and loss (G'') from primary frequency, third-order harmonics ($I_{3/1}$), third-order viscous ($v_{3/}v_1$) and elastic ($e_{3/}e_1$) chebyshev coefficients were extracted.

5.2.4 In-situ SAXS measurements

Small-angle X-ray scattering was performed at beamline 5ID-D at the Advanced Photon Source, Argonne National Laboratory with energy of 17 keV (corresponding to an X-ray wavelength of 0.7293 Å). Two-dimensional (2D) scattering patterns were collected at a pixel resolution of 1920 × 1920 pixels using a CCD detector at a sample to detector distance of 8.5 m.

For shearing samples in-situ, a linkam CSS-450 shear cell was installed on beamline. The sample disks (19 mm diameter and 1.6 mm thickness) for SAXS measurements were prepared by compression molding on a Carver Hotpress at an applied load of 4200 lbs at 230 °C. Samples were placed between two preheated parallel pates covered with kapton tape (Scheme 5.1). The shear cell was mounted such that the velocity direction (2-3 plane) is vertical and shear gradient direction (1-3 plane) is parallel to the X-ray beam. The samples were sheared with frequency of 10 rad/s at different strain amplitudes (50%, 100% and 150%). The scattering data were collected using following proctors: 1) for strain amplitudes of 100% and 150%, the data were collected 1 frame/2 seconds with exposure time of 0.628 seconds for the first 3 min, then data collection was slowed down to 1 frame/ 6 seconds with exposure time of 0.2 second for 40 min. 2) For of strain amplitudes of 50%, the data were collected 1 frame/6 seconds

with exposure time of 0.628 second for the first 30 min, then the data collection was slowed down to 1 frame/ 12 seconds with exposure time of 0.2 second for 40 min.

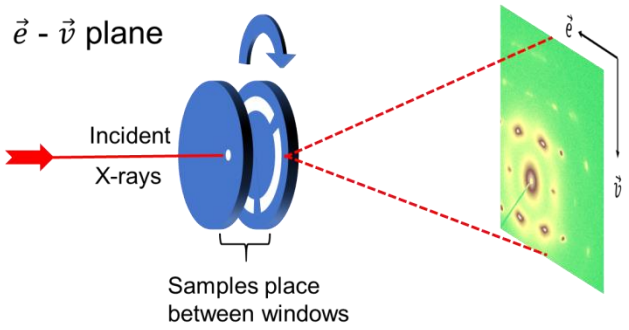

Scheme 5.1 Schematic of shear cell mounted on beamline

5.3 Disordered spherical morphology prior to shearing

The SAS triblock copolymer samples are macroscopically isotropic with randomly oriented grains, as evidenced by the isotropic ring in the 2D SAXS image (inset of Figure 5.1). The two dimensional scattering pattern was azimuthally averaged to a one dimensional profile of intensity versus scattering vector $q = 4\pi \sin(\beta/2)/\lambda$ [β is scattering angle, and λ is wavelength]. The azimuthally averaged 1D SAXS profile exhibits a sharp primary peak (q = 0.277 Å) with weak higher order peaks, indicating microphase separation. The higher order peak locations do not match with traditional equilibrium block copolymer phases (such as ordered lamellae, cylinders, or a gyroid phase), but were characteristic of a disordered spherical morphology that has been previously reported by our group.[14, 125] To better understand the morphology of unsheared sample, the 1D SAXS profile were fitted with Percus-Yevik hard spherical model (Equation 3.12-Equation 3.14). The model assumes the presence of spherical PS domains (modeled as hard spheres) with average sphere radius R_{sp}, radius of interaction R_{hs} (R_{hs} > R_{sp}) and effective volume fraction of hard spheres η.

The data fitting were performed using SasView, using combined functions of SphereModel and HardsphereStructure. The effect of size distribution of hard spheres was also incorporated into curve fitting by enabling the polydispersity function in SasView. The size distribution was characterized using $PD=\sigma / R_{sp}$, where σ is the standard deviation and R_{sp} is the hard sphere radius. The SAXS data were well-described with the Percus–Yevick model, revealing the disordered spherical morphology of SAS triblock copolymers. The parameters obtained from curve fitting were R_{sp} = 9 nm, R_{hs} = 13 nm, η = 0.55 and PD = 0.14.

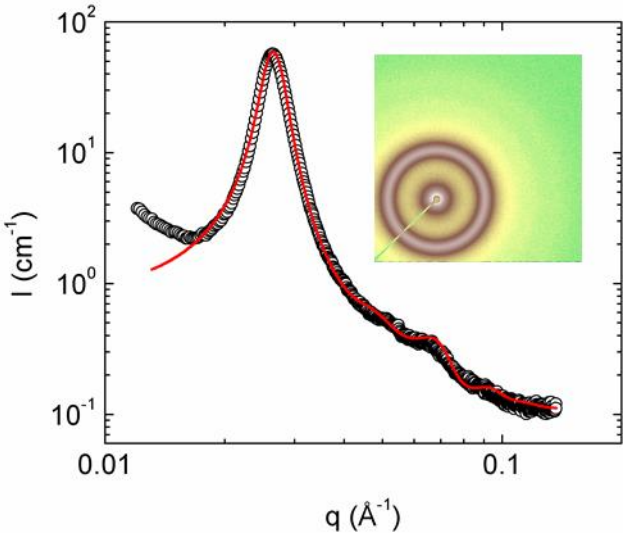

Figure 5.1 1D SAXS profile obtained from SAS triblock copolymer after compression molding (○) and Percus-Yevick hard-sphere model fit (red solid curve). Inset shows the 2D SAXS image.

5.4 Nonlinear viscoelastic behavior of SAS triblock copolymer

It is well known that the application of oscillatory shear in nonlinear regime can induce alignment of microstructure. Nonlinear regime can be determined by performing strain sweep at certain frequency. In this study, a strain sweep was performed at 10 rad/s with strain amplitudes (γ = 1%-1000%). The temperature was chosen as 130 °C, which is higher than T_g of polystyrene (103 °C) and lower than T_{ODT} of SAS triblock copolymer

(220 °C). Dynamic moduli (*G'* and *G"*) were plotted as a function of strain (Figure 5.2a). Two main regimes were observed: one is linear region, also known as small amplitude oscillatory shear (SAOS) regime in which the dynamic moduli were independent of strain (γ = 1%-10%). The other one is nonlinear regime where the dynamic moduli decreased with strain, known as strain thinning (γ = 10%-1000%). The strain thinning behavior is typically observed in polymer solution and polymer melts, originated from chain orientation and alignment of microstructure along the flow direction that reduce the local viscous drag.[218]

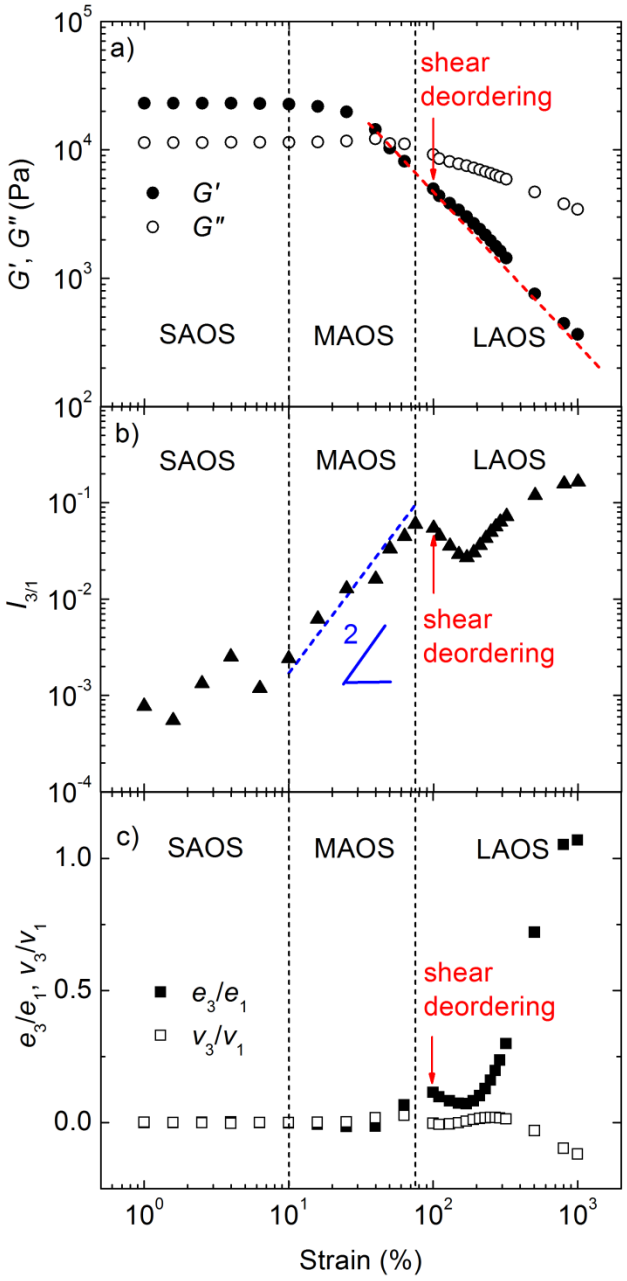

Figure 5.2 Oscillation strain sweeps of SAS triblock copolymer at 130 °C and 10 rad/s: a) dynamic moduli, b) relative third harmonic, $I_{3/1} = I_3/I_1$ and c) Chebyshev coefficients, e_3/e_1 and v_3/v_1 as functions of strain.

Even though the dynamic moduli can provide useful information in linear region, in the nonlinear regime where the higher order contributions become non-negligible, dynamic moduli are insufficient as they only provide information of first order harmonic contributions. The higher order contributions can be quantified using Fourier transform

(FT)-rheology. FT-rheology converts stress data in time domain (Figure 5.3 inset) to frequency domain (Figure 5.3), thus can quantify the weak signal of higher harmonic. Among all the higher order harmonics, the relative intensity of third order harmonics ($I_{3/1}$ = $I(3\omega)/I(\omega)$) has been proven to be powerful in quantifying the nonlinearity of materials.[218, 219] Figure 5.2b shows the $I_{3/1}$ as a function of strain. Based on different characteristics of $I_{3/1}(\gamma)$, the nonlinear region can be subdivided into two regimes: medium amplitude oscillatory shear (MAOS) and large amplitude oscillatory shear (LAOS). MAOS is an intermedium regime between SAOS and LAOS, characterized by a slope of two in the log-log plot of $I_{3/1}$ vs γ (γ = 10%-75%).[220] Interestingly, in the LAOS regime, a subregime is observed where $I_{3/1}$ decreased with strain starting at γ = 100% corresponding to a shoulder in the G' (γ). This behavior is in contract to most of the literature results that $I_{3/1}$ (γ) is sigmoidal.[215, 218, 220] The non-sigmoidal behavior has been reported for a block copolymer solution[221] and carbon black filled rubber[222]. López-Barrón *et al*[221] observed a decrease of $I_{3/1}$ in a block copolymer solution at high strain amplitude. They ascribe the non-sigmoidal behavior to be shear melting of hexagonally closed packed spheres at high strain amplitude as observed in SANS measurement. Leblanc *et al*[222] observed a "bump" in the intermediate strain amplitude due to strong interaction between a viscoelastic matrix (rubber) and a dispersed phase (carbon black). We ascribe the drop of $I_{3/1}$ at γ=100-180% to be shear deordering that will be discussed in detail in the time-resolved SAXS section.

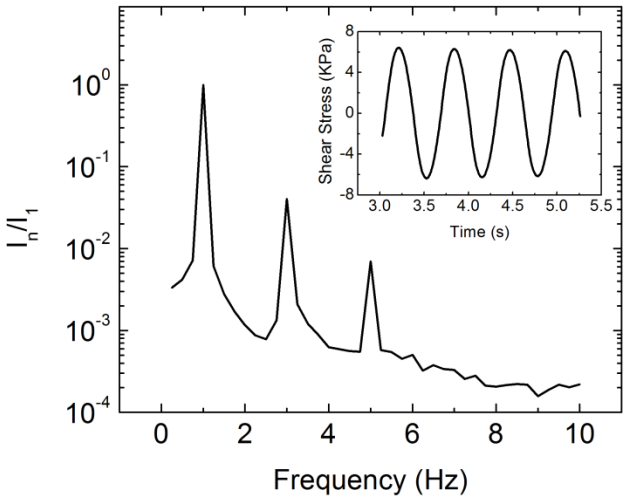

Figure 5.3 FT spectrum calculated from time-dependent shear stress (from 5th to 8th oscillation cycles) of SAS triblock copolymer under MAOS (ω = 10 rad/s, γ = 50%, T = 130 °C).

An alternative way to quantify the nonlinearity is to use the relative third order elastic and viscous Chebyshev coefficient (e_3/e_1 and v_3/v_1, respectively). Ewoldt *et al*[223] proposed stress decomposition using a set of orthogonal Chebyshev polynomials of the first kind, as defined in Equation 5.1.

$$\sigma'(\bar{x}) = \gamma_0 \sum_{\text{n=odd}} e_n(\omega, \gamma_0) T_n(\bar{x})$$

$$\sigma''(\bar{y}) = \gamma_0 \sum_{\text{n=odd}} v_n(\omega, \gamma_0) T_n(\bar{y}), \qquad \text{Equation 5.1}$$

where σ' and σ'' are the elastic stress and viscous stress, γ_0 the maximum strain, e_n and v_n the *n*th-order elastic and viscous Chebyshev coefficient, $T_n(x)$ the *n*th-order Chebyshev polynomial of the first kind, and $\bar{x} = \gamma/\gamma_0$ and $\bar{y} = \dot{\gamma}/\dot{\gamma}_0$ the normalized instantaneous strain and strain rate that provide the appropriate domains of [-1, +1] for orthogonality. The Chebyshev coefficients allow the interpretation of intracycle nonlinearity where $e_3 > 0$ indicates intracycle strain stiffening and $e_3 < 0$ represents strain

softening. Similarly, $v_3 > 0$ indicates intracycle shear thickening and $v_3 < 0$ describes shear thinning.

Figure 5.2c shows Chebyshev coefficients as function of strain. In the SAOS regime, both e_3/e_1 and v_3/v_1 are close to zero as expected. In the MAOS regime, v_3/v_1 and e_3/e_1 starts increasing with strain, indicates sample exhibits nonlinearities in both elastic and viscous response. The positive signs of v_3 and e_3 suggest intracycle shear thickening and strain stiffening. In the LAOS regime, the shear deordering starting at γ = 100% as evidenced by decrease of both v_3/v_1 and e_3/e_1, coincide with a drop of $I_{3/1}$ and a shoulder of *G'*. The decreased v_3/v_1 and e_3/e_1 suggests less contribution from strain hardening and shear thickening due to reduction of long range order as a result of shear deordering. With increasing strain amplitude (γ > 180%), e_3/e_1 increases sharply while v_3/v_1 decreases to be negative, suggests a transition from shear thickening to shear thinning at high strain values.

5.5 Time-resolved SAXS studies

To study the effect of strain on the kinetic pathway of alignment, in-situ synchrotron SAXS were performed to investigate the time dependent morphological evolution of SAS triblock copolymer under varying strain amplitude with fixed frequency (ω = 10 rad/s) at 130 °C. Three strain amplitudes were chosen at different regimes based on the results from strain sweep: 50% in the MAOS regime, 100% in the LAOS regime and 150% in the shear deordering subregime of LAOS regime. The structural evolutions were monitored over the course of 40 min and 140 min for strain amplitudes in LAOS and MAOS regimes, respectively. The data collection proctors are described in detail in experimental methods section.

The representative 2D-SAXS patterns for SAS triblock copolymer under varying strain and different time stamps are shown in Figure 5.4. At initial state (t = 0 s), the ringlike pattern in the 2D-SAXS image indicates a macroscopically isotropic morphologies with randomly oriented domains, as discussed in previous section. Upon application of oscillatory shear in nonlinear regime, diffraction spots appeared and became sharp and bright under extended shearing indicates the formation of macroscopically aligned morphologies. It is clear that the kinetics for strain amplitudes in the LAOS regime are significantly faster than that in the MAOS regime, evidenced by the fact that the well-defined diffraction spots were fully developed within 90s in the LAOS regime while in the MAOS regime, the structures were not fully developed until 40 min. The six spots pattern in the innermost ring is indicative of hexagonally-closed packed (HCP) layers (e.g., FCC [1 1 1] and HCP [0 0 0 1]).[224] The formation of HCP layers is consistent with the observed shear thinning behavior (Figure 5.2a) as the HCP layers comply easily with flow.[221, 225, 226]

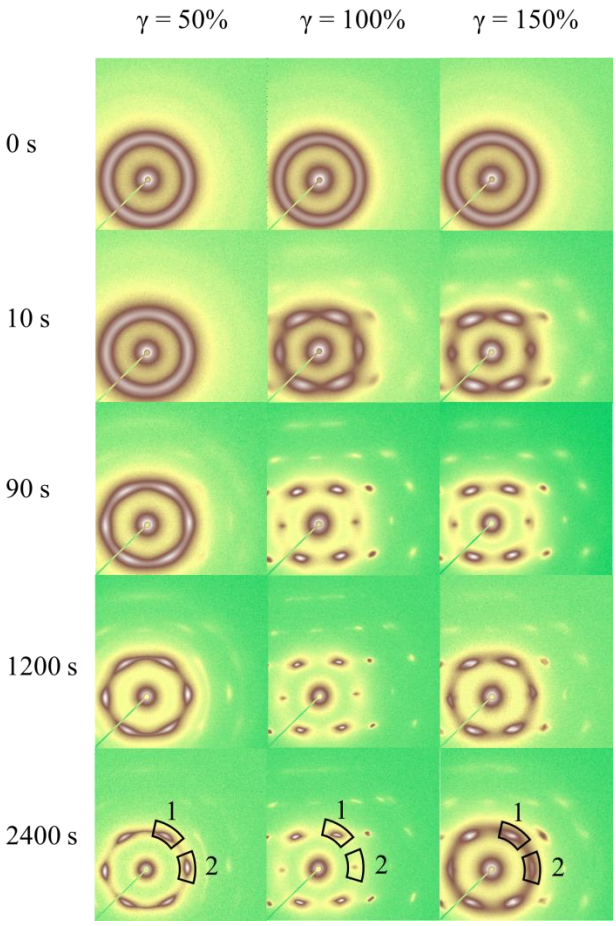

Figure 5.4 Representative 2D-SAXS data obtained on shear gradient direction with varying strain amplitudes (γ=50%, 100% and 150%) at different time stamps (t=0s, 10s, 90s, 1200s and 2400s). Shear conditions: ω = 10rad/s; T = 130 °C.

5.5.1 Effect of strain amplitudes on the orientation of HCP layers

It is worth noticing that in the LAOS regime, the two equatorial diffraction spots (Figure 5.4, peak 2) are less intensive than the other four spots. Loose and Ackerson has proposed a layer sliding mechanism that under shear, HCP layers can slide over each other in two types of motions: 1) under relatively low shear rates, the layers slide follow a zig-zag path and 2) under relatively high shear rates, the layers move follow a straight path parallel to velocity direction.[227] The theoretical calculations revealed that the zig-zag motion results in partial reduction of intensity of the two equatorial diffraction spots while the straight motion results in the disappearance of the two spots. Thus, we believe

that in the LAOS region, the HCP layers stack along shear gradient direction (the normal direction of HCP layers parallel to the shear gradient direction) and slide over each other follow a zig-zag path.

Oppositely, in the MAOS regime, the two equatorial diffraction spots are brighter than the other four spots (Figure 5.4, γ = 50%, t = 2400 s, indicated by arrows). In contrast to the fully parallel orientation in the LAOS regime, we propose that a biaxial orientation was obtained in MAOS regime with part of HCP layers perpendicular to the shear gradient direction. The hypothesis is supported by comparing the 2D SAXS data with predicted Bragg peak positions (Figure 5.5a). The locations of Bragg peaks were calculated using an internally developed program based on Microsoft Excel (freely available upon request) by inputting the space group symmetry, lattice constant and the direction of the beam. In prediction of perpendicular orientation, the [1 $\bar{1}$ 0 0] direction of HCP layer (or [1 1 $\bar{2}$] for FCC) is parallel to shear gradient direction (Figure 5.5b). The predicted Bragg peaks show good overlap with 2D SAXS data. The appearance of perpendicular orientation contributes to brighter intensity of two equatorial spots. We noticed that the biaxial orientation of HCP layers has rarely been reported. The majority of the literature results of block copolymer solutions and melts show that the HCP layers are parallel to the shear plane. Daniel *et al*[207] has reported the biaxial orientation of HCP layers for a block copolymer gel under steady shear flow at intermediate shear rate.

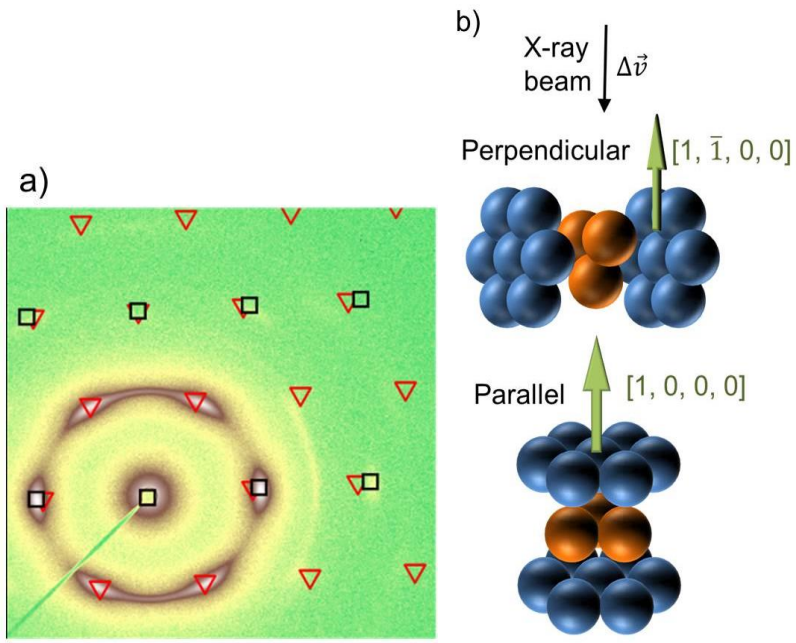

Figure 5.5 a) Comparison of 2D SAXS data obtained with γ = 50% at t = 2400 s with the predicted Bragg peaks for HCP layers parallel (red ▽) and perpendicular (black □) to the shear gradient direction. b) Scheme of relative alignment of HCP layers with the shear gradient direction (x-ray direction).

5.5.2 Kinetics of alignment process

To qualitatively study the kinetics of alignment process, the intensity as a function of azimuthal angle for innermost ring was determined, and the anisotropic factor (A_f) was calculated to characterize degree of alignment (Equation 5.2).

$$A_f = \frac{\int_0^{2\pi} I(q^*,\theta)cos[6(\theta-\theta_0)]d\theta}{\int_0^{2\pi} I(q^*,\theta)d\theta}, \qquad \text{Equation 5.2}$$

where q^* is the scattering vector of primary peak (innermost ring) and θ the azimuthal angle. The prefactor 6 was used before $(\theta-\theta_0)$ to account for six fold symmetry. A_f values are shown in Figure 6 as a function of shearing time. At early stage of shearing (180s for γ = 100% and 150%, 1800s for γ = 50%), data were collected with exposure time 0.628 s corresponds to one oscillation cycle, the curves are smooth as the stroboscopic effects were smeared out. After that, the exposure time was reduced to 0.2 s,

therefore the curves became noisy due to intracycle melting and ordering (stroboscopic effects).[221, 228]

In the MAOS region (γ = 50%), the A_f value exhibited a steep increase in the beginning and slowly approached a plateau of A_f = 0.68. In the LAOS region, both γ = 100% and 150% show much more rapid increase of A_f in the beginning than that of in the MAOS region, indicating LAOS region exhibited faster kinetics. In addition, for γ = 100%, the higher plateau value was reached with A_f = 0.75, indicating a better aligned structure was achieved. The plateau value remains constant except a slight variation due to stroboscopic effects, indicates a stable macroscopic orientation was formed despite of the continuing external mechanical excitation. In contrary, for highest strain amplitude (γ = 150%), instead of reaching a plateau, it formed a maximum at t = 180s, after which the A_f value decreased over time. The decreasing A_f indicates the macroscopic orientation was not stable under continuing mechanical stimulus. The decreased degree of alignment is also evidence as the intensity of isotropic ring (inner most ring) became stronger at t = 1200 s and 2400 s (Figure 5.5), indicating partial melting of HCP layers. Recalling from previous section that the $I_{3/1}$ decreased with strain starting at γ = 100% and G' (γ) exhibited a shoulder, we expect this behavior is related to shear deordering. The observation of shear deordering at high strain amplitude indicates that the macroscopic ordering under oscillatory shear is a complex process, the degree of alignment is not only affected by the shear conditions (frequency, strain amplitude, temperature), but also affected by the duration of applied shear.

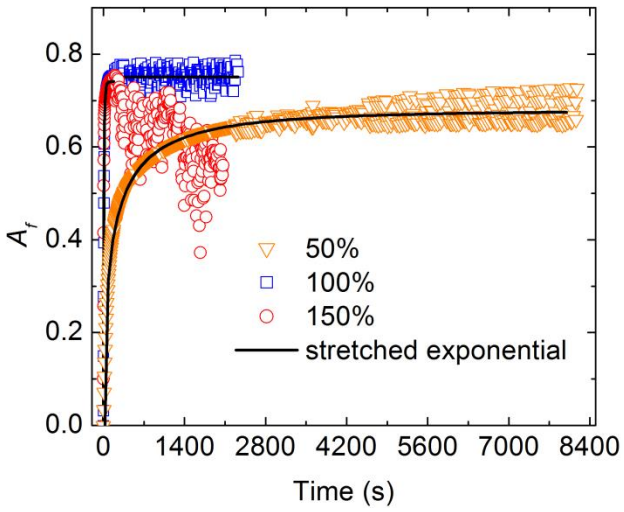

Figure 5.6 Anisotropic factor (A_f) as function of shearing time for γ = 50% (yellow ▽), 100% (blue □) and 150% (red ○). The solid lines are stretched exponential fitting.

We noticed that the shear deordering has rarely been reported. Wang et al[213] reported shear induced disordering of a concentrated diblock copolymer solution under reciprocating shear field with high frequency. At short time, a well-defined perpendicular lamellar morphology was observed. However the structure was disordered towards a poorly defined parallel orientation under continuous mechanical stimulus. Similarly, Meins and coworkers observed shear deordering of a diblock copolymer melt under LAOS with high strain amplitudes.[214] The perpendicular lamellar morphology formed in the beginning was destructed, and a biaxial orientation was formed under prolonged shearing. To the best of our knowledge, we are the first report on the shear deordering of block copolymer with closed packed spherical morphology. The question remains whether these phenomena are a common occurrence in other block copolymers with varying morphologies (e.g., cylindrical, body-centered cubic).

To quantitatively study the kinetics of shear alignment, the time dependence of A_f values are fitted with stretched exponential function (Equation 5.3). The stretched

exponential function is modified to adopt the boundary conditions for the time dependence of A_f values that when $t = 0$, $A_f = 0$ and when $t = \infty$, $A_f = A_{f,0}$

$$A_f = A_{f,0}\left(1 - e^{-\left(\frac{t}{\tau}\right)^{\beta}}\right), \qquad \text{Equation 5.3}$$

where $A_{f,0}$ is the plateau value, τ the characteristic alignment time and β the "heterogeneity index" that represents the width of alignment time distribution. The stretched exponential function has been widely used to describe the time dependent shear-induced alignment process.[186, 214, 229] The disordered polymer melts possess heterogeneous grain size, shape and orientation, thus a broad distribution of orientation time τ is usually observed which results in deviation from ideal single exponential function ($\beta = 1$). The fitted exponential function curves are shown in Figure 5.6 as solid lines and fitting results are tabulated in Table 5.2. Note that for γ = 150%, only the data for the first 180s were fitted (before the onset of shear deordering).

Table 5.2 The fitting results of time dependent A_f, normalized moduli (G', G'') and $I_{3/1}$ at various γ to stretched exponential function.

A_f			
γ	$A_{f,0}$	τ (s)	β
50%	0.67 ± 0.002	210 ± 5	0.50 ± 0.05
100%	0.75 ± 0.002	10 ± 0.5	0.67 ± 0.08
150%	0.74 ± 0.004	7 ± 0.6	0.75 ± 0.08
Normalized G'			
γ	G_0'	τ (s)	β
50%	0.55 ± 0.002	25 ± 1	0.44 ± 0.02
100%	0.82 ± 0.002	9 ± 1	0.80 ± 0.08
150%	0.86 ± 0.001	8 ± 1	0.86 ± 0.08
Normalized G''			
γ	G_0''	τ (s)	β
50%	0.70 ± 0.003	39 ± 2	0.39 ± 0.02
100%	0.84 ± 0.002	8 ± 1	0.85 ± 0.09
150%	0.91 ± 0.003	5 ± 1	0.95 ± 0.05
$I_{3/1}$			
γ	$I_{3/1,0}$	τ (s)	β
50%	-0.13 ± 0.005	43 ± 3	0.25 ± 0.02

Table 5.2 Continued

100%	0.025 ± 0.001	31 ± 2	0.72 ± 0.10
150%	0.026 ± 0.001	16 ± 2	0.71 ± 0.08

As expected, $A_{f,0}$ increased with strain amplitudes while τ decreased, indicating larger deformations results in higher degree of alignment and faster kinetics. It is obvious that orientation time τ exhibited broad distribution as β is far away from ideal case (β=1). The fact that β increased with strain amplitude indicates the defects (e.g., heterogeneity in grain size, grain orientation) can be effectively removed by applying larger deformation. The results described above are consistent with literature reports.

5.5.3. Implication of alignment mechanism

To understand the mechanism of the alignment process, the 2D SAXS data obtained at early stage of the alignment process (180s for γ = 100%) were azimuthally averaged and compared (Figure 5.7). Several noticeable changes of 1D SAXS data were taken place during the process of alignment. Firstly, the primary peak became sharper and it shifted to be at lower q value (from 0.0266 Å to 0.0255 Å), indicate the rearrangement of structure such that the domain spacing became larger and a well-ordered structure was formed. Secondly, the peak corresponds to a maximum in Percus-Yevick structure factor disappeared (indicated by black arrow in Figure 5.7) and new peaks at q = 0.0425 Å and q = 0.0512 Å corresponding to $\sqrt{3}q^*$ and $\sqrt{4}q^*$ showed up.

Previous researchers have proposed mainly two types of mechanisms: grain rotation[178, 216, 230]and domain dissolution and reformation (or melting and recrystallization)[159, 195, 231]. The grain rotation requires the initial sample to be consisting of grains with well aligned structure within each grain, but not aligned with respect to each other. Under shear, the grains remain intact and rotate as hard body to the preferred

orientation. For domain dissolution and reformation mechanism, the domains with unflavored orientation are firstly melted and then reformed piece by piece with preferred orientation to achieve globally aligned structure. In our case, on the basis of above observations, the domain dissolution and reformation mechanism were proposed for the alignment process. The dissolution of domain is confirmed by the disappearance of the peak from Percus-Yevick structure factor, indicates the melting of disordered spherical structure in the sample. Meanwhile, the new domains with closed packed spherical structure were formed as evidenced by the appearance of the new peaks at $\sqrt{3}q^*$ and $\sqrt{4}q^*$.

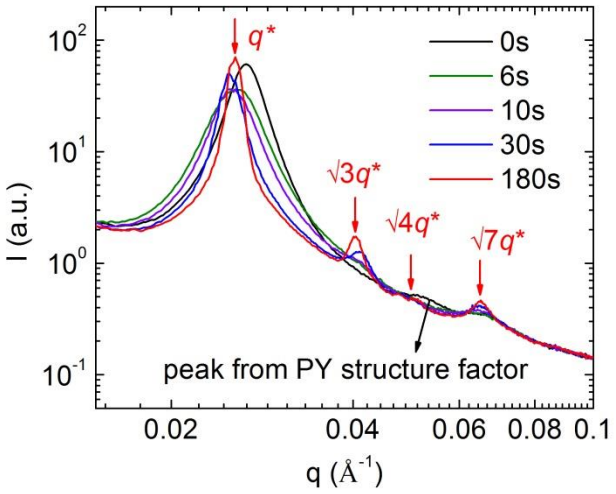

Figure 5.7 1D azimuthally averaged SAXS profile obtained at different time stamps (0s, 6s, 10s, 30s and 180s) for shear condition with γ = 100%.

5.6 Fourier-transform rheology study

To correlate morphological properties (e.g., degree of alignment, grain orientation) with rheological properties (e.g., moduli, nonlinearity), the orientation process of SAS triblock copolymer under the same shear conditions (T = 130 °C, ω = 10 rad/s, γ = 50%, 100% and 150%) were performed using ARES-G2 rheometer with cone partitioned-plate geometry. The data were recorded with transient mode, and the first-

order moduli (*G'* and *G"*) as well as relative third harmonics ($I_{3/1}$) were obtained by analyzing stress responses to imposed oscillatory shear using "MITLaos".

To qualitatively compare the time progress of moduli under different strain amplitudes, both storage and loss moduli were normalized by their maximum value (normalized $G' = G'/G'_{max}$, normalized $G'' = G''/G''_{max}$). The time dependences of normalized moduli are shown in Figure 5.8. The time progress of moduli is similar to that of A_f values discussed in previous section. Under all the shear conditions, both storage and loss moduli exhibited an initial sharp decrease due to the removal of defects and the formation of HCP layers that comply easily with flow. For both γ = 50% and 100%, the moduli reached plateau values indicating stable structures were formed, consistent with morphological observations under SAXS. In contrary, for γ = 150%, the moduli reached a minimum value at short time then increased upon continuous shearing. Recall that from in-situ SAXS, we observed that A_f value reached a maximum then decreased with time, indicates shear induced melting. Similarly, we attribute the increase of moduli to the increased number of defects as results of shear melting.

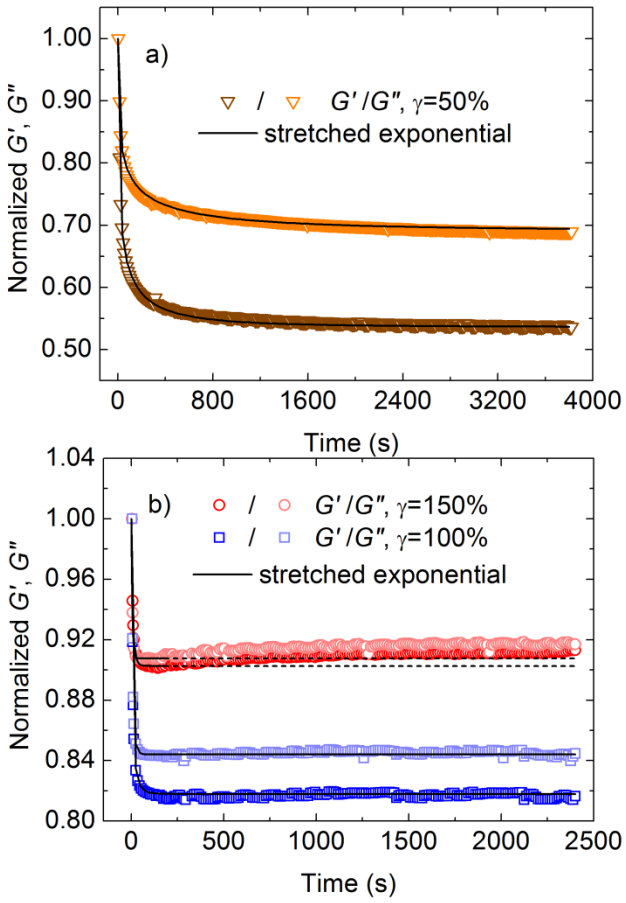

Figure 5.8 Normalized moduli (*G'* and *G"*) as a function of time under a) MAOS (γ = 50%) and b) LAOS (γ = 100% and 150%). The solid lines are stretched exponential fittings. The dashed lines are plotted for visual guides that are not part of the fitting.

The time progresses of storage modulus under various strain amplitudes are modeled with stretched exponential function (Equation 5.4).

$$\text{Normalized } G' = (1 - G_0')\left(e^{-\left(\frac{t}{\tau}\right)^{\beta}} - 1\right) + 1, \qquad \text{Equation 5.4}$$

where G_0' is the plateau value. The time progresses of normalized *G"* can be fitted similarly, with $G_0^{"}$ as the plateau value. The fitting results are plotted in Figure 5.8 as solid lines. Note that for γ = 150%, only the data for the first 180s were used for fitting. The dashed lines are plotted as visual guides. The fitting parameters are tabulated in Table 5.2. The results are similar to that observed for the time progresses of A_f values.

The speed of ordering process is greatly improved when the strain amplitudes increases from MAOS regime to LAOS regime. Same observation was found for heterogeneity index as results of better removal of defects under larger amplitudes.

However, the normalized moduli do not provide much information as the stress curves become distorted under MAOS and LAOS flow. Therefore, more analysis needs to be done to analyze the non-sinusoidal stress data. Here, we examined the nonlinear stress data using the ideas developed in FT-rheology. The relative intensity of third harmonics ($I_{3/1}$) was chosen to monitor the alignment process. Previous studies have shown that $I_{3/1}$ is sensitive to the microstructural change, thus it is suitable to be used to assess the macroscopic orientation process.[186, 214, 217, 229] The results are shown in Figure 5.9. Two completely different behaviors were observed. In the MAOS region, $I_{3/1}$ was found to increase during the shearing process while in the LAOS region, $I_{3/1}$ decreased upon shearing. Generally, $I_{3/1}$ is proportional to the number of defects. Under shear flow, the interfaces of grains (defects) undergo deformation that give rise to the nonlinear stress response. Typically, during the shear alignment process, the number of defects is anticipated to decrease as the microdomains get more and more oriented, thus results in lower $I_{3/1.}$ This rationale explains the observation in the LAOS region that $I_{3/1}$ decreased upon shearing.

It is quite unusual that $I_{3/1}$ increased with time in the MAOS region. The increase of $I_{3/1}$ has been reported by Oelschlaeger et al in the case of block copolymer with lamellar morphology, upon reorientation from parallel to perpendicular the $I_{3/1}$ become larger over time, due to the formation of differently oriented domains during reorientation process.[186] It has also been reported for the orientation of liquid crystal under oscillatory

shear. With relatively small strain amplitude (in nonlinear regime), the shear flow did not result in well-oriented lamellar structure. Thus, differently oriented grains showed various stress levels, especially at the grain boundary, which results in more distorted macroscopic stress curves. In our results, in the MAOS region, $I_{3/1}$ increased sharply then reached a plateau. Recall from in-situ SAXS section, a coexistence of parallel and perpendicular orientations of HCP layers were identified. Thus, we hypothesize that upon shearing, part of the parallel HCP layers reoriented to the perpendicular direction, which results in increased number of defects (boundary between grains) and therefore larger $I_{3/1.}$

The time progresses of $I_{3/1}$ under various strain amplitudes are also modeled with stretched exponential function:

$$I_{3/1} = I_{3/1,0} e^{-\left(\frac{t}{\tau}\right)^{\beta}} + C. \qquad \text{Equation 5.5}$$

The fitting results are plotted on Figure 5.9 as solid lines and the fitting parameters are tabulated on Table 5.2. The negative value of $I_{3/1,0}$ is indicative of increase of $I_{3/1}$ with time (e.g., γ = 50%), while positive value represent decrease with time (e.g., γ = 100% and 150%). Similar to the fitting results obtained from A_f and normalized moduli, the characteristic ordering time decreased when increasing strain amplitudes, indicating faster dynamics at higher strain amplitudes, and the heterogeneity index β increase with strain amplitudes, indicating more homogeneous grain size distribution was achieved at higher strain amplitudes. It is worth noticing that the values of τ and β are method dependent (i.e., the values of τ and β obtained from A_f differ from that obtained from $I_{3/1}$), however, the trend of each parameter change with strain amplitudes are clear that increase of strain amplitudes results in smaller τ and larger β.

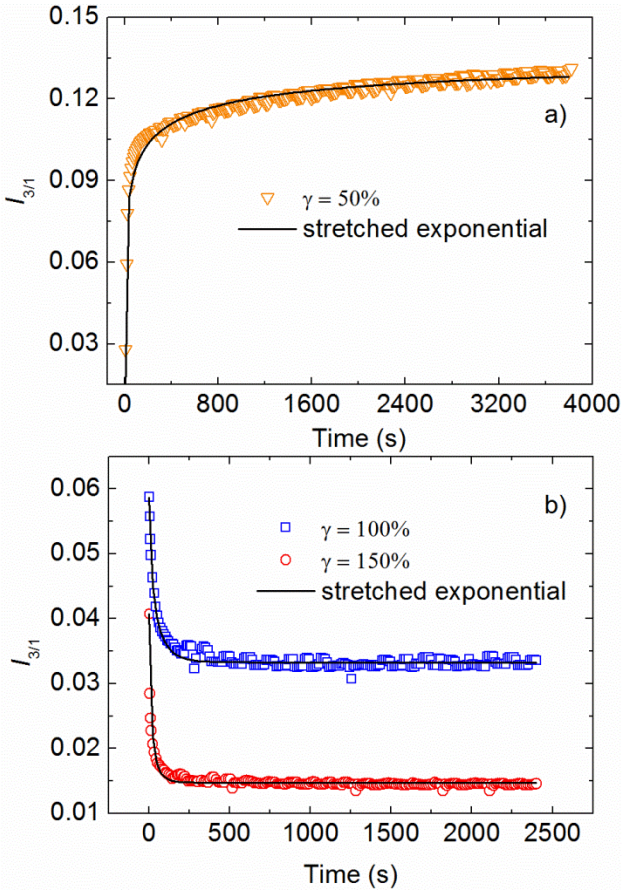

Figure 5.9 a) Time progresses of $I_{3/1}$ under MAOS (γ = 50%) and b) LAOS (γ = 100% and 150%). The solid lines are stretched exponential fittings.

5.7 Concluding remarks

In this study, we investigated kinetics and mechanism in the alignment process of poly(styrene-*b*-lauryl acrylate-*b*-styrene) triblock copolymers with initially disorder spherical morphology that transit to closed packed spherical morphology under nonlinear oscillatory shear. The time-dependent microstructural changes were evaluated using in-situ SAXS. At fixed temperature (T = 130°) and frequency (ω = 10 rad/s), change strain amplitude induced two types of orientations of HCP layers: 1) biaxial orientation in MAOS region (γ = 50%) that HCP layers are both parallel and perpendicular to shear gradient direction and 2) parallel orientation in LAOS region (γ = 100% and 150%).

Increasing strain amplitudes resulted in not only faster ordering process but also higher degree of orientation. Interestingly, for the first time, we observed shear deordering in closed packed spherical morphology under oscillatory shear at highest strain amplitude (γ = 150%). It was shown that at short time (180 s), a highly ordered closed packed spherical morphology was achieved, however, it degenerated to be less ordered structure upon extended shear. The domain dissolution and resolution mechanism was proposed for the ordering process that the unfavored disordered spherical structure was firsted melted followed by the reformation of the preferred closed packed spherical structure.

The correlation between morphological change and mechanical response was investigated by FT-rheology. For all the shear conditions, both *G'* and *G"* decreased significantly upon ordering due to the formation of HCP layers that exhibit less resistance to the flow. At γ = 150%, the moduli initially decreased sharply followed by a slight increase, manifested the shear deordering process observed with in-situ SAXS. Two completely opposite behavior of time-dependent change of nonlinearity $I_{3/1}$ were observed: 1) increase with time in MAOS region and 2) decrease with time in LAOS region. The decrease of $I_{3/1}$ in the LAOS region is anticipated during ordering process due to continuous removal of defects thus less grain boundaries. The unexpected increase of $I_{3/1}$ in the MAOS region is hypothesized to originate from the biaxial orientation which resulted in sharp grain interphase that give rise to increased $I_{3/1}$.

Chapter 6 Develop Sustainable Triblock Copolymers with Rosin Derived Endblocks

In this chapter, we report the synthesis of triblock copolymers containing a traditional acrylate midblock, poly(*n*-butyl acylate), and rosin-derived endblocks composed of poly(dehydroabietic ethyl methacrylate) (PDAEMA) via atom transfer radical polymerization (ATRP). A series of triblock copolymers with different block ratios yet constant midblock molecular weight were synthesized. The triblock copolymers exhibited microphase separated morphologies, accessible order-disorder transitions, and elastomeric behavior, suitable for TPE applications. The effect of the block ratio on the physical properties of the triblock copolymers was investigated.

6.1 Synthesis of DnBD triblock copolymers

DnBD triblock copolymers of varying block ratios, yet containing the same midblock molecular weight, were prepared in a two-step procedure using ATRP. First, the difunctional macroinitiator Br-PnBA-Br was synthesized using diethyl *meso*-2,5-dibromoadipate as difunctional initiator and $NiBr_2(PPh_3)_2$ as catalyst at 85°C following reported procedures.[109] The ^1H NMR spectrum is given in Figure 6.1. Characteristic peaks associated with the vinyl group of *n*-butyl acrylate at 6.3, 6.1 and 5.7 ppm disappeared upon polymerization, accompanied by the appearance of a broad peak associated with -OCH_2- at 4.0 ppm. The M_n of the Br-PnBA-Br macroinitiator was determined to be 76 kg/mol by GPC using a triple detection system.

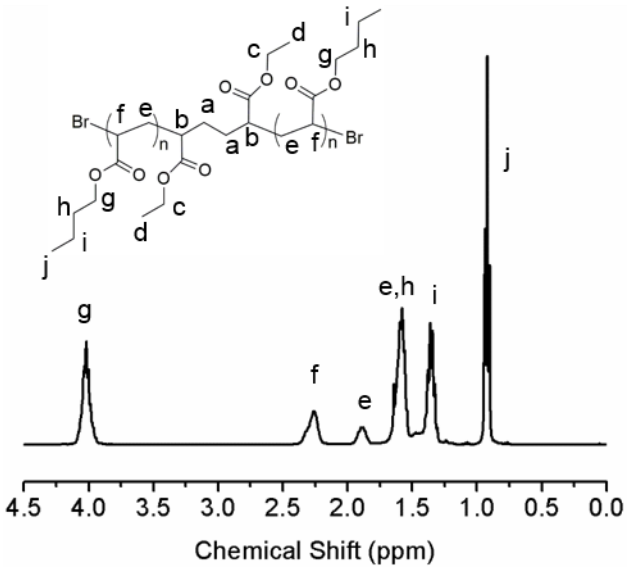

Figure 6.1 ^{1}H NMR spectrum obtained from Br-PnBA-Br (peaks a-d are not observable due to high molecular weight).

Next, DnBD triblock copolymers were synthesized by chain extension of the Br-PnBA-Br macrointiator via ATRP. CuCl was used as the Cu(I) species to invoke halogen exchange and to enhance the rate of initiation over the rate of propagation.[24] In order to optimize the synthetic condition for the chain extension, different ligands and solvents were tested. For the first series, the Me_6Tren ligand was chosen for its high activity,[232] and the reactions were carried out in three solvents (anisole, THF, DMF; Table 6.1, entries 1-3). Compared to anisole, THF and DMF gave higher conversion, likely due to the higher polarity of THF and DMF resulting in better solubility of the catalyst.[233] Thus, DMF was chosen as the suitable solvent for this reaction. Next, three ligands (PMDETA, dNbpy, Me_6Tren; Table 6.1, entries 3-5) were explored to optimize synthetic conditions. Higher conversion was achieved when PMDETA and Me_6Tren were used, likely due to the higher activity of both ligands.[232] Thus, CuCl/PMDETA and DMF were employed for all subsequent reactions to provide the highest conversion.

Table 6.1 Effect of reaction conditions on monomer conversion and dispersity of DnBD triblock copolymers[a]

Entry	[DAEMA]/ [PnBA]	Solvent	Ligand	Conversion[b] (%)	$M_{n,\ DnBD}$[b] (kg/mol) (PDAEMA-PnBA-PDAEMA)	Đ[c]
1	180	anisole	Me_6Tren	17	6.3-74-6.3	1.53
2	180	THF	Me_6Tren	33	12-74-12	2.26
3	180	DMF	Me_6Tren	32	11-81-11	1.43
4	180	DMF	dNbpy	15	5.6-74-5.6	1.36
5	180	DMF	PMDETA	35	13-81-14	1.40

[a] [PnBA]:[CuCl]:[Ligand] = 1:2:2, $[PnBA]_0=1.76\times10^{-3}$ M for all the reactions
[b] ^{1}H NMR analysis, theoretical M_n calculated from the monomer conversion.
[c] Đ was measured by GPC (light scattering, with triple detection)

A series of DnBD triblock copolymers with differing overall molecular weight and composition while keeping the M_n of midblock constant was successfully synthesized. The GPC data (Figure 6.2) show a distinct shift to higher molecular weight upon chain extension of PnBA to DnBD triblock copolymer. Chain extension was also confirmed by ^{1}H NMR (Figure 6.3), in which new signals for the aromatic protons of PDAEMA end blocks appeared at 6.80-7.15 ppm. The molar ratio of DAEMA repeat units to BA repeat units was calculated using Equation 6.1:

$$\frac{\mathrm{mol}_{DAEMA\ repeat\ units}}{\mathrm{mol}_{nBA\ repeat\ units}} = \frac{\frac{A_o}{3}}{\frac{A_{g,k}}{2} - \frac{2}{3}A_o}, \qquad \text{Equation 6.1}$$

where A_o is the integration area of aromatic protons in DAEMA moiety (labeled O_1, O_2 and O_3 in Figure 3), and $A_{g,k}$ the integration area of methylene protons next to the ester groups from both DAEMA and nBA units. The molecular weight of each PDAEMA block ($M_{n,PDAEMA}$) was further calculated using Equation 6.2:

$$M_{n,PDAEMA} = \frac{1}{2} M_{n,PnBA} \left(\frac{M_{DAEMA}}{M_{nBA}} \right), \qquad \text{Equation 6.2}$$

where $M_{n,PnBA}$ is the molecular weight of the PnBA macroinitiator (characterized by GPC), and M_{DAEMA} and M_{nBA} are the molecular weights of DAEMA and nBA monomers (412.58 and 128.17 g/mol, respectively). The characteristics of the DnBD triblock copolymers are summarized in Table 1.

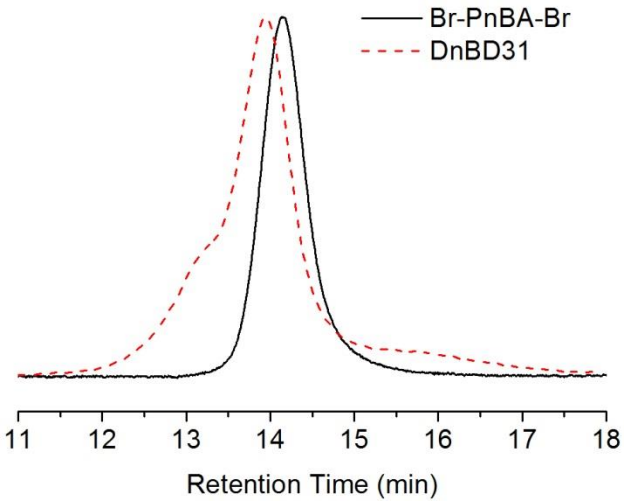

Figure 6.2 GPC data obtained from the Br-PnBA-Br macroinitiator (black solid curve) and DnBD31 triblock copolymer (red dashed curve).

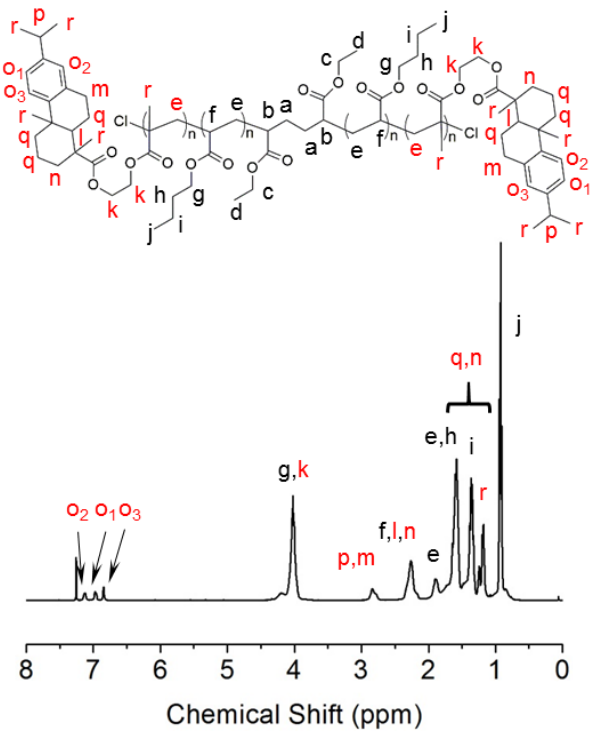

Figure 6.3 ^{1}H NMR spectrum obtained from DnBD.

In all cases, trimodal molecular weight distributions were observed, and the dispersity values were greater than 1.4 (Table 6.2 and Figure 6.2). The synthesis of PDAEMA homopolymer using ATRP has been previously reported, and the homopolymers had high dispersities (Đ =1.33 and 1.6 in ref. [75]). We therefore expect that PDAEMA blocks in DnBD have similarly high dispersities. There are several possible explanations for the presence of trimodal distributions in DnBD. The presence of the higher molecular weight shoulder is most likely due to chain coupling which is sometimes unavoidable in the synthesis of high molecular weight polymers.[234, 235] The shoulder on the right hand side of the primary peak was found to have higher retention time than that of the PnBA midblock, and therefore is not attributed to PnBA midblock which is not chain extended. One possible explanation for this low molecular weight

shoulder is the thermal self-initiation of DAEMA, as observed in other ATRP synthesis with relatively high temperature (90°C in this study).[236]

Table 6.2 Characteristics of triblock copolymers[a]

Triblock Copolymer	$M_{n,endblock}$ – $M_{n,midblock}$ – $M_{n,endblock}$ (kg/mol) [b]	Endblocks content (mol % / vol%)[b]	Đ[c]	T_{ODT} (°C)[d]	d (nm)[f]
DnBD33	20-76-20	14 / 33	1.57	185	39.2
DnBD31	18-76-18	13 / 31	1.48	175	37.6
DnBD30	17-76-17	12 / 30	1.61	175	36.9
DnBD26	14-76-14	10 / 26	1.53	155	34.9
DnBD23	12-76-12	11 / 23	1.45	145	31.4
DnBD21	10-76-10	9 / 21	1.66	<110[e]	31.3
MnBM35	21-76-21	40 / 35	1.15	> 250	34.4

[a] Macroinitiator: 76 kg/mol; Đ= 1.16, [Br-PnBA-Br]:[CuCl]:[Ligand] = 1:2:2, [DAEMA]: [Br-PnBA-Br] varied from 180:1 to 310:1. Solvent: DMF, temperature: 90°C, reaction time: 24 hours, conversion varied from 30% to 40%. [MMA]:[Br-PnBA-Br]:[CuCl]:[dNbpy] = 840:1:2:4, Solvent: DMF, temperature: 90°C.
[b] Measured by ^{1}H NMR analysis (GPC analysis with light scattering was employed to characterize the PnBA block M_n).
[c] Measured by GPC (light scattering)
[d] Measured by rheology
[e] The ODT was not observed in the rheology experiment. Above 110 °C, the rheological behavior was consistent with that of a viscoelastic liquid. The sample therefore became disordered in the vicinity of the endblock T_g.
[f] Domain spacing, d, determined from SAXS ($d = 2\pi / q^*$)

6.2 Microphase separated morphology of DnBD triblock copolymers

Small angle x-ray scattering (SAXS) was employed to study the morphology of DnBD triblock copolymers. Figure 6.4 shows 1D integrated SAXS profiles for DnBD triblock copolymers. All samples exhibited a principal scattering peak (located at q^*), indicating the presence of microphase separated structures on the order of 31-38 nm (Table 6.2, determined as $d = 2\pi / q^*$). Well-defined higher order peaks were not observed in most samples, except DnBD33, suggesting lack of long-range order. Increasing the molecular weight of the PDAEMA blocks at constant PnBA block molecular weight led

to an increase in the *d*-spacing (Table 6.2). For the case of DnBD33, higher order peaks were observed, with the ratios of the relative peak positions at q^*: $\sqrt{4}q^*$: $\sqrt{7}q^*$, where q^* is the primary peak location, consistent with a cylindrical morphology. The missing peak at $\sqrt{3}q^*$ is likely due to combined effects of a form factor minimum and structure factor peak at that location (which may coincide at certain cylinder volume fractions).[237, 238]

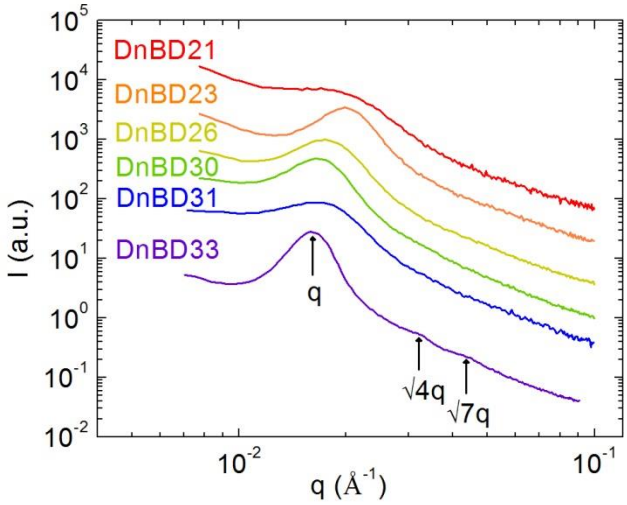

Figure 6.4 1D SAXS profiles of DnBD triblock copolymers. Data are shifted vertically for clarity.

The microphase separated morphologies of DnBD triblock copolymers were confirmed through DSC analysis of the T_g's of the PDAEMA and PnBA domains (Figure 6.5). The T_g of the PnBA block was observed at -43°C for all DnBD triblock copolymers and was consistent with that of a PnBA homopolymer (measured to be -47°C). DnBD triblock copolymers with high PDAEMA content (30-33 vol%) also exhibited a higher temperature T_g (in the range of 92-95 °C), associated with the PDAEMA block (the T_g of a PDAEMA homopolymer was reported to be 90 °C in ref. [75]). At lower PDAEMA content (21-26 vol%), the PDAEMA T_g was not observed, likely due to lack of signal based on the low fraction of PDAEMA.[239] The observance of distinct T_g's of the PnBA and PDAEMA blocks, largely in agreement of that with the corresponding

homopolymers, suggests the formation of distinct PnBA and PDAEMA domains,[240] and is thus consistent with the microphase separated morphologies indicated by SAXS analysis.

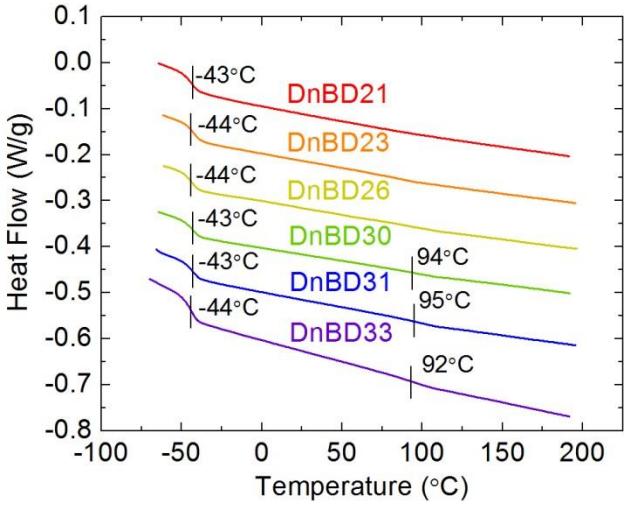

Figure 6.5 DSC data obtained from DnBD triblock copolymers. Data are shifted vertically for clarity.

For TPE applications, the midblock must exhibit a T_g well below room temperature and the endblocks must exhibit a high T_g well above room temperature. The sub-room temperature T_g of PnBA is appropriate for the rubbery block in TPE, replacing the traditionally used polydienes, and the high T_g of the PDAEMA makes it a suitable replacement for polystyrene in the glassy endblock of triblock copolymer-based thermoplastic elastomers. The thermal stability of the DnBD triblock copolymer was characterized by TGA (Figure 6.6). The onset degradation temperature for DnBD was determined to be 370°C.

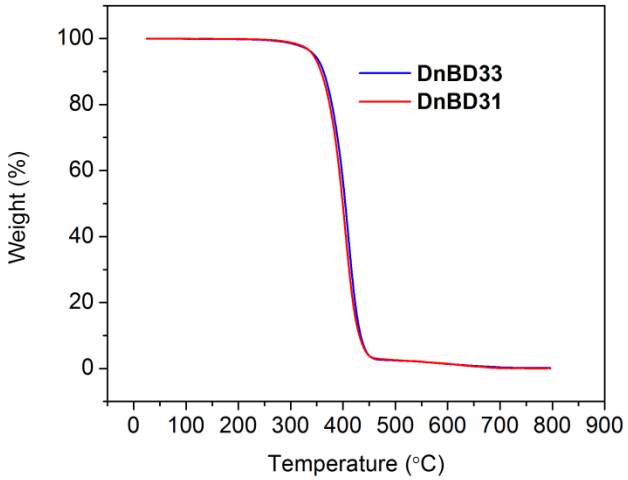

Figure 6.6 TGA data obtained from DnBD31 and DnBD33.

6.3 Accessible order-disorder transitions of DnBD triblock copolymers

The order-disorder transition temperatures (T_{ODT}) of DnBD triblock copolymers were characterized by rheology. The storage (*G'*) and loss (*G"*) moduli were first measured as functions of strain at constant frequency to characterize the linear strain region. Next, *G'* and *G"* were characterized as functions of frequency (at constant strain, choosing a value in the linear region). This process was repeated at various temperatures. A plot of log *G'* vs. T (at a chosen value of frequency) is traditionally employed to characterize the T_{ODT} and is shown in Figure 6.7a for DnBD33. An initial decrease in *G'* was observed at 110 °C, attributed to the T_g of the PDAEMA block. At higher temperatures, *G'* exhibited a second decrease at 190 °C, a signature of the T_{ODT}. We employed two additional methods to verify the location of the T_{ODT}. Following Han et al.,[241] we prepared a double logarithmic plot of *G"* vs. *G'* (Figure 6.7b). At low temperatures, the curves exhibited unique dependencies of *G'* as a function of *G"* (in the high *G"* region of the plot). As the temperature was increased above the T_{ODT}, the curves overlapped at all values of *G"*. For DnBD33 (Figure 6.7b), the curves coincided with each other between 190°C to 220°C and did not coincide between 130°C to 180°C. The

T_{ODT} was thus identified at 185 ± 5 °C, in agreement with the value determined from the plot of log *G'* vs. T. Finally, we also examined the time-temperature superposition behavior of *G'* and *G"* vs. frequency at each temperature. A change in morphology and presence of ordered structures is anticipated to lead to a failure of the data to conform to time-temperature superposition.[242] Figure 6.7c shows the dependencies of the dynamic moduli on reduced frequency ($a_T\omega$, in which a_T is the shift factor). At low temperatures (130°C to 180°C), the data were not superimposable with time-temperature superposition. Above 190°C, the data were readily superimposable. Therefore, the T_{ODT} was identified as 185 ± 5 °C, in agreement with the previously described methods.

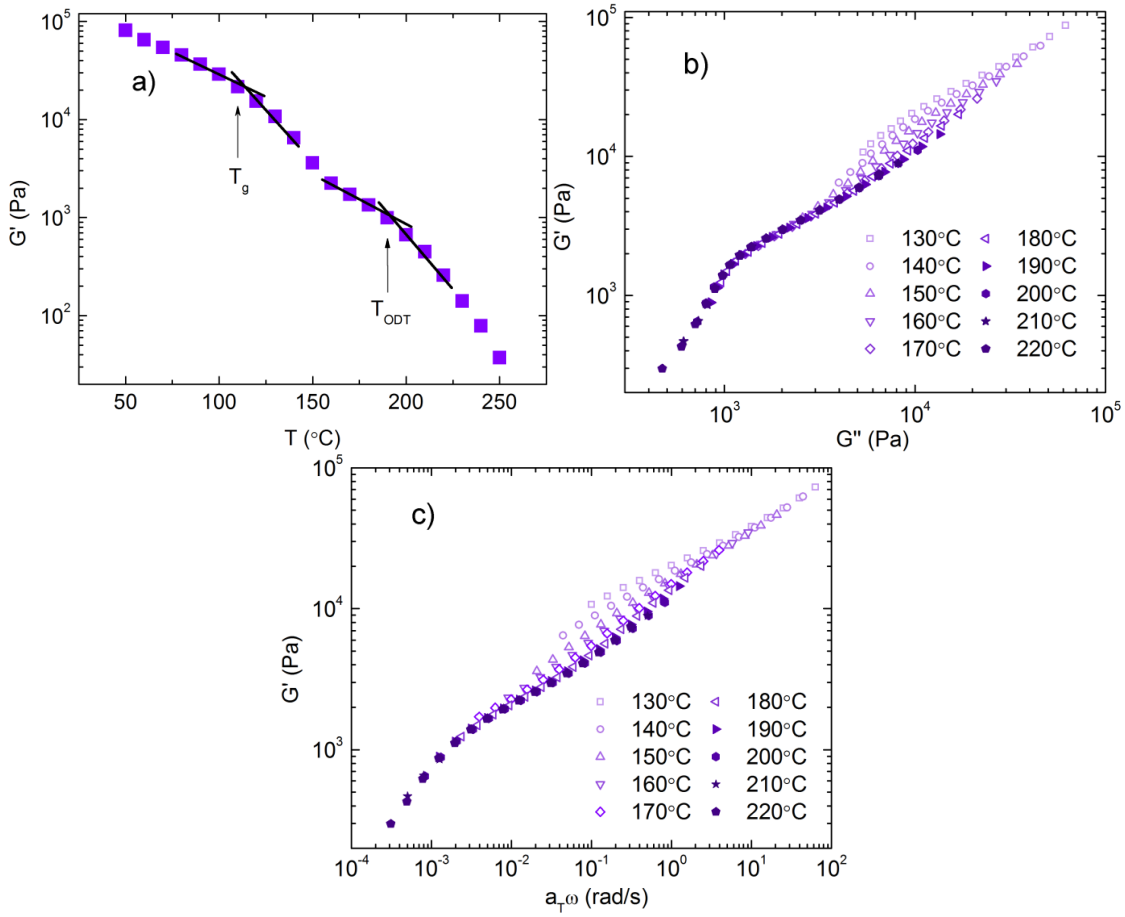

Figure 6.7 Rheology data obtained from DnDB33. a) Log *G'* vs T at an angular frequency of 0.1 rad/s. b) Log *G'* vs log *G"* at various temperatures. c) Log *G'* vs log $a_T\omega$ at various temperatures. The reference temperature was 130°C.

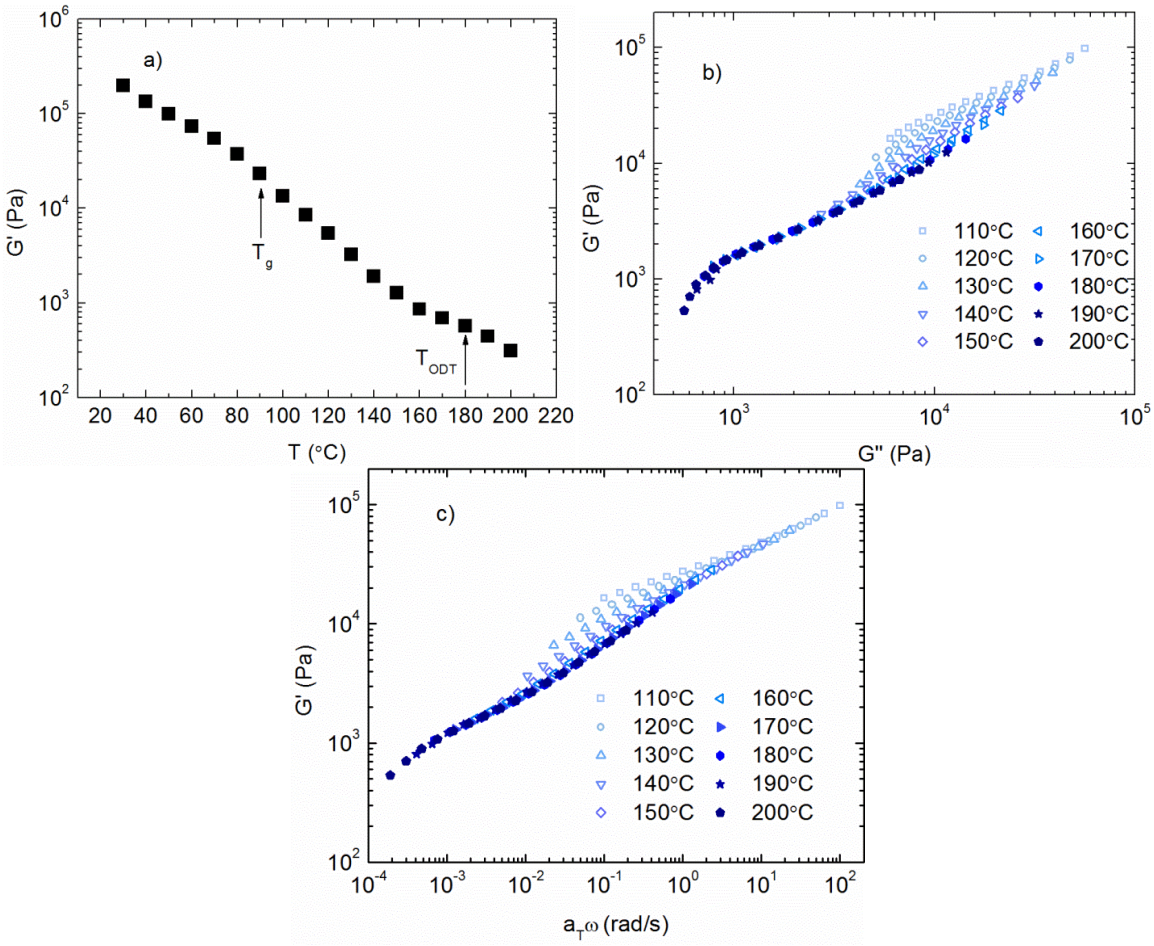

Figure 6.8 Rheology data obtained from DnBD31. a) *G'* (log scale) vs. *T* at an angular frequency of 0.1 rad/s. b) Double logarithmic plot of *G'* vs *G''* at various temperatures. c) Double logarithmic plot of *G'* vs $a_T\omega$ at various temperatures. The reference temperature was 110 °C

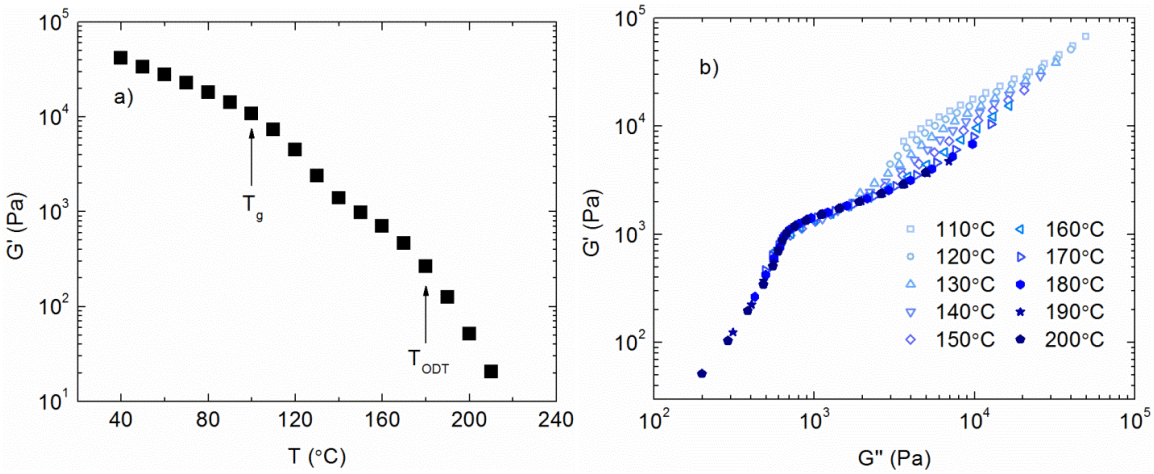

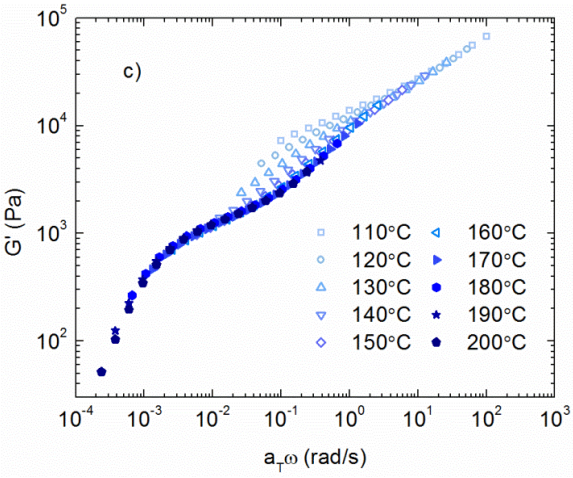

Figure 6.9 Rheology data obtained from DnBD30. a) *G'* (log scale) vs. T at an angular frequency of 0.1 rad/s. b) Double logarithmic plot of *G'* vs *G"* at various temperatures. c) Double logarithmic plot of *G'* vs $a_T\omega$ at various temperatures. The reference temperature was 110 °C

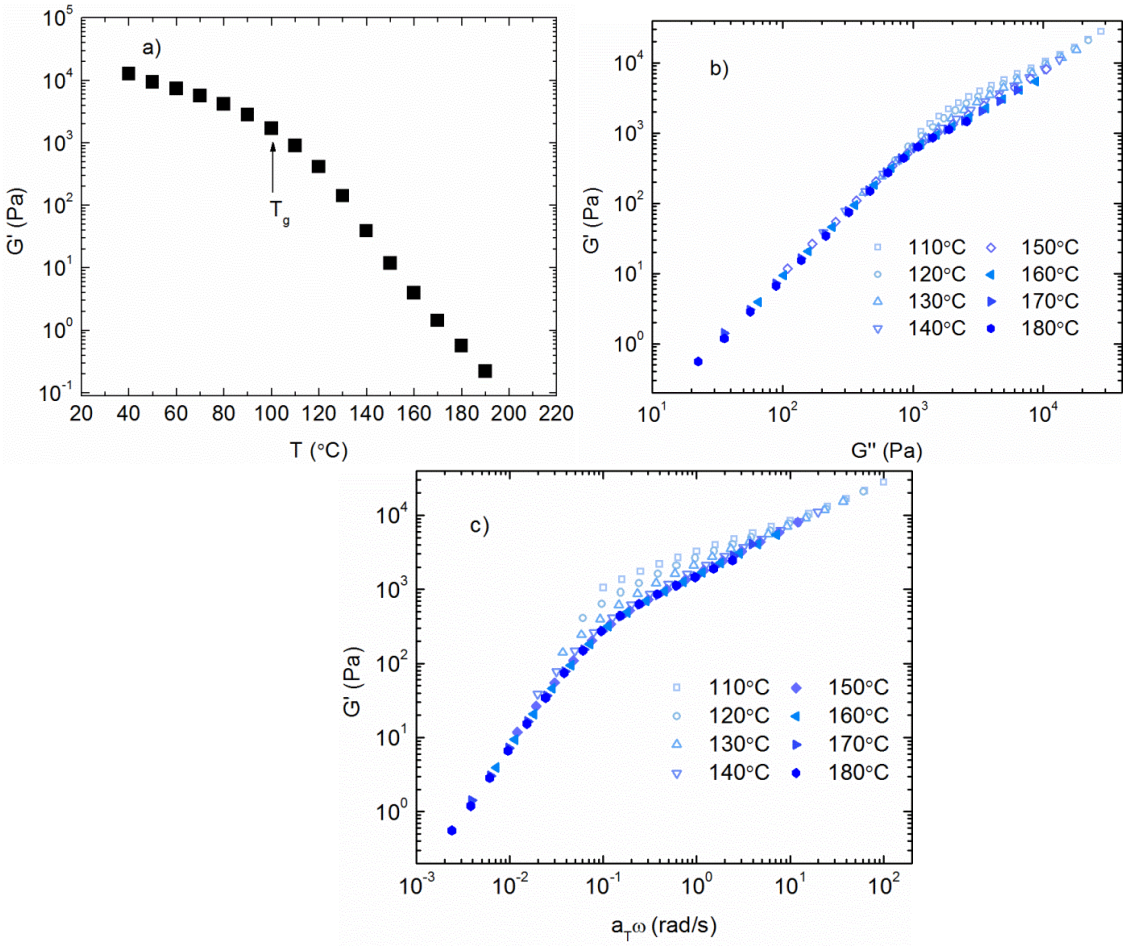

Figure 6.10 Rheology data obtained from DnBD26. a) *G'* (log scale) vs. T at an angular frequency of 0.1 rad/s. b) Double logarithmic plot of *G'* vs *G"* at various

temperatures. c) Double logarithmic plot of *G'* vs $a_T\omega$ at various temperatures. The reference temperature was 110 °C

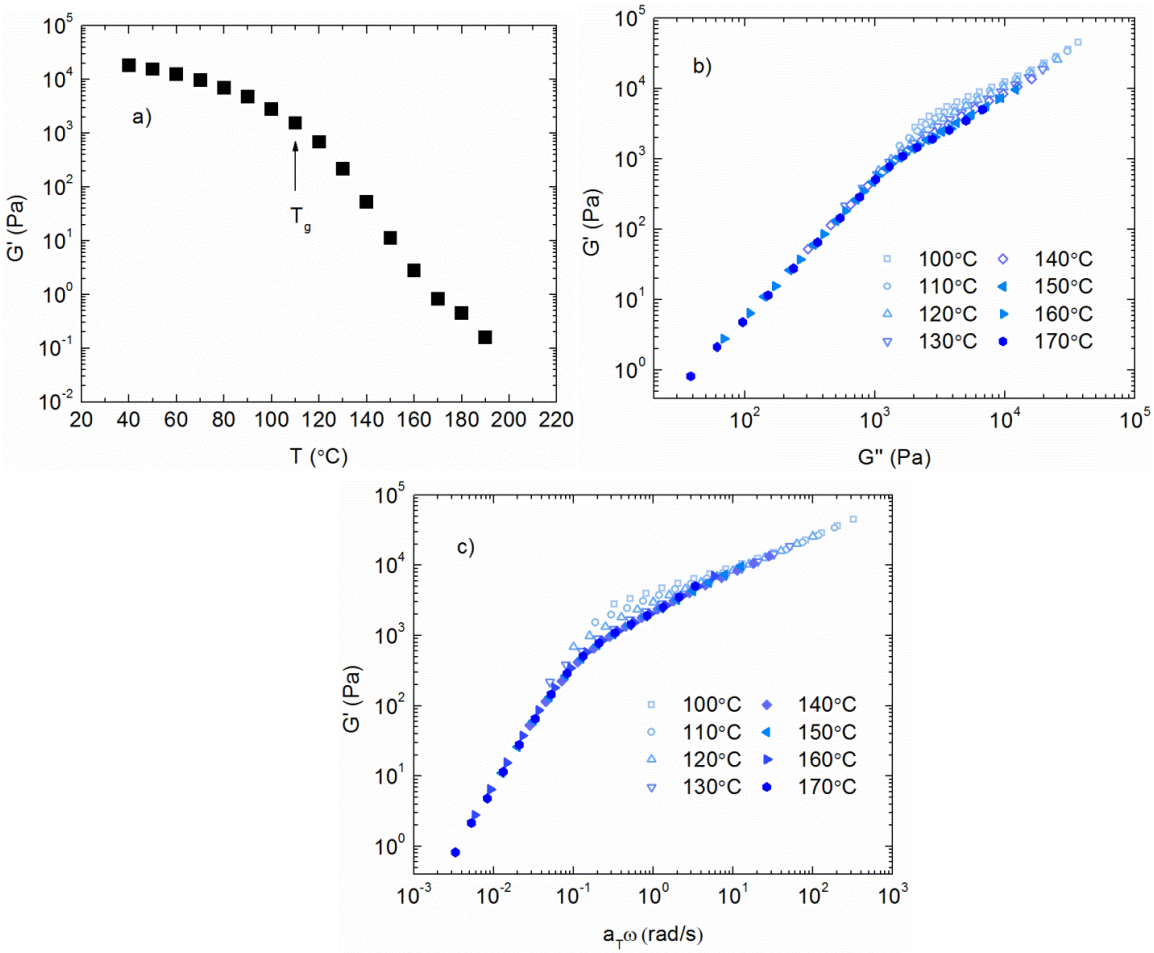

Figure 6.11 Rheology data obtained from DnBD23. a) *G'* (log scale) vs. T at an angular frequency of 0.1 rad/s. b) Double logarithmic plot of *G'* vs *G"* at various temperatures. c) Double logarithmic plot of *G'* vs $a_T\omega$ at various temperatures. The reference temperature was 110 °C.

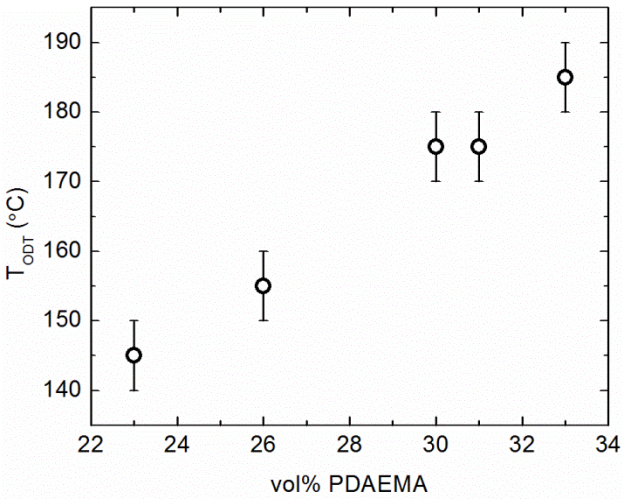

Figure 6.12 T_{ODT} as a function of vol% PDAEMA in DnBD triblock copolymers.

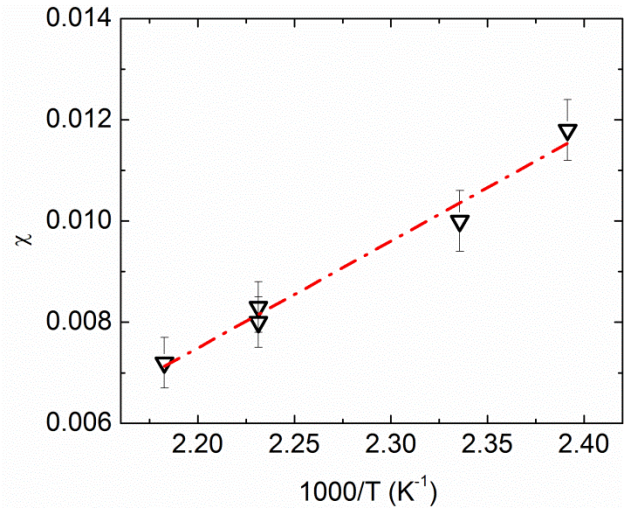

Figure 6.13 χ as a function of inverse temperature based on reference volume of 100 $Å^3$. The dashed red line represents a linear fit of data: $\chi = 21.12/T - 0.03897$

It worth noting that the order disorder transition for DnBD33 is not as sharp as that observed for other block copolymers reported in literature.[243-246] Broad order-disorder transitions have been observed for block copolymers with increased dispersity,[247] and it is notable that Đ of DnBD33 is 1.57. The three analysis methods were applied to all DnBD triblock copolymers discussed in this study, as shown in Figure 6.8-Figure 6.11. As observed in Figure 6.12, increasing the vol% of PDAEMA in the DnBD

triblock copolymer results in a higher $T_{ODT.}$ The value of χN at the order-disorder transition is dependent on the triblock copolymer composition, where N is number of repeat units and χ the temperature-dependent Flory-Huggins interaction parameter.[26, 248] In the theoretical block copolymer phase diagram,[32] as the vol% of the minor phase (PDAEMA in our case) is increased, the value of χN at the order-disorder transition decreases. For an upper critical solution temperature system, the T_{ODT} is thus predicted to increase with increasing PDAEMA content in the triblock copolymer, in agreement with the trends shown in Figure 6.12. With the knowledge of N, vol% of endblocks and ODT, χ can be estimated using theoretical phase diagram by following a previously reported procedure[32, 112]. The estimated χ at ODT are plotted in Figure 6.13 and listed in Table 6.3. The value of χ at 150°C ($\chi_{PnBA/PDAEMA}$ = 0.011) was compared to other well-studies monomer couples. The value is even lower than the well-known weakly segregating syrene/methyl methacrylate ($\chi_{PS/PMMA}$ = 0.025)[249] and it is greatly lower than styrene/isoprene ($\chi_{PS/PI}$=0.061)[250], styrene/lauryl acrylate ($\chi_{PS/PLAc}$=0.035)[112], isoprene/lactide ($\chi_{PI/PLA}$=0.15)[251] and syrene/isooctyl acrylate ($\chi_{PS/PIOA}$=0.091)[252](All the χ values are recalculated based on reference volume of 100 $Å^3$). Such a low value of χ is indicative of low incompatibility between PnBA and PDAEMA. Thus it requires larger number of N in order for DnBD triblock copolymers to self-assemble which is consistent our observation in SAXS measurements.

Table 6.3 Summary of χ estimated from T_{ODT} of DnBD triblock copolymers

Polymer	N[a]	ϕ_D[b]	Theoretical χN at T_{ODT}[c]	T_{ODT} (K)	χ at T_{ODT}[d]
DnBD33	1772	0.33	12.78	458.15 ± 5	0.0072 ± 0.0005
DnBD31	1731	0.31	13.75	448.15 ± 5	0.0080 ± 0.0005
DnBD30	1683	0.30	14.01	448.15 ± 5	0.0083 ± 0.0005

Table 6.3 Continued

DnBD26	1594	0.26	15.95	428.15 ± 5	0.0100 ± 0.0006
DnBD23	1535	0.23	18.15	418.15 ± 5	0.0118 ± 0.0006

[a] Number of repeat units (based on a reference volume of 100 Å)
[b] Volume fraction of PDAEMA in the block copolymer
[c] Theoretical χN at order-disorder transition, for a given ϕ_D (determined from ref. [32])
[d] Based on a reference volume of 100 Å

6.4 Mechanical behavior of DnBD triblock copolymers

The DnBD33 triblock copolymer was chosen to evaluate the mechanical behavior, due to its attractive features of a well-defined cylindrical morphology, observed distinct T_g's for the PDAEMA and PnBA domains, and accessible T_{ODT}. For comparison purposes, we also synthesized a conventional acrylic-based TPE, poly(methyl methacrylate-*b*-*n*-butyl acrylate-*b*-methyl methacrylate), containing 35 vol% methyl methacryate (MnBM35). The MnBM35 triblock copolymer was designed to contain the same midblock (PnBA) and comparable midblock M_n and endblock fraction, as compared to the DnBD33 triblock copolymer (Table 6.2, Figure 6.14 and Figure 6.15). The stress-strain curves of all tested specimens of DnBD33 and MnBM35 are shown in Figure 6.16, and the mechanical properties are summarized in Table 6.4. Both DnBD33 and MnBM35 exhibited elastomeric behavior at room temperature, with comparable elongation at break values of 242 and 280%, respectively.

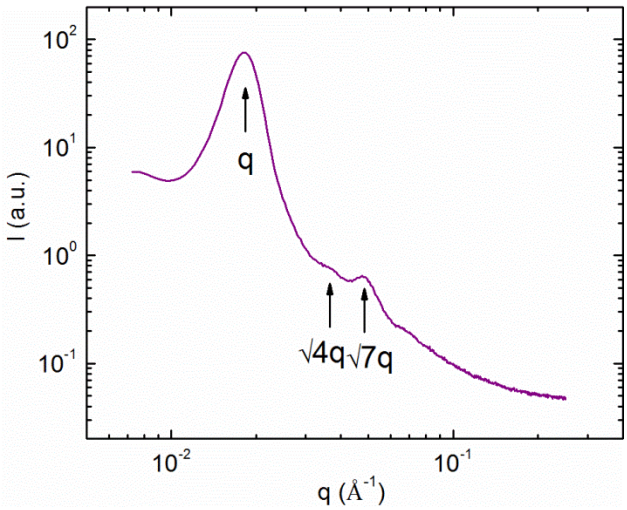

Figure 6.14 1D SAXS profile of MnBM35

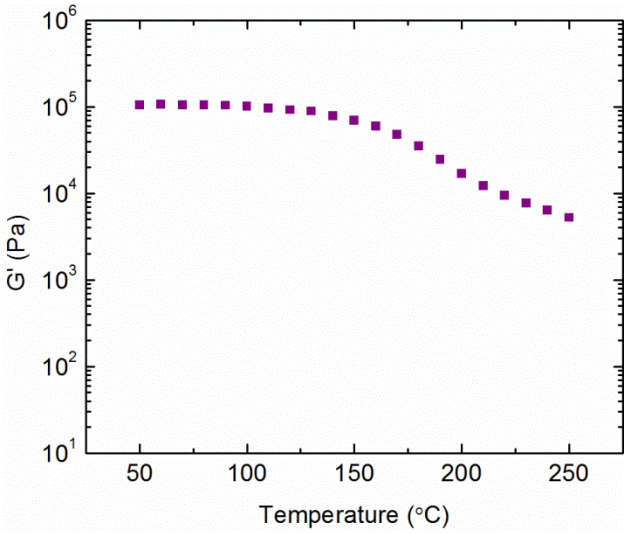

Figure 6.15 Log *G'* vs. T at an angular frequency of 1 rad/s obtained for MnBM35. The drop of *G'* starting at 150°C is the glass transition of the PMMA domain.

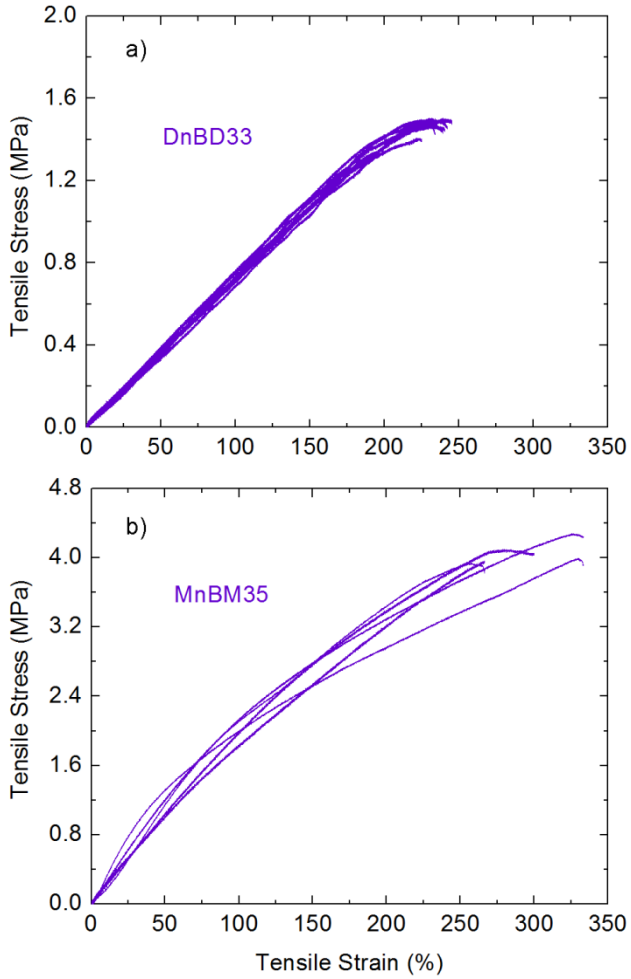

Figure 6.16 Stress vs. strain obtained from tensile testing for a) DnBD33 and b) MnBM35.

Table 6.4 Tensile properties of DnBD33 and MnbM35 triblock copolymers

Triblock Copolymer	Elongation at break (%)	Tensile strength (MPa)	Young's modulus (MPa)
DnBD33	242 ± 8	1.48 ± 0.07	0.75 ± 0.03
MnBM35	283 ± 29	4.06 ± 0.314	2.5 ± 0.5

The tensile strength and modulus of DnBD33 were significantly lower than that of MnBM35 (in both cases, by approximately a factor of 3). Acrylic-based TPEs generally exhibit lower tensile strengths and moduli as compared to polystyrene/polydiene-based TPEs,[253-255] however, the differences between the DnBD33 and MnBM35 polymers are worth examining in more detail. Two factors are known to significantly affect the

mechanical properties of triblock copolymer-based TPEs: the entanglement molecular weight and the dispersity of the polymer.

The midblock and endblock entanglements molecular weights (M_e) have a great impact on the mechanical properties of triblock copolymers. Both DnBD33 and MnBM35 contain PnBA midblocks of similar M_n (76 kg/mol). This molecular weight is 2.7 times greater than the M_e of PnBA (28 kg/mol[136]) and may not be sufficiently high to realize the full benefit of an entangled triblock copolymer matrix. Comparatively, stryrenic TPEs typically contain polydiene midblocks which have significantly lower M_e values (for example, the M_e of polybutadiene is 1.7 kg/mol[136]) and are therefore entangled at moderate molecular weights. The mechanical properties of the triblock copolymers are also affected by the strength of the rigid domains (formed by the glassy endblocks).[50, 256] Thermoplastics with molecular weight higher than M_e exhibit higher strengths.[257] The M_e of PDAEMA was not directly characterized, due to the inability to synthesize a sufficiently high molecular weight polymer (well above M_e). However, an analogue which contained a polynorbornene backbone and very similar side-chain moiety to PDAEMA was synthesized and the M_e was found to be 86 kg/mol in a prior study.[16] We therefore expect that the PDAEMA endblock M_n of DnBD33 (M_n = 20 kg/mol) is significantly lower than the M_e of PDAEMA. In the case of MnBM35, the poly(methyl methacylate) endblock molecular weight (M_n = 21 kg/mol) is approximately twice as large as its M_e (13 kg/mol),[258] thus MnBM35 may potentially contain an entangled matrix. We note that the high M_e of PDAEMA is in contrast to not only poly(methyl methacrylate) but also the polystyrene endblocks (M_e = 13 kg/mol)[259] in styrenicTPEs. Other literature studies have examined the mechanical behavior of triblock copolymer-

based TPEs which contain bulky moieties in the endblocks. Mosnáček and coworkers reported a triblock copolymer with endblocks based on butyrolactone, and the tensile stress was found to be 0.7-1.9 MPa depending on composition.[50] Hashimoto etc. reported a triblock copolymer with tricyclodecane pendant group in the endblock, which had a tensile stress of 2.4 MPa.[260] Nasiri recently synthesized a triblock copolymer with a glucose-based endblock, exhibiting a tensile stress of 0.3-0.6 MPa.[52] Thus the tensile strength of DnBD33 (1.48 MPa) is in line with other studies on TPEs containing bulky (and likely unentangled) endblocks.

Furthermore, we can consider the impact of dispersity. MnBM35 has a much lower dispersity than that of DnBD33 (Đ = 1.16 and 1.57 for MnBM35 and DnBD33, respectively). Prior studies have investigated the impact of dispersity on triblock copolymer mechanical properties, with differing results. In one study by Tong et al., triblock copolymers with higher dispersity exhibited lower modulus and tensile strength.[261] However, Luo and coworkers synthesized triblock copolymers with the same composition but very different dispersities, and they exhibited similar mechanical properties.[262] Also, Chatterjee and Mandal compared the mechanical properties of two triblock copolymers before and after removing homopolymer and diblock copolymer contamination in the triblock copoolymers, which had little effect.[263] Thus, the relationship between dispersity and mechanical properties of triblock copolymer thermoplastic elastomers remains to be elucidated.

6.5 Concluding remarks

A rosin-derived polymethacrylate, poly(dehydroabietic ethyl methacrylate) (PDAEMA), was evaluated as a sustainable endblock in triblock copolymer-based

thermoplastic elastomers. Poly(dehydroabietic ethyl methacrylate-*b*-*n*-butyl acrylate-*b*-dehydroabietic ethyl methacrylate) (DnBD) triblock copolymers were synthesized via atom transfer radical polymerization with the aid of halogen exchange. The polymers exhibited two distinct glass transition temperatures that were commensurate to the corresponding homopolymers, indicating microphase separation of the triblock copolymers with little phase intermixing. SAXS measurements confirmed microphase separation: the triblock copolymer with the highest PDAEMA content exhibited a well-defined cylindrical morphology and the others exhibited microphase separation lacking long-range order. The order-disorder transition temperature increased with increasing PDAEMA content, consistent with an upper critical solution temperature system. Mechanical testing revealed elastomeric behavior at room temperature. Whereas the elongation at break of a DnBD triblock copolymer containing 33 vol% PDAEMA was comparable to that measured for a conventional petroleum derived acrylic-based triblock copolymer, poly(methyl methacrylate-*b*-*n*-butyl acrylate-*b*-methyl methacrylate) (containing similar end-block content, 35 vol%), the tensile strength and modulus were lower for the rosin-based triblock copolymer, attributed to significantly higher entanglement molecular weight of rosin-derived end-blocks. This work demonstrates the utility of a renewable, abundant, and non-toxic feedstock, rosin, to produce sustainable TPE components. Rosin-based polymethacrylates, with high glass transition temperatures, were suitable endblocks in ABA triblock copolymer TPEs, exhibiting elastomeric behavior and accessible order-disorder transitions.

Chapter 7 Summary and Future Work

7.1 Conclusion of this work

Given the challenges that the majority of the sustainable TPEs exhibited inferior mechanical properties to the petroleum-based TPEs due to the presence of bulky moieties in the polymer repeat units, in this work, we demonstrated that the incorporation of supramolecular networks, formed by hydrogen bonds and ionic bonds, effectively enhanced the mechanical properties of sustainable TPEs. In addition, we explored the kinetics and mechanism of shear alignment of the fatty acid-derived triblock copolymer forming a closed packed spherical morphology which has rarely been reported in the literature. Finally, we broadened the library of sustainable building blocks with high glass transition temperatures by examining a rosin derived polymethacrylate as endblock for sustainable TPEs.

In first project, hydrogen bonds were incorporated into fatty acid-derived triblock copolymer as a mean to improve the mechanical properties. The impact of hydrogen bonding on the physical properties was evaluated. The triblock copolymers were synthesized by copolymerization of fatty acid-based lauryl acrylate and the hydrogen bonding comonomer acrylamide to form the midblock, followed by chain extension with styrene to form the endblocks. FTIR confirmed the presence of hydrogen bonding at low temperatures, and effective dissociation of hydrogen bonds at elevated temperatures, facilitating melt processing of these polymers. The incorporation of acrylamide greatly reduced the order-disorder transition temperature due to more favorable thermodynamic interactions between the midblock and endblocks. SAXS analyses revealed the presence of a disordered spherical morphology that was unaffected by the presence of hydrogen

bonding. Mechanical testing revealed that the incorporation of hydrogen bonding significantly improved the tensile strength and strain at break of the triblock copolymers. Indeed, this work demonstrates the utility of hydrogen bonding to improve the mechanical properties of triblock copolymer thermoplastic elastomers which contain bulky constituents in the midblock (such as the long alkyl side-chains in the fatty acid-based polymers explored in this work).

In second project, ionic interactions were incorporated into fatty acid-derived triblock copolymer as a mean to improve the mechanical properties. The triblock copolymers poly(methyl methacrylate-b-(lauryl methacrylate-co-methacrylic acid)-b-methyl methacrylate) were synthesized with reversible addition-fragmentation transfer polymerization. The comonomer methacrylic acid in the midblock was further neutralized with sodium hydroxide to introduce ionic interactions into the system. The effects of acid content and degree of neutralization on the physical properties were evaluated. Rheological measurement of the midblocks revealed that the relaxation time increase with increasing acid content and degree of neutralization. Incorporation of ionic interaction into the midblock greatly improved the both tensile strength and modulus. However, the strain at break decreased upon neutralization. Interestingly, the extent of enhancement of mechanical propertied was found to correlate with the relaxation time of midblock.

In third project, we investigated kinetics and mechanism in the alignment process of poly(styrene-*b*-lauryl acrylate-*b*-styrene) triblock copolymers with initially disorder spherical morphology that transition to closed packed spherical morphology under nonlinear oscillatory shear. The time-dependent microstructural changes were evaluated

using in-situ SAXS. Change strain amplitude induced two types of orientations of HCP layers: 1) biaxial orientation in MAOS region and 2) parallel orientation in LAOS region. Increasing strain amplitudes resulted in not only faster ordering process but also higher degree of orientation. Interestingly, for the first time, we observed shear deordering in closed packed spherical morphology under oscillatory shear at highest strain amplitude. The domain dissolution and resolution mechanism was proposed for the ordering process. The mechanical response detected by FT-rheology is correlated with morphological changes.

Finally, a rosin-derived polymethacrylate, poly(dehydroabietic ethyl methacrylate) (PDAEMA), was evaluated as a sustainable endblock in triblock copolymer-based thermoplastic elastomers. Poly(dehydroabietic ethyl methacrylate-*b*-*n*-butyl acrylate-*b*-dehydroabietic ethyl methacrylate) (DnBD) triblock copolymers were synthesized via atom transfer radical polymerization. SAXS measurements confirmed microphase separation: the triblock copolymer with the highest PDAEMA content exhibited a well-defined cylindrical morphology and the others exhibited microphase separation lacking long-range order. The order-disorder transition temperature increased with increasing PDAEMA content, consistent with an upper critical solution temperature system. Mechanical testing revealed elastomeric behavior at room temperature. This work demonstrates the utility of a renewable, abundant, and non-toxic feedstock, rosin, to produce sustainable TPE components. Rosin-based polymethacrylates, with high glass transition temperatures, were suitable endblocks in ABA triblock copolymer TPEs, exhibiting elastomeric behavior and accessible order-disorder transitions.

7.2 Outlook and future work

The hydrogen bond-containing comonomer acrylamide used in this study is derived from petroleum. Furthermore, the length of the acrylamide side chain is much shorter compared to that of fatty acid derived lauryl acrylate, which might affect the chain dynamics and degree of hydrogen bonding in the midblock. Future work could replace the acrylamide with a hydrogen bond-containing monomer with long side chain and derived from sustainable sources. For example, vegetable oil-derived fatty amide can be a good candidate.[100]

The valence and size of metal cation have a great impact on the ionic interactions. In this study, only sodium cation was employed. Future work could explore the effect of different metal cations on the physical properties of ion-containing triblock copolymers, including zinc, magnesium and cobalt. They are anticipated to affect midblock chain dynamics that affect the mechanical properties of the triblock copolymers.[146]

Even though the mechanical properties of fatty acid-derived triblock copolymers were significantly improved by the incorporation of either hydrogen bonds or ionic interactions, they are still inferior to commercial TPEs which limit the application of sustainable TPEs. To achieve better mechanical performance, one approach is to reduce the size of alkyl side chain through metathesis. By cutting off the length of the side chain, the entanglement molecular weight could drop significantly, thus can enhance the mechanical properties of the triblock copolymers. Another approach is to explore other types of transient networks, such as metal-ligand interactions. Recently, metal-ligand interactions have received a lot of success in enhancing the mechanical properties of

elastomers.[264-266] By careful design of the ligand structure, the relaxation time and bond strength can be tuned for targeted applications.

References

1. Paul C. Hiemenz, T. P. L., *Polymer Chemistry*. CRC Press: 2007.

2. Zhu, Y.; Romain, C.; Williams, C. K. Sustainable polymers from renewable resources. *Nature* **2016,** 540, 354.

3. Okkerse, C.; Van Bekkum, H. From fossil to green. *Green Chemistry* **1999,** 1 (2), 107-114.

4. Weisz, P. B. Basic choices and constraints on long-term energy supplies. *PHYSICS TODAY*. **2004,** 57 (7), 47-52.

5. Grand View Research, I. Elastomers Market Size. **2019,** Retrieved from D&B Global Business Browser database.

6. The Freedonia Group, I. World Thermoplastic Elastomers. **2018,** Retrieved from D&B Global Business Browser database.

7. Wang, S.; Kesava, S. V.; Gomez, E. D.; Robertson, M. L. Sustainable Thermoplastic Elastomers Derived from Fatty Acids. *Macromolecules* **2013,** 46 (18), 7202-7212.

8. Shin, J.; Lee, Y.; Tolman, W. B.; Hillmyer, M. A. Thermoplastic Elastomers Derived from Menthide and Tulipalin A. *Biomacromolecules* **2012,** 13 (11), 3833-3840.

9. Zhou, C.; Wei, Z. Y.; Lei, X. F.; Li, Y. Fully biobased thermoplastic elastomers: synthesis and characterization of poly(L-lactide)-b-polymyrcene-b-poly(L-lactide) triblock copolymers. *Rsc Advances* **2016,** 6 (68), 63508-63514.

10. Frick, E. M.; Zalusky, A. S.; Hillmyer, M. A. Characterization of Polylactide-b-polyisoprene-b-polylactide Thermoplastic Elastomers. *Biomacromolecules* **2003,** 4 (2), 216-223.

11. Ding, W.; Wang, S.; Yao, K.; Ganewatta, M. S.; Tang, C.; Robertson, M. L. Physical Behavior of Triblock Copolymer Thermoplastic Elastomers Containing Sustainable Rosin-Derived Polymethacrylate End Blocks. *ACS Sustainable Chemistry & Engineering* **2017**.

12. Wang, S.; Ding, W.; Yang, G.; Robertson, M. L. Biorenewable Thermoplastic Elastomeric Triblock Copolymers Containing Salicylic Acid‐Derived End‐Blocks and a Fatty Acid‐Derived Midblock. *Macromolecular Chemistry and Physics* **2016,** 217 (2), 292-303.

13. Bolton, J. M.; Hillmyer, M. A.; Hoye, T. R. Sustainable thermoplastic elastomers from terpene-derived monomers. *ACS Macro Letters* **2014,** 3 (8), 717-720.

14. Wang, S.; Ding, W.; Yang, G.; Robertson, M. L. Biorenewable Thermoplastic Elastomeric Triblock Copolymers Containing Salicylic Acid-Derived End-Blocks and a Fatty Acid-Derived Midblock. *Macromolecular Chemistry and Physics* **2016,** 217 (2), 292-303.

15. Wang, Z.; Yuan, L.; Trenor, N. M.; Vlaminck, L.; Billiet, S.; Sarkar, A.; Du Prez, F. E.; Stefik, M.; Tang, C. Sustainable thermoplastic elastomers derived from plant oil and their "click-coupling" via TAD chemistry. *Green Chemistry* **2015,** 17 (7), 3806-3818.

16. Ganewatta, M. S.; Ding, W.; Rahman, M. A.; Yuan, L.; Wang, Z.; Hamidi, N.; Robertson, M. L.; Tang, C. Biobased Plastics and Elastomers from Renewable Rosin via “Living” Ring-Opening Metathesis Polymerization. *Macromolecules* **2016,** 49 (19), 7155-7164.

17. Tong, J. D.; Moineau, G.; Leclère, P.; Brédas; Lazzaroni, R.; Jérôme, R. Synthesis, Morphology, and Mechanical Properties of Poly(methyl methacrylate)-b-

poly(n-butyl acrylate)-b-poly(methyl methacrylate) Triblocks. Ligated Anionic Polymerization vs Atom Transfer Radical Polymerization. *Macromolecules* **2000,** 33 (2), 470-479.

18. Holden, G.; Legge, N. R.; Quirk, R.; Schroeder, H. E. Thermoplastic Elastomers 2nd Edition. *Thermoplastic Elastomers 2nd Edition* **1996**.

19. Singh, R.; Desai, S.; Solanky, S.; Thanki, P. Photodegradation and stabilization of styrene–butadiene–styrene rubber. *Journal of applied polymer science* **2000,** 75 (9), 1103-1114.

20. Cortizo, M.; Larsen, D.; Bianchetto, H.; Alessandrini, J. Effect of the thermal degradation of SBS copolymers during the ageing of modified asphalts. *Polymer Degradation and Stability* **2004,** 86 (2), 275-282.

21. Xu, J.; Zhang, A.; Zhou, T.; Cao, X.; Xie, Z. A study on thermal oxidation mechanism of styrene–butadiene–styrene block copolymer (SBS). *Polymer Degradation and Stability* **2007,** 92 (9), 1682-1691.

22. Tong, J. D.; Jerome, R. Synthesis of poly(methyl methacrylate)-b-poly(n-butyl acrylate)-b-poly(methyl methacrylate) triblocks and their potential as thermoplastic elastomers. *Polymer* **2000,** 41 (7), 2499-2510.

23. Chatterjee, D. P.; Mandal, B. M. Triblock thermoplastic elastomers with poly(lauryl methacrylate) as the center block and poly(methyl methacrylate) or poly(tert-butyl methacrylate) as end blocks. Morphology and thermomechanical properties. *Macromolecules* **2006,** 39 (26), 9192-9200.

24. Shipp, D. A.; Wang, J. L.; Matyjaszewski, K. Synthesis of acrylate and methacrylate block copolymers using atom transfer radical polymerization. *Macromolecules* **1998,** 31 (23), 8005-8008.

25. Jeusette, M.; Leclere, P.; Lazzaroni, R.; Simal, F.; Vaneecke, J.; Lardot, T.; Roose, P. New "all-acrylate" block copolymers: Synthesis and influence of the architecture on the morphology and the mechanical properties. *Macromolecules* **2007,** 40 (4), 1055-1065.

26. Bates, F. S.; Fredrickson, G. H. Block Copolymer Thermodynamics: Theory and Experiment. *Annual Review of Physical Chemistry* **1990,** 41 (1), 525-557.

27. Flory, P. J. Thermodynamics of high polymer solutions. *The Journal of Chemical Physics* **1942,** 10 (1), 51-61.

28. Huggins, M. L. Some properties of solutions of long-chain compounds. *The Journal of Physical Chemistry* **1942,** 46 (1), 151-158.

29. Matsen, M. W.; Thompson, R. B. Equilibrium behavior of symmetric ABA triblock copolymer melts. *The Journal of Chemical Physics* **1999,** 111 (15), 7139-7146.

30. Ye, X.; Yu, X.; Sun, Z.; An, L. Comparing the Morphology and Phase Diagram of H-Shaped ABC Block Copolymers and Linear ABC Block Copolymers. *The Journal of Physical Chemistry B* **2006,** 110 (24), 12042-12046.

31. Matsen, M. W. Comparison of A-block polydispersity effects on BAB triblock and AB diblock copolymer melts. *The European Physical Journal E* **2013,** 36 (4), 44.

32. Matsen, M. W. Effect of architecture on the phase behavior of AB-type block copolymer melts. *Macromolecules* **2012,** 45 (4), 2161-2165.

33. Tang, P.; Qiu, F.; Zhang, H.; Yang, Y. Morphology and Phase Diagram of Complex Block Copolymers: ABC Star Triblock Copolymers. *The Journal of Physical Chemistry B* **2004,** 108 (24), 8434-8438.

34. Pochan, D. J.; Gido, S. P.; Pispas, S.; Mays, J. W.; Ryan, A. J.; Fairclough, J. P. A.; Hamley, I. W.; Terrill, N. J. Morphologies of Microphase-Separated A2B Simple Graft Copolymers. *Macromolecules* **1996,** 29 (15), 5091-5098.

35. Pochan, D. J.; Gido, S. P.; Pispas, S.; Mays, J. W. Morphological Transitions in an I2S Simple Graft Block Copolymer: From Folded Sheets to Folded Lace to Randomly Oriented Worms at Equilibrium. *Macromolecules* **1996,** 29 (15), 5099-5105.

36. Gido, S. P.; Lee, C.; Pochan, D. J.; Pispas, S.; Mays, J. W.; Hadjichristidis, N. Synthesis, Characterization, and Morphology of Model Graft Copolymers with Trifunctional Branch Points. *Macromolecules* **1996,** 29 (22), 7022-7028.

37. Beyer, F. L.; Gido, S. P.; Poulos, Y.; Avgeropoulos, A.; Hadjichristidis, N. Morphology of Vergina Star 16-Arm Block Copolymers and Scaling Behavior of Interfacial Area with Graft Point Functionality. *Macromolecules* **1997,** 30 (8), 2373-2376.

38. Xenidou, M.; Beyer, F. L.; Hadjichristidis, N.; Gido, S. P.; Tan, N. B. Morphology of Model Graft Copolymers with Randomly Placed Trifunctional and Tetrafunctional Branch Points. *Macromolecules* **1998,** 31 (22), 7659-7667.

39. Lee, C.; Gido, S. P.; Poulos, Y.; Hadjichristidis, N.; Tan, N. B.; Trevino, S. F.; Mays, J. W. π-Shaped double-graft copolymers: effect of molecular architecture on morphology. *Polymer* **1998,** 39 (19), 4631-4638.

40. Wang, Z.; Yuan, L.; Trenor, N. M.; Vlaminck, L.; Billiet, S.; Sarkar, A.; Du Prez, F. E.; Stefik, M.; Tang, C. Sustainable thermoplastic elastomers derived from plant oil and their "click-coupling" via TAD chemistry. *Green Chemistry* **2015,** 17 (7), 3806-3818.

41. Lee, S.; Lee, K.; Kim, Y.-W.; Shin, J. Preparation and characterization of a renewable pressure-sensitive adhesive system derived from ε-decalactone, l-lactide, epoxidized soybean oil, and rosin ester. *ACS Sustainable Chemistry & Engineering* **2015,** 3 (9), 2309-2320.

42. Martello, M. T.; Schneiderman, D. K.; Hillmyer, M. A. Synthesis and melt processing of sustainable poly (ε-decalactone)-block-poly (lactide) multiblock thermoplastic elastomers. *ACS Sustainable Chemistry & Engineering* **2014,** 2 (11), 2519-2526.

43. Liu, S. S.; Zhang, X. J.; Li, M. S.; Ren, X. Y.; Tao, Y. H. Precision Synthesis of Sustainable Thermoplastic Elastomers from Lysine-Derived Monomers. *Journal of Polymer Science Part a-Polymer Chemistry* **2017,** 55 (2), 349-355.

44. Shin, J.; Martello, M. T.; Shrestha, M.; Wissinger, J. E.; Tolman, W. B.; Hillmyer, M. A. Pressure-sensitive adhesives from renewable triblock copolymers. *Macromolecules* **2010,** 44 (1), 87-94.

45. Qian, H.; Bei, J.; Wang, S. Synthesis, characterization and degradation of ABA block copolymer of L-lactide and ε-caprolactone. *Polymer Degradation and Stability* **2000,** 68 (3), 423-429.

46. Cohn, D.; Hotovely-Salomon, A. Biodegradable multiblock PEO/PLA thermoplastic elastomers: molecular design and properties. *Polymer* **2005,** 46 (7), 2068-2075.

47. Frick, E. M.; Hillmyer, M. A. Synthesis and characterization of polylactide ‐ block ‐ polyisoprene ‐ block ‐ polylactide triblock copolymers: new thermoplastic elastomers containing biodegradable segments. *Macromolecular rapid communications* **2000,** 21 (18), 1317-1322.

48. Lebarbé, T.; Ibarboure, E.; Gadenne, B.; Alfos, C.; Cramail, H. Fully bio-based poly (L-lactide)-b-poly (ricinoleic acid)-b-poly (L-lactide) triblock copolyesters: investigation of solid-state morphology and thermo-mechanical properties. *Polymer Chemistry* **2013,** 4 (11), 3357-3369.

49. Shin, J.; Kim, Y.-W.; Kim, G.-J. Sustainable Block Copolymer-based Thermoplastic Elastomers. *Applied Chemistry for Engineering* **2014,** 25 (2), 121-133.

50. Mosnáček, J.; Yoon, J. A.; Juhari, A.; Koynov, K.; Matyjaszewski, K. Synthesis, morphology and mechanical properties of linear triblock copolymers based on poly (α-methylene-γ-butyrolactone). *Polymer* **2009,** 50 (9), 2087-2094.

51. Gallagher, J. J.; Hillmyer, M. A.; Reineke, T. M. Acrylic Triblock Copolymers Incorporating Isosorbide for Pressure Sensitive Adhesives. *ACS Sustainable Chemistry & Engineering* **2016,** 4 (6), 3379-3387.

52. Nasiri, M.; Reineke, T. M. Sustainable glucose-based block copolymers exhibit elastomeric and adhesive behavior. *Polymer Chemistry* **2016,** 7 (33), 5233-5240.

53. Xia, Y.; Larock, R. C. Vegetable Oil-Based Polymeric Materials: Synthesis, Properties, and Applications. *Green Chem.* **2010,** 12 (11), 1893-1909.

54. Shogren, R. L.; Petrovic, Z.; Liu, Z.; Erhan, S. Z. Biodegradation Behavior of Some Vegetable Oil-Based Polymers. *Journal of Polymers and the Environment* **2004,** 12 (3), 173-178.

55. Ronda, J. C.; Lligadas, G.; Galià, M.; Cádiz, V. Vegetable oils as platform chemicals for polymer synthesis. *European Journal of Lipid Science and Technology* **2011,** 113 (1), 46-58.

56. Lu, Y.; Larock, R. Novel Polymeric Materials from Vegetable Oils and Vinyl Monomers: Preparation, Properties, and Applications. *ChemSusChem* **2009,** 2 (2), 136-147.

57. Domb, A. J.; Nudelman, R. Biodegradable polymers derived from natural fatty acids. *Journal of Polymer Science Part A: Polymer Chemistry* **1995,** 33 (4), 717-725.

58. Jain, J. P.; Sokolsky, M.; Kumar, N.; Domb, A. J. Fatty Acid Based Biodegradable Polymer. *Polymer Reviews* **2008,** 48 (1), 156-191.

59. Vilela, C.; Rua, R.; Silvestre, A. J. D.; Gandini, A. Polymers and Copolymers from Fatty Acid-based Monomers. *Ind. Crop. Prod.* **2010,** 32 (2), 97-104.

60. Gupta, A. P.; Ahmad, S.; Dev, A. Modification of Novel Bio-Based Resin-Epoxidized Soybean Oil by Conventional Epoxy Resin. *Polym. Eng. Sci.* **2011,** 51 (6), 1087-1091.

61. Park, S. J.; Jin, F. L.; Lee, J. R. Synthesis and Thermal Properties of Epoxidized Vegetable Oil. *Macromolecular Rapid Communications* **2004,** 25 (6), 724-727.

62. Ionescu, M.; Petrovic, Z. S.; Wan, X. M. Ethoxylated Soybean Polyols for Polyurethanes. *Journal of Polymers and the Environment* **2010,** 18 (1), 1-7.

63. Lligadas, G.; Ronda, J. C.; Galia, M.; Biermann, U.; Metzger, J. O. Synthesis and Characterization of Polyurethanes from Epoxidized Methyl Oleate Based Polyether Polyols as Renewable Resources. *Journal of Polymer Science Part A: Polymer Chemistry* **2006,** 44 (1), 634-645.

64. Campanella, A.; La Scala, J. J.; Wool, R. P. The Use of Acrylated Fatty Acid Methyl Esters as Styrene Replacements in Triglyceride-based Thermosetting Polymers. *Polym. Eng. Sci.* **2009,** 49 (12), 2384-2392.

65. Beers, K. L.; Matyjaszewski, K. The Atom Transfer Radical Polymerization of Lauryl Acrylate. *J. Macromol. Sci., Pure Appl. Chem.* **2001,** 38 (7), 731-739.

66. Zhu, J.; Zhu, X. L.; Cheng, Z. P.; Lu, J. M.; Liu, F. Reversible Addition-Fragmentation Chain-Transfer Polymerization of Octadecyl Acrylate. *J. Macromol. Sci., Pure Appl. Chem.* **2003,** A40 (9), 963-975.

67. O'Leary, K. A.; Paul, D. R. Physical Properties of Poly(n-alkyl acrylate) Copolymers. Part 1. Crystalline/Crystalline Combinations. *Polymer* **2006,** 47 (4), 1226-1244.

68. Henna, P.; Larock, R. C. Novel Thermosets Obtained by the Ring-opening Metathesis Polymerization of a Functionalized Vegetable Oil and Dicyclopentadiene. *Journal of Applied Polymer Science* **2009,** 112 (3), 1788-1797.

69. Mauldin, T. C.; Haman, K.; Sheng, X.; Henna, P.; Larock, R. C.; Kessler, M. R. Ring-Opening Metathesis Polymerization of a Modified Linseed Oil with Varying Levels of Crosslinking. *Journal of Polymer Science Part A: Polymer Chemistry* **2008,** 46 (20), 6851-6860.

70. Henna, P. H.; Larock, R. C. Rubbery Thermosets by Ring-Opening Metathesis Polymerization of a Functionalized Castor Oil and Cyclooctene. *Macromol. Mater. Eng.* **2007,** 292 (12), 1201-1209.

71. Mutlu, H.; Meier, M. A. R. Ring-Opening Metathesis Polymerization of Fatty Acid Derived Monomers. *Journal of Polymer Science Part a-Polymer Chemistry* **2010,** 48 (24), 5899-5906.

72. Takeda, Y.; Nakagawa, Y.; Tomishige, K. Selective Hydrogenation of Higher Saturated Carboxylic Acids to Alcohols Using a ReOx-Pd/SiO_2 Catalyst. *Catal. Sci. Eng.* **2012,** 2 (11), 2221-2223.

73. Toba, M.; Tanaka, S.; Niwa, S.; Mizukami, F.; Koppány, Z.; Guczi, L.; Cheah, K. Y.; Tang, T. S. Synthesis of Alcohols and Diols by Hydrogenation of Carboxylic Acids and Esters over Ru–Sn–Al_2O_3 Catalysts. *Appl. Catal., A* **1999,** 189 (2), 243-250.

74. Dutta, P.; Gogoi, B.; Dass, N. N.; Sen Sarma, N. Efficient Organic Solvent and Oil Sorbent co-Polyesters: Poly-9-octadecenylacrylate/Methacrylate with 1-Hexene. *Reactive and Functional Polymers* **2013,** 73 (3), 457-464.

75. Zheng, Y. J.; Yao, K. J.; Lee, J.; Chandler, D.; Wang, J. F.; Wang, C. P.; Chu, F. X.; Tang, C. B. Well-Defined Renewable Polymers Derived from Gum Rosin. *Macromolecules* **2010,** 43 (14), 5922-5924.

76. An, S. Y.; Hong, S. H.; Tang, C.; Oh, J. K. Rosin-based block copolymer intracellular delivery nanocarriers with reduction-responsive sheddable coronas for cancer therapy. *Polymer Chemistry* **2016,** 7 (29), 4751-4760.

77. Chen, Y.; Wilbon, P. A.; Chen, Y. P.; Zhou, J.; Nagarkatti, M.; Wang, C.; Chu, F.; Decho, A. W.; Tang, C. Amphipathic antibacterial agents using cationic methacrylic polymers with natural rosin as pendant group. *RSC Advances* **2012,** 2 (27), 10275-10282.

78. Chen, Y.; Wilbon, P. A.; Zhou, J.; Nagarkatti, M.; Wang, C.; Chu, F.; Tang, C. Multifunctional self-fluorescent polymer nanogels for label-free imaging and drug delivery. *Chemical Communications* **2013,** 49 (3), 297-299.

79. PináChen, Y. Bio-inspired resin acid-derived materials as anti-bacterial resistance agents with unexpected activities. *Chemical Science* **2014,** 5 (5), 2011-2016.

80. Ganewatta, M. S.; Miller, K. P.; Singleton, S. P.; Mehrpouya-Bahrami, P.; Chen, Y. P.; Yan, Y.; Nagarkatti, M.; Nagarkatti, P.; Decho, A. W.; Tang, C. Antibacterial and biofilm-disrupting coatings from resin acid-derived materials. *Biomacromolecules* **2015,** 16 (10), 3336-3344.

81. Liu, Y.; Yao, K.; Chen, X.; Wang, J.; Wang, Z.; Ploehn, H. J.; Wang, C.; Chu, F.; Tang, C. Sustainable thermoplastic elastomers derived from renewable cellulose, rosin and fatty acids. *Polymer Chemistry* **2014,** 5 (9), 3170-3181.

82. Feldman, K. E.; Kade, M. J.; Meijer, E. W.; Hawker, C. J.; Kramer, E. J. Model Transient Networks from Strongly Hydrogen-Bonded Polymers. *Macromolecules* **2009,** 42 (22), 9072-9081.

83. Shabbir, A.; Goldansaz, H.; Hassager, O.; van Ruymbeke, E.; Alvarez, N. J. Effect of Hydrogen Bonding on Linear and Nonlinear Rheology of Entangled Polymer Melts. *Macromolecules* **2015,** 48 (16), 5988-5996.

84. Lewis, C. L.; Stewart, K.; Anthamatten, M. The Influence of Hydrogen Bonding Side-Groups on Viscoelastic Behavior of Linear and Network Polymers. *Macromolecules* **2014,** 47 (2), 729-740.

85. Lillie, L. M.; Tolman, W. B.; Reineke, T. M. Structure/property relationships in copolymers comprising renewable isosorbide, glucarodilactone, and 2,5-bis(hydroxymethyl)furan subunits. *Polymer Chemistry* **2017,** 8 (24), 3746-3754.

86. Jiang, F.; Fang, C.; Zhang, J.; Wang, W.; Wang, Z. Triblock Copolymer Elastomers with Enhanced Mechanical Properties Synthesized by RAFT Polymerization and Subsequent Quaternization through Incorporation of a Comonomer with Imidazole Groups of about 2.0 Mass Percentage. *Macromolecules* **2017,** 50 (16), 6218-6226.

87. Wang, W.; Wang, X.; Jiang, F.; Wang, Z. Synthesis, order-to-disorder transition, microphase morphology and mechanical properties of BAB triblock copolymer elastomers with hard middle block and soft outer blocks. *Polymer Chemistry* **2018,** 9 (22), 3067-3079.

88. Cheng, S.; Beyer, F. L.; Mather, B. D.; Moore, R. B.; Long, T. E. Phosphonium-Containing ABA Triblock Copolymers: Controlled Free Radical Polymerization of Phosphonium Ionic Liquids. *Macromolecules* **2011,** 44 (16), 6509-6517.

89. Yang, J.-X.; Long, Y.-Y.; Pan, L.; Men, Y.-F.; Li, Y.-S. Spontaneously Healable Thermoplastic Elastomers Achieved through One-Pot Living Ring-Opening Metathesis Copolymerization of Well-Designed Bulky Monomers. *ACS Applied Materials & Interfaces* **2016,** 8 (19), 12445-12455.

90. Hayashi, M.; Noro, A.; Matsushita, Y. Highly Extensible Supramolecular Elastomers with Large Stress Generation Capability Originating from Multiple Hydrogen Bonds on the Long Soft Network Strands. *Macromolecular Rapid Communications* **2016,** 37 (8), 678-684.

91. Hayashi, M.; Matsushima, S.; Noro, A.; Matsushita, Y. Mechanical Property Enhancement of ABA Block Copolymer-Based Elastomers by Incorporating Transient Cross-Links into Soft Middle Block. *Macromolecules* **2015,** 48 (2), 421-431.

92. Rungswang, W.; Kotaki, M.; Shimojima, T.; Kimura, G.; Sakurai, S.; Chirachanchai, S. Directing Thermoplastic Elastomer Microdomain Parallel to Fiber Axis: A Model Case of SEBS with Benzoxazine through π–π Stacking. *Macromolecules* **2011,** 44 (23), 9276-9285.

93. Xing, W.; Li, H.; Huang, G.; Cai, L.-H.; Wu, J. Graphene oxide induced crosslinking and reinforcement of elastomers. *Composites Science and Technology* **2017,** 144, 223-229.

94. Araby, S.; Zaman, I.; Meng, Q.; Kawashima, N.; Michelmore, A.; Kuan, H.-C.; Majewski, P.; Ma, J.; Zhang, L. Melt compounding with graphene to develop functional, high-performance elastomers. *Nanotechnology* **2013,** 24 (16), 165601.

95. Wang, C.; Liu, N.; Allen, R.; Tok, J. B.-H.; Wu, Y.; Zhang, F.; Chen, Y.; Bao, Z. A Rapid and Efficient Self-Healing Thermo-Reversible Elastomer Crosslinked with Graphene Oxide. *Advanced Materials* **2013,** 25 (40), 5785-5790.

96. Liu, X.; Zhao, R.-Y.; Zhao, T.-P.; Liu, C.-Y.; Yang, S.; Chen, E.-Q. An ABA triblock containing a central soft block of poly[2,5-di(n-hexogycarbonyl)styrene] and outer hard block of poly(4-vinylpyridine): synthesis, phase behavior and mechanical enhancement. *RSC Advances* **2014,** 4 (35), 18431-18441.

97. Xie, F.; Huang, C.; Wang, F.; Huang, L.; Weiss, R. A.; Leng, J.; Liu, Y. Carboxyl-Terminated Polybutadiene–Poly(styrene-co-4-vinylpyridine) Supramolecular

Thermoplastic Elastomers and Their Shape Memory Behavior. *Macromolecules* **2016,** 49 (19), 7322-7330.

98. Mather, B. D.; Baker, M. B.; Beyer, F. L.; Berg, M. A. G.; Green, M. D.; Long, T. E. Supramolecular Triblock Copolymers Containing Complementary Nucleobase Molecular Recognition. *Macromolecules* **2007,** 40 (19), 6834-6845.

99. Song, L.; Wang, Z.; Lamm, M. E.; Yuan, L.; Tang, C. Supramolecular Polymer Nanocomposites Derived from Plant Oils and Cellulose Nanocrystals. *Macromolecules* **2017,** 50 (19), 7475-7483.

100. Wang, Z.; Zhang, Y.; Yuan, L.; Hayat, J.; Trenor, N. M.; Lamm, M. E.; Vlaminck, L.; Billiet, S.; Du Prez, F. E.; Wang, Z.; Tang, C. Biomass Approach toward Robust, Sustainable, Multiple-Shape-Memory Materials. *ACS Macro Letters* **2016,** 5 (5), 602-606.

101. Cordier, P.; Tournilhac, F.; Soulié-Ziakovic, C.; Leibler, L. Self-healing and thermoreversible rubber from supramolecular assembly. *Nature* **2008,** 451, 977.

102. Feng, X.; Kawabata, K.; Whang, D. M.; Osuji, C. O. Polymer Nanosheets from Supramolecular Assemblies of Conjugated Linoleic Acid–High Surface Area Adsorbents from Renewable Materials. *Langmuir* **2017,** 33 (40), 10690-10697.

103. Hu, J.; Wang, Z.; Lu, Z.; Chen, C.; Shi, M.; Wang, J.; Zhao, E.; Zeng, K.; Yang, G. Bio-based adenine-containing high performance polyimide. *Polymer* **2017,** 119 (Supplement C), 59-65.

104. Woranuch, S.; Pangon, A.; Puagsuntia, K.; Subjalearndee, N.; Intasanta, V. Rice flour-based nanostructures via a water-based system: transformation from powder to electrospun nanofibers under hydrogen-bonding induced viscosity, crystallinity and improved mechanical property. *RSC Advances* **2017,** 7 (32), 19960-19966.

105. Loveday, D.; Wilkes, G.; Lee, Y.; Storey, R. F. Structure--Property Relationships in Poly (Isobutene) Telechelic Ionomers With Narrow or Broad Polydispersity. *Polymer Preprints(USA)* **1992,** 33 (2), 288-289.

106. Ghosh, S. K.; Khastgir, D.; De, S.; De, P.; Albalak, R.; Cohen, R. Sulphonation of maleated block-copoly (styrene ethylene-butylene. *Plastics rubber and composites processing and applications* **1998,** 27 (7), 310-316.

107. Ghosh, S. K.; De, P. P.; Khastgir, D.; De, S. K. Zinc ionomer based on sulfonated maleated styrene-ethylene/butylene-styrene block copolymer. *Macromolecular Rapid Communications* **1999,** 20 (9), 505-509.

108. Halbrook, N. J.; Lawrence, R. V. The Isolation of Dehydroabietic Acid from Disproportionated Rosin. *The Journal of Organic Chemistry* **1966,** 31 (12), 4246-4247.

109. Moineau, G.; Minet, M.; Dubois, P.; Teyssie, P.; Senninger, T.; Jerome, R. Controlled radical polymerization of (meth)acrylates by ATRP with NiBr2(PPh3)(2) as catalyst. *Macromolecules* **1999,** 32 (1), 27-35.

110. Patton, D. L.; Mullings, M.; Fulghum, T.; Advincula, R. C. A Facile Synthesis Route to Thiol-Functionalized α,ω-Telechelic Polymers via Reversible Addition Fragmentation Chain Transfer Polymerization. *Macromolecules* **2005,** 38 (20), 8597-8602.

111. Wang, S.; Vajjala Kesava, S.; Gomez, E. D.; Robertson, M. L. Sustainable Thermoplastic Elastomers Derived from Fatty Acids. *Macromolecules* **2013,** 46 (18), 7202-7212.

112. Wang, S.; Robertson, M. L. Thermodynamic Interactions between Polystyrene and Long-Chain Poly(n-Alkyl Acrylates) Derived from Plant Oils. *ACS Applied Materials & Interfaces* **2015,** 7 (22), 12109-12118.

113. Choy, C.; Hunt, R.; Salinger, G. d. Specific heat of amorphous polymethyl methacrylate and polystyrene below 4 K. *The Journal of Chemical Physics* **1970,** 52 (7), 3629-3633.

114. Luo, Y.; Liu, X. Reversible addition–fragmentation transfer (RAFT) copolymerization of methyl methacrylate and styrene in miniemulsion. *Journal of Polymer Science Part A: Polymer Chemistry* **2004,** 42 (24), 6248-6258.

115. Chen, M.; Moad, G.; Rizzardo, E. Thiocarbonylthio end group removal from RAFT-synthesized polymers by a radical-induced process. *Journal of Polymer Science Part A: Polymer Chemistry* **2009,** 47 (23), 6704-6714.

116. Barner-Kowollik, C.; Buback, M.; Charleux, B.; Coote, M. L.; Drache, M.; Fukuda, T.; Goto, A.; Klumperman, B.; Lowe, A. B.; Mcleary, J. B.; Moad, G.; Monteiro, M. J.; Sanderson, R. D.; Tonge, M. P.; Vana, P. Mechanism and kinetics of dithiobenzoate-mediated RAFT polymerization. I. The current situation. *Journal of Polymer Science Part A: Polymer Chemistry* **2006,** 44 (20), 5809-5831.

117. Hill, M. R.; Carmean, R. N.; Sumerlin, B. S. Expanding the Scope of RAFT Polymerization: Recent Advances and New Horizons. *Macromolecules* **2015,** 48 (16), 5459-5469.

118. Das, D.; Gerboth, D.; Postma, A.; Srinivasan, S.; Kern, H.; Chen, J.; Ratner, D. M.; Stayton, P. S.; Convertine, A. J. Synthesis of zwitterionic, hydrophobic, and

amphiphilic polymers via RAFT polymerization induced self-assembly (PISA) in acetic acid. *Polymer Chemistry* **2016,** 7 (39), 6133-6143.

119. Li, S.-J.; Xie, S.-J.; Li, Y.-C.; Qian, H.-J.; Lu, Z.-Y. Influence of molecular-weight polydispersity on the glass transition of polymers. *Physical Review E* **2016,** 93 (1), 012613.

120. Claudy, P.; Létoffé, J. M.; Camberlain, Y.; Pascault, J. P. Glass transition of polystyrene versus molecular weight. *Polymer Bulletin* **1983,** 9 (4), 208-215.

121. Coleman, M. M.; Lee, K. H.; Skrovanek, D. J.; Painter, P. C. Hydrogen bonding in polymers. 4. Infrared temperature studies of a simple polyurethane. *Macromolecules* **1986,** 19 (8), 2149-2157.

122. Rogers, S.; Mandelkern, L. Glass Transitions of the Poly-(n-Alkyl Methacrylates). *The Journal of Physical Chemistry* **1957,** 61 (7), 985-991.

123. Lynd, N. A.; Hillmyer, M. A. Effects of Polydispersity on the Order−Disorder Transition in Block Copolymer Melts. *Macromolecules* **2007,** 40 (22), 8050-8055.

124. Coleman, M. M.; Serman, C. J.; Bhagwagar, D. E.; Painter, P. C. A practical guide to polymer miscibility. *Polymer* **1990,** 31 (7), 1187-1203.

125. Wang, S.; Xie, R.; Vajjala Kesava, S.; Gomez, E. D.; Cochran, E. W.; Robertson, M. L. Close-Packed Spherical Morphology in an ABA Triblock Copolymer Aligned with Large-Amplitude Oscillatory Shear. *Macromolecules* **2016,** 49 (13), 4875-4888.

126. Kinning, D. J.; Thomas, E. L. Hard-sphere interactions between spherical domains in diblock copolymers. *Macromolecules* **1984,** 17 (9), 1712-1718.

127. Hashimoto, T.; Fujimura, M.; Kawai, H. Domain-Boundary Structure of Styrene-Isoprene Block Copolymer Films Cast from Solutions. 5. Molecular-Weight Dependence of Spherical Microdomains. *Macromolecules* **1980,** 13 (6), 1660-1669.

128. Helfand, E.; Wasserman, Z. R. Block Copolymer Theory. 5. Spherical Domains. *Macromolecules* **1978,** 11 (5), 960-966.

129. Sakamoto, J.; Sakurai, S.; Doi, K.; Nomura, S. Molecular orientation of poly(styrene-block-butadiene-block-styrene) triblock copolymer with cylindrical microdomains of polystyrene. *Polymer* **1993,** 34 (23), 4837-4840.

130. Kok, C. M.; Yee, V. H. The effects of crosslink density and crosslink type on the tensile and tear strengths of NR, SBR and EPDM gum vulcanizates. *European Polymer Journal* **1986,** 22 (4), 341-345.

131. Gee, G. Tensile strengths of pure gum natural rubber compounds. *Journal of Polymer Science* **1947,** 2 (5), 451-462.

132. Kajita, T.; Noro, A.; Matsushita, Y. Design and properties of supramolecular elastomers. *Polymer* **2017,** 128 (Supplement C), 297-310.

133. Holden, G.; Bishop, E.; Legge, N. R. In *Thermoplastic elastomers*, Journal of Polymer Science: Polymer Symposia, 1969; Wiley Online Library: 1969; pp 37-57.

134. Moineau, C.; Minet, M.; Teyssié, P.; Jérôme, R. Synthesis and Characterization of Poly(methyl methacrylate)-block-poly(n-butyl acrylate)-block-poly(methyl methacrylate) Copolymers by Two-Step Controlled Radical Polymerization (ATRP) Catalyzed by NiBr2(PPh3)2, 1. *Macromolecules* **1999,** 32 (25), 8277-8282.

135. Luo, Y.; Wang, X.; Zhu, Y.; Li, B.-G.; Zhu, S. Polystyrene-block-poly(n-butyl acrylate)-block-polystyrene Triblock Copolymer Thermoplastic Elastomer Synthesized via RAFT Emulsion Polymerization. *Macromolecules* **2010,** 43 (18), 7472-7481.

136. Tong, J.; Jérôme, R. Synthesis of poly (methyl methacrylate)-b-poly (n-butyl acrylate)-b-poly (methyl methacrylate) triblocks and their potential as thermoplastic elastomers. *Polymer* **2000,** 41 (7), 2499-2510.

137. Morton, M.; McGrath, J. E.; Juliano, P. C. Structure-property relationships for styrene-diene thermoplastic elastomers. *Journal of Polymer Science Part C: Polymer Symposia* **1969,** 26 (1), 99-115.

138. Zhang, Z.; Grijpma, D. W.; Feijen, J. Triblock Copolymers Based on 1,3-Trimethylene Carbonate and Lactide as Biodegradable Thermoplastic Elastomers. *Macromolecular Chemistry and Physics* **2004,** 205 (7), 867-875.

139. Dair, B. J.; Honeker, C. C.; Alward, D. B.; Avgeropoulos, A.; Hadjichristidis, N.; Fetters, L. J.; Capel, M.; Thomas, E. L. Mechanical Properties and Deformation Behavior of the Double Gyroid Phase in Unoriented Thermoplastic Elastomers. *Macromolecules* **1999,** 32 (24), 8145-8152.

140. Adhikari, R.; Michler, G. H. Influence of molecular architecture on morphology and micromechanical behavior of styrene/butadiene block copolymer systems. *Progress in polymer science* **2004,** 29 (9), 949-986.

141. Adhikari, R.; Michler, G. H.; Lebek, W.; Goerlitz, S.; Weidisch, R.; Knoll, K. Morphology and micromechanical deformation behavior of SB-block copolymers. II. Influence of molecular architecture of asymmetric star block copolymers. *Journal of Applied Polymer Science* **2002,** 85 (4), 701-713.

142. Weidisch, R.; Stamm, M.; Schubert, D. W.; Arnold, M.; Budde, H.; Höring, S. Correlation between Phase Behavior and Tensile Properties of Diblock Copolymers. *Macromolecules* **1999,** 32 (10), 3405-3411.

143. Weidisch, R.; Ensslen, M.; Michler, G. H.; Fischer, H. Deformation Behavior of Weakly Segregated Block Copolymers. 1. Influence of Morphology of Poly(styrene-b-butyl methacrylate) Diblock Copolymers. *Macromolecules* **1999,** 32 (16), 5375-5382.

144. Serpe, M. J.; Craig, S. L. Physical Organic Chemistry of Supramolecular Polymers. *Langmuir* **2007,** 23 (4), 1626-1634.

145. Herbst, F.; Seiffert, S.; Binder, W. H. Dynamic supramolecular poly(isobutylene)s for self-healing materials. *Polymer Chemistry* **2012,** 3 (11), 3084-3092.

146. Bose, R. K.; Hohlbein, N.; Garcia, S. J.; Schmidt, A. M.; van der Zwaag, S. Connecting supramolecular bond lifetime and network mobility for scratch healing in poly(butyl acrylate) ionomers containing sodium, zinc and cobalt. *Physical Chemistry Chemical Physics* **2015,** 17 (3), 1697-1704.

147. Chen, Q.; Huang, C.; Weiss, R. A.; Colby, R. H. Viscoelasticity of Reversible Gelation for Ionomers. *Macromolecules* **2015,** 48 (4), 1221-1230.

148. Stukalin, E. B.; Cai, L.-H.; Kumar, N. A.; Leibler, L.; Rubinstein, M. Self-Healing of Unentangled Polymer Networks with Reversible Bonds. *Macromolecules* **2013,** 46 (18), 7525-7541.

149. Sauer, J. A. Mechanical Properties of lonomers AU - Hara, M. *Journal of Macromolecular Science, Part C* **1994,** 34 (3), 325-373.

150. Middleton, L. R.; Winey, K. I. Nanoscale Aggregation in Acid- and Ion-Containing Polymers. *Annual Review of Chemical and Biomolecular Engineering* **2017,** 8 (1), 499-523.

151. Rubinstein, M.; Semenov, A. N. Thermoreversible Gelation in Solutions of Associating Polymers. 2. Linear Dynamics. *Macromolecules* **1998,** 31 (4), 1386-1397.

152. Huang, C.; Wang, C.; Chen, Q.; Colby, R. H.; Weiss, R. A. Reversible Gelation Model Predictions of the Linear Viscoelasticity of Oligomeric Sulfonated Polystyrene Ionomer Blends. *Macromolecules* **2016,** 49 (10), 3936-3947.

153. Jeong, S.-J.; Kim, J. Y.; Kim, B. H.; Moon, H.-S.; Kim, S. O. Directed self-assembly of block copolymers for next generation nanolithography. *Materials Today* **2013,** 16 (12), 468-476.

154. Black, C. T.; Ruiz, R.; Breyta, G.; Cheng, J. Y.; Colburn, M. E.; Guarini, K. W.; Kim, H.-C.; Zhang, Y. Polymer self assembly in semiconductor microelectronics. *IBM Journal of Research and Development* **2007,** 51 (5), 605-633.

155. Chan, V. Z.-H.; Hoffman, J.; Lee, V. Y.; Iatrou, H.; Avgeropoulos, A.; Hadjichristidis, N.; Miller, R. D.; Thomas, E. L. Ordered Bicontinuous Nanoporous and Nanorelief Ceramic Films from Self Assembling Polymer Precursors. *Science* **1999,** 286 (5445), 1716-1719.

156. Ma, W.; Yang, C.; Gong, X.; Lee, K.; Heeger, A. J. Thermally Stable, Efficient Polymer Solar Cells with Nanoscale Control of the Interpenetrating Network Morphology. *Advanced Functional Materials* **2005,** 15 (10), 1617-1622.

157. Guo, C.; Lin, Y.-H.; Witman, M. D.; Smith, K. A.; Wang, C.; Hexemer, A.; Strzalka, J.; Gomez, E. D.; Verduzco, R. Conjugated Block Copolymer Photovoltaics

with near 3% Efficiency through Microphase Separation. *Nano Letters* **2013,** 13 (6), 2957-2963.

158. Borges, B. G. A. L.; Veiga, A. G.; Tzounis, L.; Laskarakis, A.; Logothetidis, S.; Rocco, M. L. M. Molecular Orientation and Ultrafast Charge Transfer Dynamics Studies on the P3HT:PCBM Blend. *The Journal of Physical Chemistry C* **2016,** 120 (43), 25078-25082.

159. Chen, Z.-R.; Kornfield, J. A. Flow-induced alignment of lamellar block copolymer melts. *Polymer* **1998,** 39 (19), 4679-4699.

160. Hermel, T. J.; Wu, L.; Hahn, S. F.; Lodge, T. P.; Bates, F. S. Shear-Induced Lamellae Alignment in Matched Triblock and Pentablock Copolymers. *Macromolecules* **2002,** 35 (12), 4685-4689.

161. Stangler, S.; Abetz, V. Orientation behavior of AB and ABC block copolymers under large amplitude oscillatory shear flow. *Rheologica Acta* **2003,** 42 (6), 569-577.

162. Olszowka, V.; Hund, M.; Kuntermann, V.; Scherdel, S.; Tsarkova, L.; Böker, A. Electric Field Alignment of a Block Copolymer Nanopattern: Direct Observation of the Microscopic Mechanism. *ACS Nano* **2009,** 3 (5), 1091-1096.

163. Liedel, C.; Pester, C. W.; Ruppel, M.; Lewin, C.; Pavan, M. J.; Urban, V. S.; Shenhar, R.; Bösecke, P.; Böker, A. Block Copolymer Nanocomposites in Electric Fields: Kinetics of Alignment. *ACS Macro Letters* **2013,** 2 (1), 53-58.

164. Hammond, M. R.; Dietsch, H.; Pravaz, O.; Schurtenberger, P. Mutual Alignment of Block Copolymer−Magnetic Nanoparticle Composites in a Magnetic Field. *Macromolecules* **2010,** 43 (20), 8340-8343.

165. Gopinadhan, M.; Choo, Y.; Kawabata, K.; Kaufman, G.; Feng, X.; Di, X.; Rokhlenko, Y.; Mahajan, L. H.; Ndaya, D.; Kasi, R. M.; Osuji, C. O. Controlling orientational order in block copolymers using low-intensity magnetic fields. *Proceedings of the National Academy of Sciences* **2017,** 114 (45), E9437-E9444.

166. Hashimoto, T.; Bodycomb, J.; Funaki, Y.; Kimishima, K. The Effect of Temperature Gradient on the Microdomain Orientation of Diblock Copolymers Undergoing an Order−Disorder Transition. *Macromolecules* **1999,** 32 (3), 952-954.

167. Singh, G.; Yager, K. G.; Smilgies, D.-M.; Kulkarni, M. M.; Bucknall, D. G.; Karim, A. Tuning Molecular Relaxation for Vertical Orientation in Cylindrical Block Copolymer Films via Sharp Dynamic Zone Annealing. *Macromolecules* **2012,** 45 (17), 7107-7117.

168. Singh, G.; Yager, K. G.; Berry, B.; Kim, H.-C.; Karim, A. Dynamic Thermal Field-Induced Gradient Soft-Shear for Highly Oriented Block Copolymer Thin Films. *ACS Nano* **2012,** 6 (11), 10335-10342.

169. Kim, S. H.; Misner, M. J.; Xu, T.; Kimura, M.; Russell, T. P. Highly Oriented and Ordered Arrays from Block Copolymers via Solvent Evaporation. *Advanced Materials* **2004,** 16 (3), 226-231.

170. Park, S.; Wang, J.-Y.; Kim, B.; Chen, W.; Russell, T. P. Solvent-Induced Transition from Micelles in Solution to Cylindrical Microdomains in Diblock Copolymer Thin Films. *Macromolecules* **2007,** 40 (25), 9059-9063.

171. Albert, J. N. L.; Young, W.-S.; Lewis, R. L.; Bogart, T. D.; Smith, J. R.; Epps, T. H. Systematic Study on the Effect of Solvent Removal Rate on the Morphology of

Solvent Vapor Annealed ABA Triblock Copolymer Thin Films. *ACS Nano* **2012,** 6 (1), 459-466.

172. Segalman, R. A.; Yokoyama, H.; Kramer, E. J. Graphoepitaxy of Spherical Domain Block Copolymer Films. *Advanced Materials* **2001,** 13 (15), 1152-1155.

173. Cheng, J. Y.; Ross, C. A.; Thomas, E. L.; Smith, H. I.; Vancso, G. J. Fabrication of nanostructures with long-range order using block copolymer lithography. *Applied Physics Letters* **2002,** 81 (19), 3657-3659.

174. Cheng, J. Y.; Zhang, F.; Chuang, V. P.; Mayes, A. M.; Ross, C. A. Self-Assembled One-Dimensional Nanostructure Arrays. *Nano Letters* **2006,** 6 (9), 2099-2103.

175. Shin, G.; Sakamoto, N.; Saijo, K.; Suehiro, S.; Hashimoto, T.; Ito, K.; Amemiya, Y. Time-resolved SAXS studies of a sphere-forming block copolymer under large oscillatory shear deformation. *Macromolecules* **2000,** 33 (24), 9002-9014.

176. Huang, Y.-Y.; Hsu, J.-Y.; Chen, H.-L.; Hashimoto, T. Existence of fcc-Packed Spherical Micelles in Diblock Copolymer Melt. *Macromolecules* **2007,** 40 (3), 406-409.

177. Lee, S.; Bluemle, M. J.; Bates, F. S. Discovery of a Frank-Kasper σ Phase in Sphere-Forming Block Copolymer Melts. *Science* **2010,** 330 (6002), 349-353.

178. Morrison, F. A.; Winter, H. H. The effect of unidirectional shear on the structure of triblock copolymers. I. Polystyrene-polybutadiene-polystyrene. *Macromolecules* **1989,** 22 (9), 3533-3540.

179. Pakula, T.; Saijo, K.; Kawai, H.; Hashimoto, T. Deformation behavior of styrene-butadiene-styrene triblock copolymer with cylindrical morphology. *Macromolecules* **1985,** 18 (6), 1294-1302.

180. Osuji, C.; Zhang, Y.; Mao, G.; Ober, C. K.; Thomas, E. L. Transverse Cylindrical Microdomain Orientation in an LC Diblock Copolymer under Oscillatory Shear. *Macromolecules* **1999,** 32 (22), 7703-7706.

181. Vigild, M. E.; Almdal, K.; Mortensen, K.; Hamley, I. W.; Fairclough, J. P. A.; Ryan, A. J. Transformations to and from the Gyroid Phase in a Diblock Copolymer. *Macromolecules* **1998,** 31 (17), 5702-5716.

182. Wang, C.-Y.; Lodge, T. P. Kinetics and Mechanisms for the Cylinder-to-Gyroid Transition in a Block Copolymer Solution. *Macromolecules* **2002,** 35 (18), 6997-7006.

183. Koppi, K. A.; Tirrell, M.; Bates, F. S.; Almdal, K.; Colby, R. H. Lamellae orientation in dynamically sheared diblock copolymer melts. *J. Phys. II France* **1992,** 2 (11), 1941-1959.

184. Kannan, R. M.; Kornfield, J. A. Evolution of Microstructure and Viscoelasticity during Flow Alignment of a Lamellar Diblock Copolymer. *Macromolecules* **1994,** 27 (5), 1177-1186.

185. Okamoto, S.; Saijo, K.; Hashimoto, T. Real-Time SAXS Observations of Lamella-Forming Block Copolymers under Large Oscillatory Shear Deformation. *Macromolecules* **1994,** 27 (20), 5547-5555.

186. Oelschlaeger, C.; Gutmann, J. S.; Wolkenhauer, M.; Spiess, H. W.; Knoll, K.; Wilhelm, M. Kinetics of Shear Microphase Orientation and Reorientation in Lamellar Diblock and Triblock Copolymer Melts as Detected via FT‐Rheology and 2D‐SAXS. *Macromolecular Chemistry and Physics* **2007,** 208 (16), 1719-1729.

187. Gupta, V. K.; Krishnamoorti, R.; Chen, Z. R.; Kornfield, J. A.; Smith, S. D.; Satkowski, M. M.; Grothaus, J. T. Dynamics of Shear Alignment in a Lamellar Diblock

Copolymer: Interplay of Frequency, Strain Amplitude, and Temperature. *Macromolecules* **1996,** 29 (3), 875-884.

188. Polis, D. L.; Smith, S. D.; Terrill, N. J.; Ryan, A. J.; Morse, D. C.; Winey, K. I. Shear-Induced Lamellar Rotation Observed in a Diblock Copolymer by in Situ Small-Angle X-ray Scattering. *Macromolecules* **1999,** 32 (14), 4668-4676.

189. Qiao, L.; Winey, K. I.; Morse, D. C. Dynamics of Kink Bands in Layered Liquids: Theory and in Situ SAXS Experiments on a Block Copolymer Melt. *Macromolecules* **2001,** 34 (22), 7858-7867.

190. Fredrickson, G. H. Steady shear alignment of block copolymers near the isotropic–lamellar transition. *Journal of Rheology* **1994,** 38 (4), 1045-1067.

191. Hu, H.; Gopinadhan, M.; Osuji, C. O. Directed self-assembly of block copolymers: a tutorial review of strategies for enabling nanotechnology with soft matter. *Soft Matter* **2014,** 10 (22), 3867-3889.

192. Chen, Z.-R.; Kornfield, J. A.; Smith, S. D.; Grothaus, J. T.; Satkowski, M. M. Pathways to Macroscale Order in Nanostructured Block Copolymers. *Science* **1997,** 277 (5330), 1248-1253.

193. Osuji, C. O.; Chen, J. T.; Mao, G.; Ober, C. K.; Thomas, E. L. Understanding and controlling the morphology of styrene–isoprene side-group liquid crystalline diblock copolymers. *Polymer* **2000,** 41 (25), 8897-8907.

194. Marencic, A. P.; Wu, M. W.; Register, R. A.; Chaikin, P. M. Orientational Order in Sphere-Forming Block Copolymer Thin Films Aligned under Shear. *Macromolecules* **2007,** 40 (20), 7299-7305.

195. Marencic, A. P.; Adamson, D. H.; Chaikin, P. M.; Register, R. A. Shear alignment and realignment of sphere-forming and cylinder-forming block-copolymer thin films. *Physical Review E* **2010,** 81 (1), 011503.

196. Torija, M. A.; Choi, S. H.; Lodge, T. P.; Bates, F. S. Large Amplitude Oscillatory Shear of Block Copolymer Spheres on a Body-Centered Cubic Lattice: Are Micelles Like Metals? *Journal of Physical Chemistry B* **2011,** 115 (19), 5840-5848.

197. Takagi, H.; Yamamoto, K. Phase Boundary of Frank–Kasper σ Phase in Phase Diagrams of Binary Mixtures of Block Copolymers and Homopolymers. *Macromolecules* **2019,** 52 (5), 2007-2014.

198. Zhang, J.; Bates, F. S. Dodecagonal Quasicrystalline Morphology in a Poly(styrene-b-isoprene-b-styrene-b-ethylene oxide) Tetrablock Terpolymer. *Journal of the American Chemical Society* **2012,** 134 (18), 7636-7639.

199. Lee, S.; Leighton, C.; Bates, F. S. Sphericity and symmetry breaking in the formation of Frank–Kasper phases from one component materials. *Proceedings of the National Academy of Sciences* **2014,** 111 (50), 17723-17731.

200. Gillard, T. M.; Lee, S.; Bates, F. S. Dodecagonal quasicrystalline order in a diblock copolymer melt. *Proceedings of the National Academy of Sciences* **2016,** 113 (19), 5167-5172.

201. Imaizumi, K.; Ono, T.; Kota, T.; Okamoto, S.; Sakurai, S. Transformation of cubic symmetry for spherical microdomains from face-centred to body-centred cubic upon uniaxial elongation in an elastomeric triblock copolymer. *Journal of applied crystallography* **2003,** 36 (4), 976-981.

202. Sakamoto, N.; Hashimoto, T.; Han, C. D.; Kim, D.; Vaidya, N. Y. Order−Order and Order−Disorder Transitions in a Polystyrene-block-Polyisoprene-block-Polystyrene Copolymer. *Macromolecules* **1997,** 30 (6), 1621-1632.

203. Sakamoto, N.; Hashimoto, T. Ordering Dynamics of Cylindrical and Spherical Microdomains in Polystyrene-block-Polyisoprene-block-Polystyrene. 1. SAXS and TEM Observations for the Grain Formation. *Macromolecules* **1998,** 31 (24), 8493-8502.

204. Dormidontova, E. E.; Lodge, T. P. The Order−Disorder Transition and the Disordered Micelle Regime in Sphere-Forming Block Copolymer Melts. *Macromolecules* **2001,** 34 (26), 9143-9155.

205. Castelletto, V.; Hamley, I. W.; Holmqvist, P.; Rekatas, C.; Booth, C.; Grossmann, J. G. Small-angle X-ray scattering study of a poly(oxyphenylethylene)–poly(oxyethylene) diblock copolymer gel under shear flow. *Colloid and Polymer Science* **2001,** 279 (7), 621-628.

206. Bang, J.; Lodge, T. P. Mechanisms and Epitaxial Relationships between Close-Packed and BCC Lattices in Block Copolymer Solutions. *The Journal of Physical Chemistry B* **2003,** 107 (44), 12071-12081.

207. Daniel, C.; Hamley, I. W.; Mingvanish, W.; Booth, C. Effect of shear on the face-centered cubic phase in a diblock copolymer gel. *Macromolecules* **2000,** 33 (6), 2163-2170.

208. Matsen, M. W. Phase Behavior of Block Copolymer/Homopolymer Blends. *Macromolecules* **1995,** 28 (17), 5765-5773.

209. Matsen, M. W. Stabilizing New Morphologies by Blending Homopolymer with Block Copolymer. *Physical Review Letters* **1995,** 74 (21), 4225-4228.

210. Lynd, N. A.; Meuler, A. J.; Hillmyer, M. A. Polydispersity and block copolymer self-assembly. *Progress in Polymer Science* **2008,** 33 (9), 875-893.

211. Hamley, I. W.; Pople, J. A.; Booth, C.; Yang, Y. W.; King, S. M. A Small-Angle Neutron-Scattering Study of Shear-Induced Ordering in the Cubic Phase of a Block Copolymer Gel. *Langmuir* **1998,** 14 (12), 3182-3186.

212. Wang, H.; Newstein, M. C.; Krishnan, A.; Balsara, N. P.; Garetz, B. A.; Hammouda, B.; Krishnamoorti, R. Ordering Kinetics and Alignment of Block Copolymer Lamellae under Shear Flow. *Macromolecules* **1999,** 32 (11), 3695-3711.

213. Wang, H.; Kesani, P. K.; Balsara, N. P.; Hammouda, B. Undulations and Disorder in Block Copolymer Lamellae under Shear Flow. *Macromolecules* **1997,** 30 (4), 982-992.

214. Meins, T.; Hyun, K.; Dingenouts, N.; Ardakani, M. F.; Struth, B.; Wilhelm, M. New Insight to the Mechanism of the Shear-Induced Macroscopic Alignment of Diblock Copolymer Melts by a Unique and Newly Developed Rheo-SAXS Combination. *Macromolecules* **2012,** 45 (1), 455-472.

215. Manfred, W. Fourier‐Transform Rheology. *Macromolecular Materials and Engineering* **2002,** 287 (2), 83-105.

216. Meins, T.; Dingenouts, N.; Kubel, J.; Wilhelm, M. In Situ Rheodielectric, ex Situ 2D-SAXS, and Fourier Transform Rheology Investigations of the Shear-Induced Alignment of Poly(styrene-b-1,4-isoprene) Diblock Copolymer Melts. *Macromolecules* **2012,** 45 (17), 7206-7219.

217. Langela, M.; Wiesner, U.; Spiess, H. W.; Wilhelm, M. Microphase reorientation in block copolymer melts as detected via FT rheology and 2D SAXS. *Macromolecules* **2002,** 35 (8), 3198-3204.

218. Hyun, K.; Wilhelm, M.; Klein, C. O.; Cho, K. S.; Nam, J. G.; Ahn, K. H.; Lee, S. J.; Ewoldt, R. H.; McKinley, G. H. A review of nonlinear oscillatory shear tests: Analysis and application of large amplitude oscillatory shear (LAOS). *Progress in Polymer Science* **2011,** 36 (12), 1697-1753.

219. Hyun, K.; Wilhelm, M. Establishing a New Mechanical Nonlinear Coefficient Q from FT-Rheology: First Investigation of Entangled Linear and Comb Polymer Model Systems. *Macromolecules* **2009,** 42 (1), 411-422.

220. Hyun, K.; Baik, E. S.; Ahn, K. H.; Lee, S. J.; Sugimoto, M.; Koyama, K. Fourier-transform rheology under medium amplitude oscillatory shear for linear and branched polymer melts. *Journal of Rheology* **2007,** 51 (6), 1319-1342.

221. López-Barrón, C. R.; Wagner, N. J.; Porcar, L. Layering, melting, and recrystallization of a close-packed micellar crystal under steady and large-amplitude oscillatory shear flows. *Journal of Rheology* **2015,** 59 (3), 793-820.

222. Leblanc, J. L. Large amplitude oscillatory shear experiments to investigate the nonlinear viscoelastic properties of highly loaded carbon black rubber compounds without curatives. *Journal of Applied Polymer Science* **2008,** 109 (2), 1271-1293.

223. Ewoldt, R. H.; Hosoi, A. E.; McKinley, G. H. New measures for characterizing nonlinear viscoelasticity in large amplitude oscillatory shear. *Journal of Rheology* **2008,** 52 (6), 1427-1458.

224. Ackerson, B. J.; Pusey, P. N. Shear-Induced Order in Suspensions of Hard Spheres. *Physical Review Letters* **1988,** 61 (8), 1033-1036.

225. Jiang, J.; Burger, C.; Li, C.; Li, J.; Lin, M. Y.; Colby, R. H.; Rafailovich, M. H.; Sokolov, J. C. Shear-Induced Layered Structure of Polymeric Micelles by SANS. *Macromolecules* **2007,** 40 (11), 4016-4022.

226. Chen, L. B.; Ackerson, B. J.; Zukoski, C. F. Rheological consequences of microstructural transitions in colloidal crystals. *Journal of Rheology* **1994,** 38 (2), 193-216.

227. Loose, W.; Ackerson, B. J. Model calculations for the analysis of scattering data from layered structures. *The Journal of chemical physics* **1994,** 101 (9), 7211-7220.

228. López-Barrón, C. R.; Porcar, L.; Eberle, A. P.; Wagner, N. J. Dynamics of melting and recrystallization in a polymeric micellar crystal subjected to large amplitude oscillatory shear flow. *Physical review letters* **2012,** 108 (25), 258301.

229. Lee, S. H.; Yong Song, H.; Hyun, K.; Hyup Lee, J. Nonlinearity from FT-rheology for liquid crystal 8CB under large amplitude oscillatory shear (LAOS) flow. *Journal of Rheology* **2014,** 59 (1), 1-19.

230. Morrison, F.; Le Bourvellec, G.; Winter, H. H. Flow-induced structure and rheology of a triblock copolymer. *Journal of Applied Polymer Science* **1987,** 33 (5), 1585-1600.

231. Scott, D. B.; Waddon, A. J.; Lin, Y. G.; Karasz, F. E.; Winter, H. H. Shear-induced orientation transitions in triblock copolymer styrene-butadiene-styrene with cylindrical domain morphology. *Macromolecules* **1992,** 25 (16), 4175-4181.

232. Tang, W.; Matyjaszewski, K. Effect of ligand structure on activation rate constants in ATRP. *Macromolecules* **2006,** 39 (15), 4953-4959.

233. Wang, G. Synthesis of poly (n-butyl acrylate) homopolymers by activators generated by electron transfer (AGET) ATRP using FeCl 3· 6H 2 O/succinic acid catalyst. *Iran Polym J* **2011,** 20, 931-938.

234. Nguyen, N. H.; Kulis, J.; Sun, H.-J.; Jia, Z.; Van Beusekom, B.; Levere, M. E.; Wilson, D. A.; Monteiro, M. J.; Percec, V. A comparative study of the SET-LRP of oligo (ethylene oxide) methyl ether acrylate in DMSO and in H2O. *Polymer Chemistry* **2013,** 4 (1), 144-155.

235. Basuki, J. S.; Esser, L.; Duong, H. T.; Zhang, Q.; Wilson, P.; Whittaker, M. R.; Haddleton, D. M.; Boyer, C.; Davis, T. P. Magnetic nanoparticles with diblock glycopolymer shells give lectin concentration-dependent MRI signals and selective cell uptake. *Chemical Science* **2014,** 5 (2), 715-726.

236. Hui, C. M.; Dang, A.; Chen, B.; Yan, J.; Konkolewicz, D.; He, H.; Ferebee, R.; Bockstaller, M. R.; Matyjaszewski, K. Effect of thermal self-initiation on the synthesis, composition, and properties of particle brush materials. *Macromolecules* **2014,** 47 (16), 5501-5508.

237. Funaki, Y.; Kumano, K.; Nakao, T.; Jinnai, H.; Yoshida, H.; Kimishima, K.; Tsutsumi, K.; Hirokawa, Y.; Hashimoto, T. Influence of casting solvents on microphase-separated structures of poly (2-vinylpyridine)-block-polyisoprene. *Polymer* **1999,** 40 (25), 7147-7156.

238. Hashimoto, T.; Kawamura, T.; Harada, M.; Tanaka, H. Small-angle scattering from hexagonally packed cylindrical particles with paracrystalline distortion. *Macromolecules* **1994,** 27 (11), 3063-3072.

239. Alfonzo, C. G.; Fleury, G.; Chaffin, K. A.; Bates, F. S. Synthesis and Characterization of Elastomeric Heptablock Terpolymers Structured by Crystallization. *Macromolecules* **2010,** 43 (12), 5295-5305.

240. Hashimoto, T.; Imaeda, T.; Irie, S.; Urushisaki, M.; Sakaguchi, T. Synthesis of Poly(vinyl ether)-Based, ABA Triblock-Type Thermoplastic Elastomers with Functionalized Soft Segments and their Gas Permeability. *Journal of Polymer Science Part a-Polymer Chemistry* **2015,** 53 (9), 1114-1124.

241. Han, C. D.; Kim, J. W.; Kim, J. K. DETERMINATION OF THE ORDER-DISORDER TRANSITION-TEMPERATURE OF BLOCK COPOLYMERS. *Macromolecules* **1989,** 22 (1), 383-394.

242. He, P.; Shen, W.; Yu, W.; Zhou, C. Mesophase Separation and Rheology of Olefin Multiblock Copolymers. *Macromolecules* **2014,** 47 (2), 807-820.

243. Han, C. D.; Baek, D. M.; Kim, J. K. Effect of microdomain structure on the order-disorder transition temperature of polystyrene-block-polyisoprene-block-polystyrene copolymers. *Macromolecules* **1990,** 23 (2), 561-570.

244. Kothari, R.; Winter, H. H.; Watkins, J. J. Rheological Study of Order-to-Disorder Transitions and Phase Behavior of Block Copolymer Surfactant Complexes Containing Hydrogen-Bonded Small Molecule Additives. *Macromolecules* **2014,** 47 (22), 8048-8055.

245. Song, J.; Cho, B.-K. Nanostructured poly(ethylene oxide)-like dendron-block-linear poly(ethylene-alt-propylene) copolymers: design, synthesis, and thermal and assembling properties. *Soft Matter* **2012,** 8 (12), 3419-3428.

246. Sugimoto, M.; Sakai, K.; Aoki, Y.; Taniguchi, T.; Koyama, K.; Ueda, T. Rheology and Morphology Change with Temperature of SEBS/Hydrocarbon Oil Blends. *Journal of Polymer Science Part B-Polymer Physics* **2009,** 47 (10), 955-965.

247. Almdal, K.; Rosedale, J. H.; Bates, F. S. The order-disorder transition in binary mixtures of nearly symmetric diblock copolymers. *Macromolecules* **1990,** 23 (19), 4336-4338.

248. Thomas, E.; Lescanec, R.; Frank, F.; Higgins, J.; Klug, A.; Hamley, I. Phase morphology in block copolymer systems [and discussion]. *Philosophical Transactions of the Royal Society of London A: Mathematical, Physical and Engineering Sciences* **1994,** 348 (1686), 149-166.

249. Russell, T. P.; Hjelm, R. P.; Seeger, P. A. Temperature dependence of the interaction parameter of polystyrene and poly(methyl methacrylate). *Macromolecules* **1990,** 23 (3), 890-893.

250. Sakamoto, N.; Hashimoto, T. Order-Disorder Transition of Low Molecular Weight Polystyrene-block-Polyisoprene. 1. SAXS Analysis of Two Characteristic Temperatures. *Macromolecules* **1995,** 28 (20), 6825-6834.

251. Lee, S.; Gillard, T. M.; Bates, F. S. Fluctuations, Order, and Disorder in Short Diblock Copolymers. *AIChE Journal* **2013,** 59 (9), 3502-3513.

252. Lee, J.; Ahn, H.; Ryu, D. Y.; Shin, K.; Cho, J. Anomaly in SANS χ for polydisperse polystyrene-b-poly(isooctyl acrylate). *Polymer* **2012,** 53 (12), 2495-2499.

253. Haloi, D. J.; Ata, S.; Singha, N. K.; Jehnichen, D.; Voit, B. Acrylic AB and ABA Block Copolymers Based on Poly(2-ethylhexyl acrylate) (PEHA) and Poly(methyl

methacrylate) (PMMA) via ATRP. *Acs Applied Materials & Interfaces* **2012,** 4 (8), 4200-4207.

254. Nese, A.; Mosnacek, J.; Juhari, A.; Yoon, J. A.; Koynov, K.; Kowalewski, T.; Matyjaszewski, K. Synthesis, Characterization, and Properties of Starlike Poly(n-butyl acrylate)-b-poly(methyl methacrylate) Block Copolymers. *Macromolecules* **2010,** 43 (3), 1227-1235.

255. Holden, G. L., N. R.; Quirk, R.; Schroeder, H. E., Thermoplastic elastomers. Hanser Publishers: Munish: 1996.

256. Yi, Y.; Fan, X. H.; Wan, X. H.; Li, L.; Zhao, N.; Chen, X. F.; Xu, J.; Zhou, Q. F. ABA type triblock copolymer based on mesogen-jacketed liquid crystalline polymer: Design, synthesis, and potential as thermoplastic elastomer. *Macromolecules* **2004,** 37 (20), 7610-7618.

257. Bhargava, A.; Sharma, C., *Mechanical Behaviour and testing of materials*. PHI Learning Pvt. Ltd.: 2011.

258. Graessley, W. W., The entanglement concept in polymer rheology. In *The Entanglement Concept in Polymer Rheology*, Springer: 1974; pp 1-179.

259. Fetters, L.; Lohse, D.; Richter, D.; Witten, T.; Zirkel, A. Connection between polymer molecular-weight, density, chain dimensions, and melt viscoelastic properties. *Macromolecules* **1994,** 27 (17), 4639-4647.

260. Hashimoto, T.; Namikoshi, T.; Irie, S.; Urushisaki, M.; Sakaguchi, T.; Nemoto, T.; Isoda, S. Synthesis and microphase-separated structure of poly(tricyclodecyl vinyl ether)-block-poly(n-butyl vinyl Ether)-block-poly(tricyclodecyl vinyl ether): New triblock

copolymer as thermoplastic elastomer composed solely of poly(vinyl ether) backbones. *Journal of Polymer Science Part a-Polymer Chemistry* **2008,** 46 (5), 1902-1906.

261. Tong, J.-D.; Moineau, G.; Leclere, P.; Brédas, J.-L.; Lazzaroni, R.; Jérôme, R. Synthesis, Morphology, and Mechanical Properties of Poly (methyl methacrylate)-b-poly (n-butyl acrylate)-b-poly (methyl methacrylate) Triblocks. Ligated Anionic Polymerization vs Atom Transfer Radical Polymerization. *Macromolecules* **2000,** 33 (2), 470-479.

262. Luo, Y. W.; Wang, X. G.; Zhu, Y.; Li, B. G.; Zhu, S. P. Polystyrene-block-poly(n-butyl acrylate)-block-polystyrene Triblock Copolymer Thermoplastic Elastomer Synthesized via RAFT Emulsion Polymerization. *Macromolecules* **2010,** 43 (18), 7472-7481.

263. Chatterjee, D. P.; Mandal, B. M. Triblock thermoplastic elastomers with poly (lauryl methacrylate) as the center block and poly (methyl methacrylate) or poly (tert-butyl methacrylate) as end blocks. Morphology and thermomechanical properties. *Macromolecules* **2006,** 39 (26), 9192-9200.

264. Zhang, Q.; Zhu, X.; Li, C.-H.; Cai, Y.; Jia, X.; Bao, Z. Disassociation and Reformation Under Strain in Polymer with Dynamic Metal–Ligand Coordination Cross-Linking. *Macromolecules* **2019,** 52 (2), 660-668.

265. Tang, Z.; Huang, J.; Guo, B.; Zhang, L.; Liu, F. Bioinspired Engineering of Sacrificial Metal–Ligand Bonds into Elastomers with Supramechanical Performance and Adaptive Recovery. *Macromolecules* **2016,** 49 (5), 1781-1789.

266. Li, C.-H.; Wang, C.; Keplinger, C.; Zuo, J.-L.; Jin, L.; Sun, Y.; Zheng, P.; Cao, Y.; Lissel, F.; Linder, C.; You, X.-Z.; Bao, Z. A highly stretchable autonomous self-healing elastomer. *Nature Chemistry* **2016,** 8, 618.